COMPUTER MODELLING METHODOLOGY FOR SHREDDING OF END OF LIFE CONSUMER ELECTRONIC DEVICES

BY

YUN XING
Master of Material Process Engineering,
University of Science and Technology Beijing, China, March 1997

THESIS

Submitted as partial fulfillment of the requirements
for the degree of Doctor of Philosophy in Mechanical Engineering
in the Graduate College of the
University of Illinois at Chicago, 2007

Chicago, Illinois

ACKNOWLEDGMENTS

I would like to thank my advisors, Professor Michael J. McNallan, Professor Michael J. Scott, and Professor Simon Song, for their continuous guidance and feedback. They have been a constant source of great ideas and useful guidelines during my graduate program at UIC.

I wish to extend my thankfulness to the members of my thesis committee Dr. Sabri Cetinkunt, Dr. David He, and Dr. Peipei Hsu for providing me interesting suggestions about this research.

The support of the Department of Mechanical & Industrial Engineering is gratefully acknowledged.

SUMMARY

Increased environmental concerns in recent years as well as potential economic benefits and, in some cases, mandatory regulations have placed more challenges on the recycling of end of life electronic products. The first step of the recycling system is to disassemble the pre-collected end of life electronic products either by hand or to shred by machine in preparation for the following recycling steps. Since the volume of the end of life electronic products for recycling is huge, a great deal of manual labor is required for hand disassembly. Because of the high cost of labor, shredding is often a more economical choice than manual operation.

Quality control of the intermediate recycling products is of critical importance to reach recycling targets determined by economic and environmental considerations. Thus the shredding operation plays an important role in the whole recycling system since it affects the characteristics (size, composition, etc.) of the intermediate recycling streams and thus the ultimate material recovery and the recycling rate. Accurate knowledge of the shredder output is needed to optimise the mutual compatibility of the successive processes in the recycling system. To optimise material recovery and to minimise waste generation in recycling end of life electronic products, and to get better understanding of the shredding process and thus better quality control of the intermediate products created during shredding, a computer simulation model for shredder is developed and presented in this thesis. This is of critical importance to reach recycling targets. Results from the simulation model may also provide suggestions for the designer of electronic products in the view of the relationship between product design and recycling rate.

The computer simulation model presented in this dissertation is developed based on advanced mathematical matrix operations and manipulation. The model simulates the size reduction and material

liberation during the shredding process for end of life electronic products. The following steps are essential to build the simulation model for shredder:

1. Model the EOL products as minerals.
2. Model the comminution and liberation evolution in the shredding process.
3. Calculate the size distribution and liberation distribution after shredding.

The following figure shows a typical shredding block diagram, with a telephone as the end of life product to be recycled:

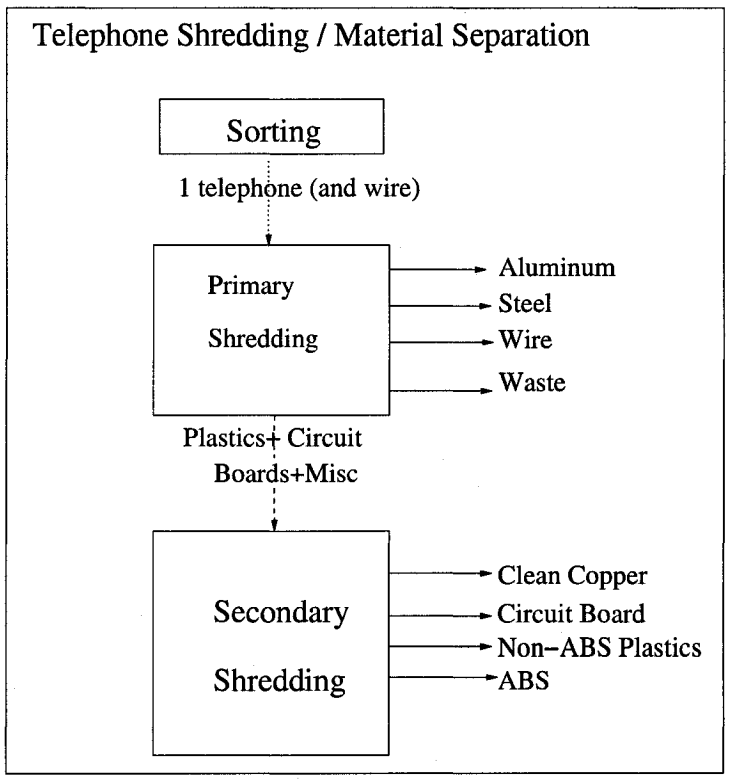

Figure 1: Typical shredding block

SUMMARY (Continued)

Based on the simulation of the transition of size distribution and liberation distribution of end of life electronic products during the shredding process, we can investigate the interrelationship between product design and its recycling rate at its life cycle closure.

To evaluate the validity of the computer model, an image-analysis based procedure is proposed which measures the size distribution and liberation distribution data and uses those data to construct size distribution and liberation distribution matrices for inputs to and outputs from the shredder. The image analysis procedure and the accompanying algorithm to transform the collected 2-D data to 3-D data can be used to evaluate the computer simulation model.

The computer model assumes that all materials constituting end of life electronic products defined in the shredder model break according to the same shredding transformation matrix. This is obviously a simplification since various materials will break differently due to their specific mechanical properties, joint methods, designs, and complexities. How to take those differences in the shredder simulation model into consideration is a subject of future work.

TABLE OF CONTENTS

CHAPTER PAGE

LIST OF FIGURES

LIST OF TABLES

LIST OF ABBREVIATIONS

ELV	End of Life Vehicle
CFC	Chlorofluorocarbon
EOL	End of Life
FEM	Finite Element Method
STMS	Size Transformation Matrix of Shredder
LMM	Liberation Matrix of Minerals
DE	Dispersion Entropy
CMM	Composition Matrix of Minerals
SM	Survival Matrix
UIC	University of Illinois at Chicago

CHAPTER 1

RECYCLING OF END OF LIFE ELECTRONIC PRODUCTS

This chapter introduces the recycling of end of life (EOL) electronic products. First, a literature survey and background investigation about recycling of modern electronic "minerals" are briefly presented. The significance and motivation for the recycling project are then introduced. The related recycling processing and simulation techniques which are essential for developing the shredder simulation model are summarised.

Traditional mineral processing technologies are rich resources to adapt to the recycling of modern end of life electronic products. Still, attention should be paid to the differences between the two fields. The adaption of mineral processing techniques to the area of electronic products recycling is implemented here with appropriate care.

What makes end of life electronic products distinct is the complexity of modern electronic products and their fast development and changes in manufacturing technologies. Taking into consideration environmental impacts, economic advantages, and legal requirements, the life cycle management of modern electronic products is an urgent task.

The physical structure of the recycling system is also briefly discussed in this chapter. The function of each processing station that is part of the recycling system is discussed sufficiently to present a whole picture of the overall system.

1.1 Motivation

In 2005, some estimate that 130,000 computers were discarded in a single day. Along with computers, TVs, VCRs, cell phones, and monitors – an estimated 304 million electronics – were removed from

US households in 2005 according to the Consumer Electronics Association's 2005 Market Research Report [Consumer Electronics Association 2005]. To protect the environment, these must be processed and recycled rather than discarded at their life cycle closure. Legislative regulations also require that a certain material ratio of those products must be recyclable before they can enter the market. Finally, a carefully developed optimised recycling procedure for these end of life electronic products offers economic benefits. Advancements in information systems have given rise to a new trend to identify and recycle value from end of life electronic products. The growth of worldwide legislative requirements for recycling and miniaturisation of components in consumer electronic products are likely to make recycling by hand disassembly infeasible in the near future. An approach based on the shredding of return end of life electronic products, followed by separation into component materials, is more appropriate to handle large quantities of material. The economic efficiency of such a recycling system depends on the efficiencies of the shredding and separation processes. A computer model of the shredder that is sensitive to changes in design of the end of life electronic products recycled will be greatly helpful to optimise the recycling system. These factors are all motivations to research the methodology for shredding which is an important portion of the whole recycling system of end of life electronic products.

Traditional mineral processing and simulation technologies have been adapted to apply to the field of recycling modern products for years [van Schaik, Reuter & Heiskanen 2004]. Nevertheless, there is a basic difference between the two fields: the design of modern products combines and connects various materials in many complex different ways, making a complex "mineralogy" of the products and their components which changes rapidly and continuously over time [van Schaik, Reuter & Heiskanen 2004]. On the other hand, the mineralogy of traditional ores and minerals originating from mines, from which the composition is well known, does not vary drastically within a particular mine site or

even between mine sites. The traditional mineral processing methods need to be modified and updated if they are to be used to research the recycling of modern end of life electronic product because of those differences in characteristic properties between traditional primary ores and modern end of life electronic products "minerals". What should be emphasised here is that because the modern "minerals" are so complex, so diverse and changing so rapidly, the fundamental descriptions of their "mineral" properties are incomplete and thus make the calibration of fundamental models extremely difficult.

With new technology leading to new and better electronic products come new challenges associated with the life cycle management of these products. What is to be done with the obsolete products? The industry practice is to extract useful materials from the end of life electronic products instead of disposal directly to the environment. Reclamation and recycling products produce certain benefits such as decreased solid waste, but these processes also result in adverse environmental impacts such as energy and water consumption, air emissions, and waste generation. A computer simulation of the recycling system is helpful to optimise the procedure to recycle end of life electronic products and thus get the maximum economic benefits from recycling these products while fulfilling legislative requirements and assuring minimum environmental impacts.

1.2 Literature survey

Social demand for end of life electronic products recycling and waste management is stronger than ever in history [Kotera & Sato 1997]. Large streams of waste create the potential for environmental pollution in areas adjoining the limited space remaining in landfill sites. The development of landfill sites also comsumes large amounts of energy.

The laws in developed countries promote the use of recycled resources of end of life electronic products, such as televisions, refrigerators, air-conditioners and washing machines. Figure 2 lists the

compositions of these major appliances. Air-conditioners and refrigerators contain large amounts of pure steel, copper and aluminum, and televisions contain mostly high-quality glass by weight. Recycling recovers these resources, saves energy that would otherwise be spent on processing raw materials, and helps conserve supplies of rare earth materials and scare metals. Recycling is also preferable over disposal because old appliances often contain lead, CFC's and other substances that have a negative impact on the environment.

Electronic products are manufactured using a wide spectrum of different raw materials. At their life's end those products return as complex multi-component materials that can not directly be converted into products once more. The manufacturing of electronic products should be carried out in an energy efficient and environmentally friendly way. These products and their use or operations should also contribute to the overall sustainability. Figure 3 shows the spectrum of activities that can be performed in a sustainable manner.

Society asks that as much as possible end of life electronic products find their way back into the industrial and comsumer cycle while minimising both energy input and the impact to the environment and at the same time maximising the economic advantage. The blue circle (perpendicular) in Figure 3 that maintains the golden (plane) and grey (horizontal) circles illustrates this idea. It is impossible to fulfill this requirement without combining knowledge and technology from the simplest separation and sorting technology to the most complex metallurgical reactor optimisation via fundamental studies on flow and kinetics in pyrometallurgical reactors, process layout, and product design. Innovative designs and production methods must be developed. The optimisation of the material cycle in a world in which products change rapidly is only possible if the interactions between all technological aspects of creating, using, discarding, and recycling products are considered in relationship to fundamental studies including

Product	Refrigerator*1		Television*2	
Substances used	Weight (kg)	% of product weight	Weight (kg)	% of product weight
Steel	28.50	49.78	3.93	10.70
Copper	2.32	4.05	1.06	2.88
Aluminum	0.54	0.94	0.16	0.44
Phosphor bronze	—	—	0.09	0.24
Stainless steel	—	—	0.01	0.03
Ferrite	—	—	0.39	1.06
Polyurethane foam	6.36	11.11	—	—
Rubber	0.77	1.34	—	—
Other plastics	17.48	30.53	8.15	22.19
Paper	0.10	0.17	0.10	0.27
Glass	0.04	0.07	18.18	49.48
CFCs and refrigerant oil	0.30	0.52	—	—
PCBs*3	0.16	0.28	1.95	5.31
Condenser*3	0.03	0.05	—	—
Electron gun*3	—	—	0.06	0.16
Transformers*3	—	—	0.93	2.53
Loss during disassembly	0.65	1.14	1.73	4.71
Total	57.25	100.00	36.74	100.00

Note 1: A company's 320-liter 1987 model
Note 2: B company's 25-inch 1989 model
Note 3: Not reduced to raw materials

Figure 2: Materials composition of refrigerators and television. [Kotera & Sato 1997]

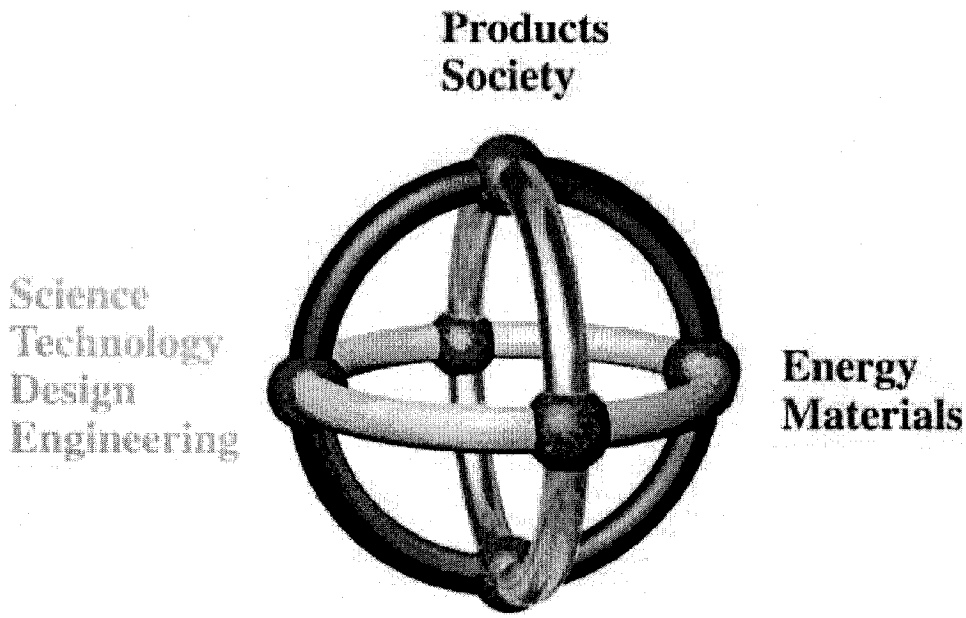

Figure 3: Sustainability represented as the interaction between society, products, materials, science and engineering. [Reuter & van Schaik 2004]

environmental control and policy. It is therefore imperative to achieve sustainability change at various system levels, from global material cycles down to plant and process equipment design and operation. The grey plane (horizontal) in Figure 3 represents all technological disciplines involved to achieve this. In the golden circle these will be dealing with complex, large-scale systems, where company/plant/sector boundaries are crossed. Therefore the process of changes will involve and affect a great variety of stakeholders represented in the blue circle.

One of the major purpose of shredding the end of life electronic products is to increase the liberation of shredded products. To fulfill this goal the particles need to be broken as fine as possible, however by decreasing particle size, energy costs substantially increase, and it becomes more difficult to separate

particles. The particle's properties (see Figure 4), especially the size and chemical composition, play a critical role in the shredding model.

Gay [2004] proposed a schematic procedure to model the particle composition distribution and its change due to breakage as shown in (Figure 5). Single-sized multiphase parent particles (there are three minerals) and a set of one size-class of the product particles (also called progeny) are illustrated in this figure. The problem is to estimate the probability distribution that each particular parent formed each particular progeny particle. The core idea of Gay's model is to treat the process as two main processes, *comminution* and *separation*. The relationship between the feed and product particles can be estimated using a probability method, with the probability defined as the probability that a feed particle of particular composition and size will form a product particle of a particular size and composition. The method is based on maximising the entropy of the probability subject to mass and composition constraints. Not only does this method allow a liberation model to be developed for binary particles, but also particles consisting of many minerals.

Wei & Gay [1999] proposed an approach to model liberation for comminution. The liberation distribution is characterised by a dispersion rate function, which is related to the texture of the ore. Once this function is determined, the dispersion model predicts the liberation of the mill product when the feed or operating conditions change. That model was validated using computer simulation and the dolomite-sphalerite data made available by Schneider [1995]. The results show that the dispersion model is capable of describing and predicting the liberation of particles as size changes when breakage is non-preferential.

The recycling system for end of life electronic products consists of a complex network of inter-connected processes, each with its own recoveries, products, residues, etc., and material and energy

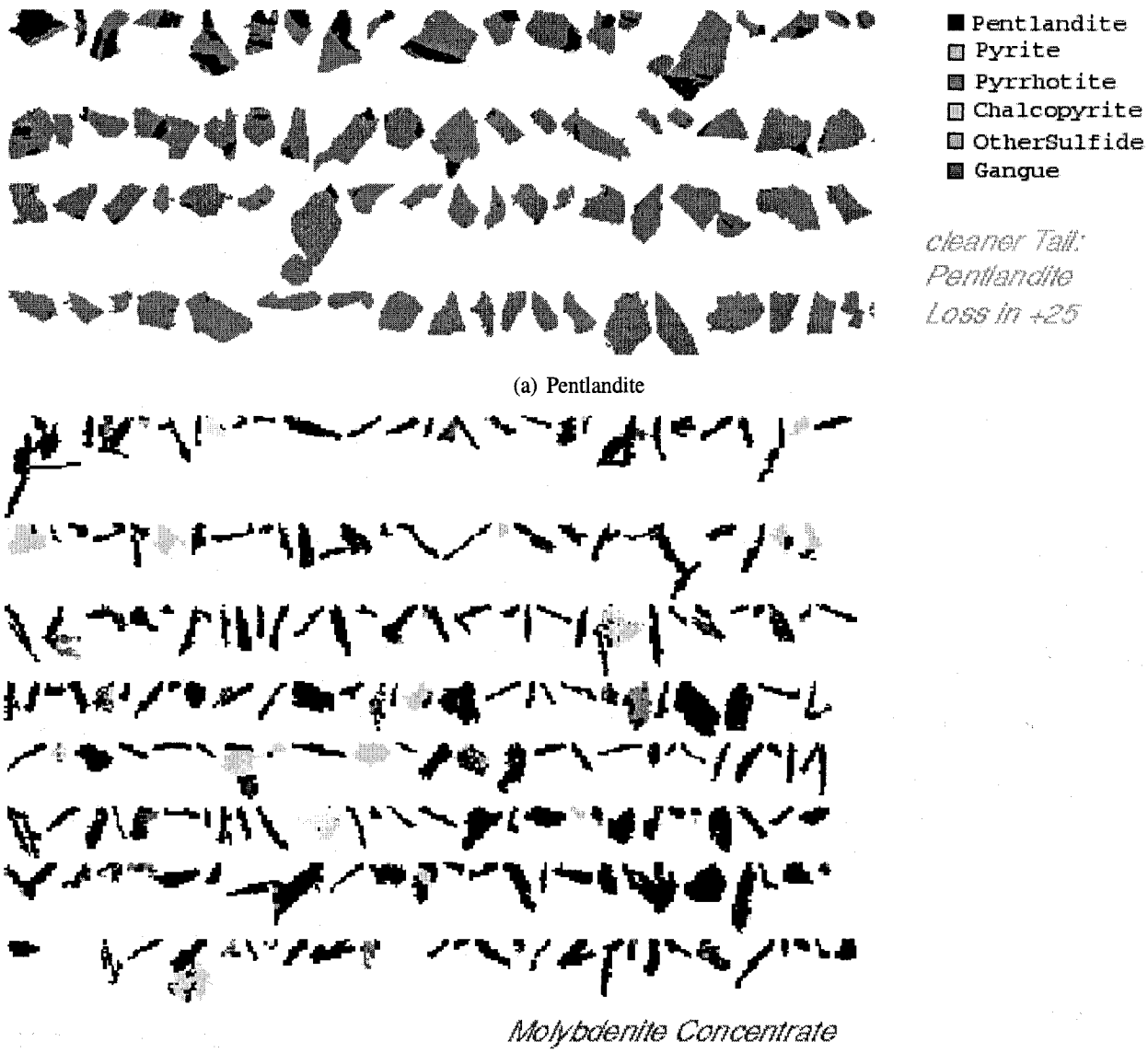

(a) Pentlandite

(b) Molybdenite Concentrate

Figure 4: Figures of particles. (http://www.sgs.com)

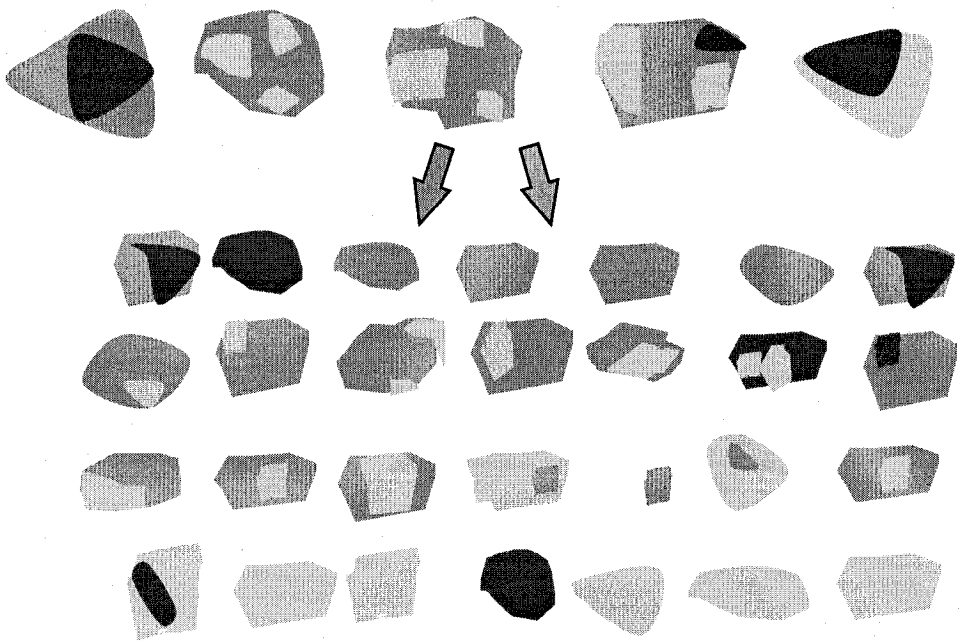

Figure 5: Single-sized parent particles and one size-class of the progeny particles.

streams. In order to define the recycling rate as a dynamic function of distributed parameters determining the recovery rate for each of the materials, the recycling process must be fully understood. This is only possible if recycling systems are defined more fundamentally than is the case at present. This requires sound technological knowledge about the behaviour of material and processes within the recycling flow sheet, also in relation to the changing design of the products and their distributed properties. This will assist in ensuring a sustainable development of our society, in which products have to comply with recycling targets.

The continuously changing design of products and the application of new material combinations raise questions about the influence of product design, materials applied, and their mutual interactions on the recyclability of products. It is known from the interrelation between recovery and grade of physical

separation methods for scrap that it is impossible to obtain simultaneously a high recovery and a high grade for a certain material stream. Increasing the recovery of a certain material will simutaneously lead to an increased amount of unwanted elements in the recovered stream, since separation processes are not perfectly selective. The combination of materials and in particular the way they are connected in product design will affect the degree of liberation, the composition of the material streams after shredding, the amount as well as the composition of the non-liberated particles, and the quality of the material streams after mechanical separation which will be the feed for metallurgical processing. The development of products that bring togther metals that are not linked in the natural resource systems (see Figure 6) has increased the complexity of recycling pyrometallurgy. As a consequence, many of these materials are not completely compatible with current processes in the metals production network, which were developed for the processing of primary natural resources, optimised for the processing not only for the primary metal but also for all mineralogically associated minor valuable and harmful elements. The formation of complex residue streams or undesired harmful emissions therefore inhibits the processing and recovery of products at their end of life phase. Mineralogy and liberation will affect the possibilities of material recovery and the recycling rate of product. Product designers, physical liberation and separation plants, waste processors and metal producers must cooperate to realise optimal metal/material recovery in designing and recycling comsumer electronic products. This ensures that each created stream has a destination.

To simplify programming, image analyzers commonly measure either intercepts or the areas of particles and grains to determine liberation based on polished section amounts. The concentration of minerals by flotation is based on reagents that interact with the exposed surfaces of minerals. Thus, it is often perceived that image analyzers should measure the perimeter of the mineral of interest in

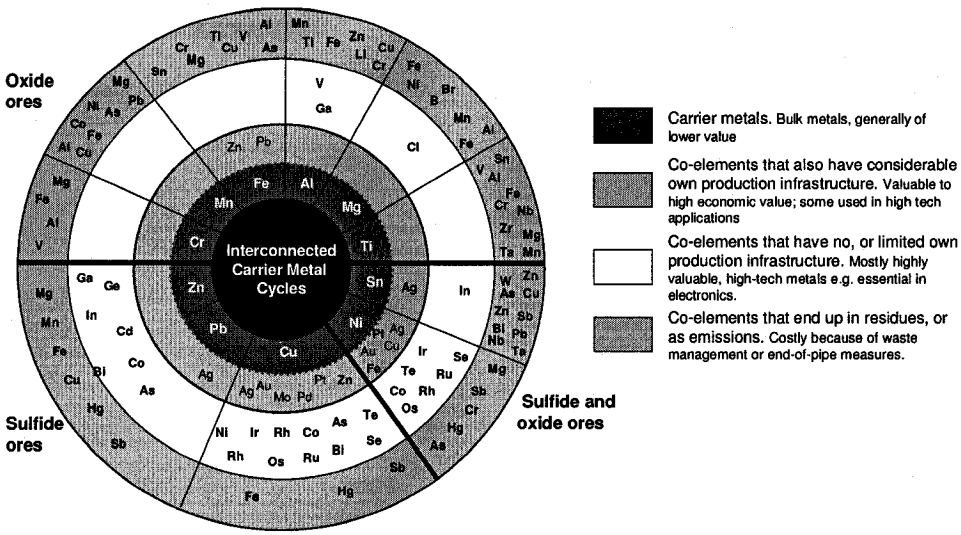

Figure 6: Linkage of metals as found in natural resources-map to sustainable recycling of metals (legend top to bottom equivalent to rings from the inside to the outside) [Reuter & van Schaik 2004]

the ore particles. A comparative liberation study of thirteen samples collected from a flotation plant processing a complex base metal sulfide ore showed that the liberation of the ore materials determined by area measurement is very similar to the liberation determined by the exposed perimeters [Lastra 2002]. The liberation determined by exposed perimeters is more appropriate only for those cases where the mineral texture is so complex that it is retained in the small particles generated in conventional grinding operations. These experiences "should be" taken into consideration in the design of the experimental procedure to evaluate the simulation model for shredding of end of life electronic products.

CHAPTER 2

FUNDAMENTALS OF SHREDDERS

In this chapter we discuss fundamentals of shredders, important equipment for the recycling system of end of life electronic products. We begin with definitions to give a better understanding of the concept of shredder and shredding operation. We then discuss and illustrate pictorially the different types of shredders. After that we focus on one specific shredder type, the swing-hammer type shredder, to expand the discussion of the fundamental structure of shredders, basic operation principles, and characteristics of shredding. The relationship between the characteristics of particles after shredding and the characteristics of the physical structure of shredder and operation parameters are also discussed to sufficient degree to explain the fundamentals of shredders.

2.1 Definitions

A *shredder* is a size reduction machine that tears objects into small pieces [Web 2006*h*]. Shredders are used in end of life electronic products recycling systems to obtain a fragment size distribution suitable for the subsequent processing steps, to increase the bulk density and liberate the valuable components of composites and assemblies. Materials size reduction and liberation inside a shredder experience complex stressing modes, such as tension, bending, torsion, shear, and impact.

Comminution is one of the four main types of mechanical processing and describes the movement of the particle size distribution (grains, drops, bubbles) into a range of finer particle sizes [Web 2006*e*]. The three other types are agglomeration, separation and mixing. Examples of comminution from daily life are cutting, crushing, grinding and rasping to reduce the size of different foods. Industrial applications include the extraction of raw materials in mineral processing, production of cement in the chemical and

ceramic industries, and processing of food. In this dissertation comminution is treated as a synonym for shredding.

Compaction is the process by which a material is packed more closely together [Web 2006*f*]. Compaction is often used to reduce the size of waste material. Garbage compactors and garbage trucks squeeze garbage so that more of it can be stored in the same space. It is compacted again, more thoroughly, at the landfill to preserve valuable space. In this dissertation, compaction refers to a the process that produces a more closely packed state of the shredded particles.

Minerals here refer to the valuable components to be recycled from the end of life electronics. Minerals can be simple substances, compounds, or alloys. The recoverable value of a material (or component) in such an end of life consumer electronic device is influenced by many factors including technology for manufacturing, secondary materials avaiability, and environmental considerations, which may favor recovery over disposal.

Feed in this dissertation refers to the input materials to the shredder.

2.2 Types of shredders

There are many different types of shredders used in industry today for different kind of applications; Figure 7 shows some shredder types. Figure 7a and Figure 7b are products of the Shred-Tech company. Figure 7a shows a four shaft shredder designed to process bulk materials including wood, plastics, paper, tires, textiles, electronic equipments and manufactured products to a uniform particle size in a single pass. Figure 7b shows a metal granulator whose interchangeable screen sizes allow for maximum flexibility when determining desired particle size. Models range from 40 hp (30 kw) up to 200 hp (150 kw) and are available in a wide variety of cutting chamber sizes to meet the demands of various materials in all possible shapes, sizes and material loading methods. Figure 7c shows a shear

shredder made by Shredding Systems, Inc. which is used for wood, paper, hard plastics, and other brittle materials with limited metal contamination, where small, uniform particle size is important. Figure 7d shows a low speed, high torque dual shaft shredder from Gensco Equipment, Inc. Figure 7e shows the Delumper® Twin-LP from Franklin Miller, Inc., a crusher which processes massive quantities of lumps or agglomerates with a powerful crushing action.

2.3 Shredder structure

Among the many types of shredders, the swing-hammer shredder is a good example to illustrate the basic inner structure. This swing-hammer shredder is typically utilised for comminution of automobile scrap, other types of light steel scrap, electronic appliances, lead-acid accumulators, non-ferrous metals and metal chips.

The input material is fed from one side, and the mass flow is controlled by the power consumption of the shredder. Any material that is sufficiently small after shredding is discharged from the shredding chamber of shredding by means of grates. The configuration of the discharge grates most common for the light comminution of light steel is shown in Figure 8a (model Lindmann/Newell). One grate is usually placed above the rotor and in some cases a second one below it. The vertical discharge grate is accompanied by a modified design of the upper part of the housing, which must be narrower (Figure 8b, model Thyssen HRT). This design decreases the specific energy consumption for the process. Figure 8c shows the Kondirator, by which is characterised by a reverse rotor, in which the feed is carried into the space above the rotor first. Items which are unshreddable can be discharged by means of the swivelling grate (4) before the material is transported into the narrow gap underneath the rotor. This kind of shredder is well suited for the size reduction of light steel scrap containing small portions of scrap from demolished steel constructions.

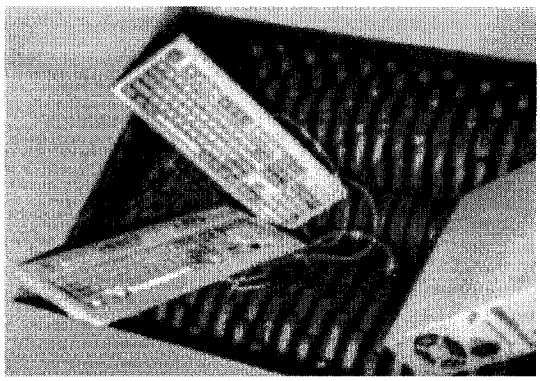

(a) Quad Shaft Shredders (http://www.shred-tech.com)

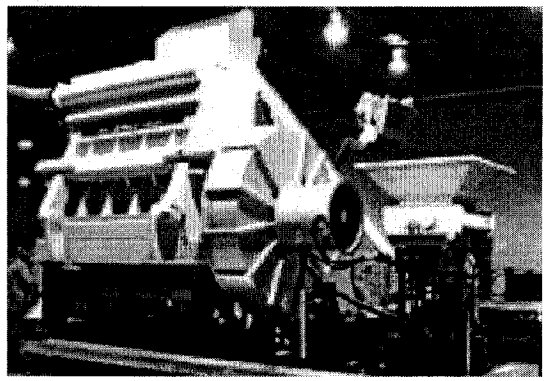

(b) STG Metals Granulator (http://www.shred-tech.com)

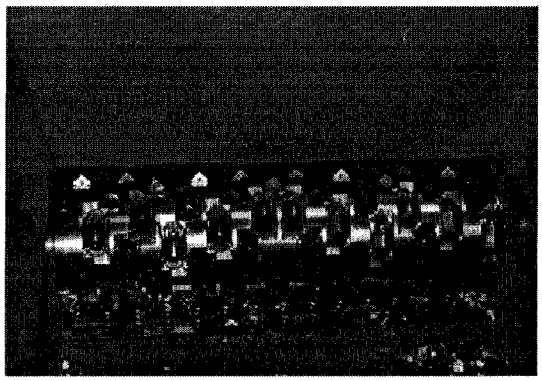

(c) SR-300 Unil-Shear Shredder(http://www.ssiworld.com)

(d) Slow speed, high torque shredder(http://www.genscoequip.com)

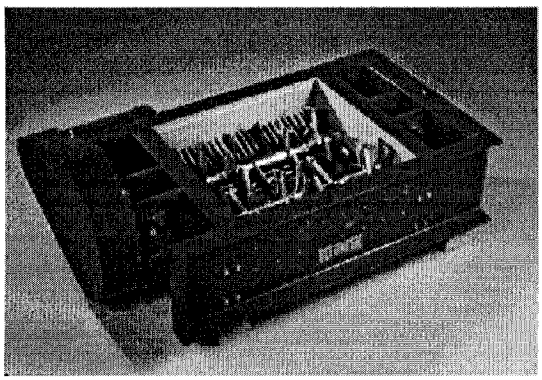

(e) DELUMPER Model 2830LP Twin-LP Crusher(http://www.franklinmiller.com)

Figure 7: Shredders of different types

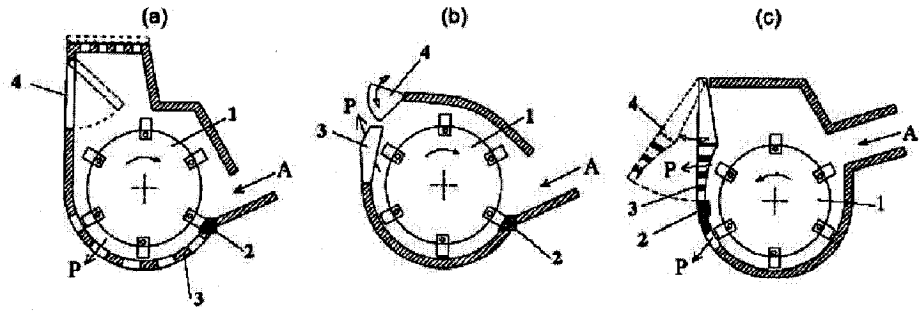

Figure 8: Swing-hammer shredders for the comminution of automobile scrap and other types of light steel scrap. (a) model Lindmann/Newell; (b) model Thyssen HRT; (C) model Kondirator
(1) rotor and impacting tools (swing-hammers); (2) anvil; (3) discharge grate; (4) device for discharging unshreddable items; (A) feed; (P) product. [Sander 2004]

2.4 Comminution in shredders of the swing-hammer type

Sander [2004] investigated the processes that take place inside the swing-hammer shredder. Its important components are a small-scale horizontal shaft shredder, a modified Izod pendulum and an impact apparatus (refer to Figure 9). In order to make sure that the process of shredding can be examined separately from the kinetics of classifying taking place simultaneously, the discharge grates (5) in Figure 9 located above and underneath the rotor of the small scale horizontal shaft shredder are replaced by steel plates. The lower part of the housing is designed to act as a flap (3) in Figure 9. After a predetermined period of time, the material can quickly be discharged from the chamber of comminution by lowering this flap. The mechanical power can be drawn as a function of shredding time with the help of a torque measurement shaft. The area enclosed by such a power-versus-time plot is equal to the energy consumption. An example of this kind of power-time plot is given in Figure 11a.

As a result of the intensive deformation of the material, the characterisation of the products of the shredding has proven to be difficult. The distributions and median values of fragment size and fragment

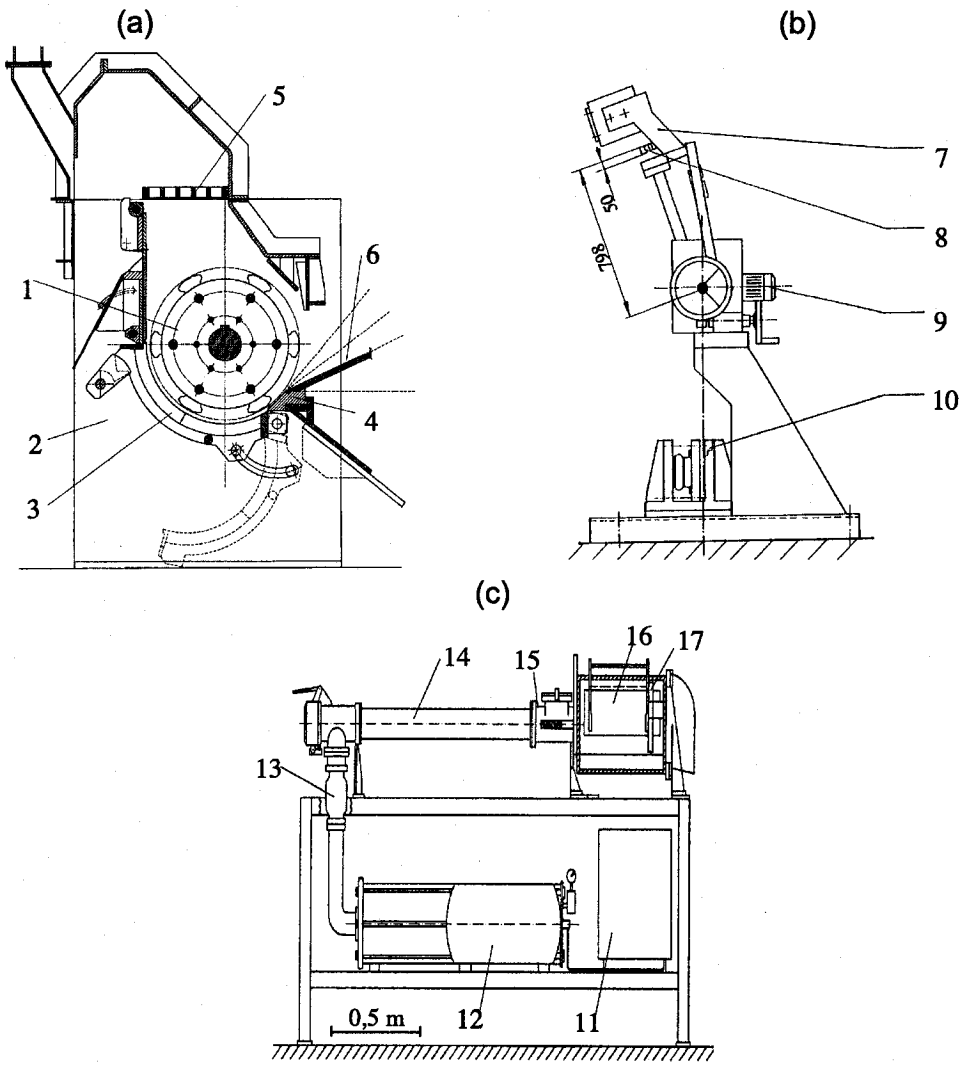

Figure 9: Small-scaled shredder (a), modified Izod pendulum (b), and impact apparatus (c).
(1) Rotor with impacting tools (swing-hammers); (2) upper part of housing; (3) lower part of housing (flap, discharge in the case of batch tests); (4) anvil; (5) discharge grate (closed in the case of batch tests); (6) feed chute; (7) weights of impacting tool (50kg); (8) impacting tool with strain gages; (9) lifting and breaking device for the impacting tool; (10) anvil construction ;(11) compressor; (12) compressed air tank; (13) magnetic valve; (14) acceleration tube; (15) chock block; (16) impact chamber with velocity measurement (light barrier); (17)baffle plate (deflection 0...37°)

mass were used to characterise the results of comminution. The fragments can be described in three main dimensions: a, b and c, where $a \geq b \geq c$ (see Figure 10a). The dimension b was modified to characterise the fragment size. It is estimated by the dimension of b_{ell} of the best fitting ellipse of equal area of projection (refer to Figure 10b).

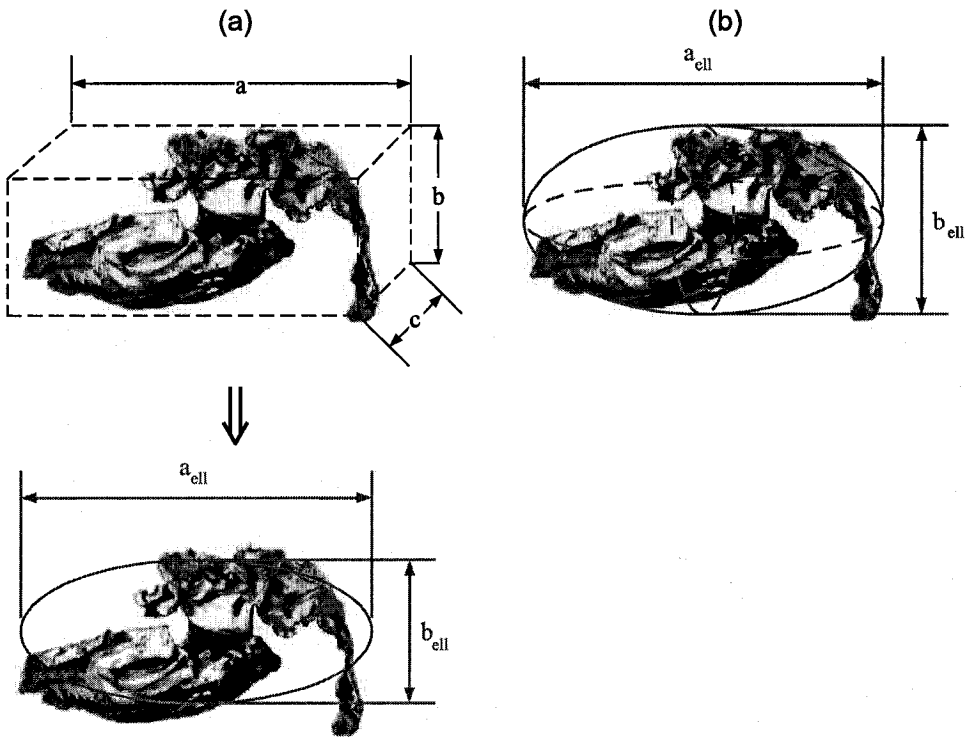

Figure 10: Measurement of the main dimensions a and b of a fragment by the determination of the best fitting ellipse of equal area (a) and estimation of the fragment volume by the calculation of the ellipsoid of rotation having the dimensions a_{ell} and b_{ell} (b). [Sander 2004]

The increase in surface area can be determined by bending open the fragments and measuring the lengths of fractures and cracks. The degree of bending B and the degree of compaction K are determined in order to characterise the deformation of the fragments. B can be calculated according to:

$$B = \frac{A_{äq} - A_{Pr}}{A_{äq} - A_K} \tag{2.1}$$

A_{Pr} and A_K represent the projection areas of the fragment and of the sphere of equal mass therein respectively. The equivalent fragment $A_{äq}$ area can be obtained using the following formula:

$$A_{äq} = \frac{m}{\rho_M d} \tag{2.2}$$

in which m, ρ_M and d are the fragment mass, the material density and the wall thickness of the test body. The compaction degree is calculated according to the following formula:

$$K = \frac{6m}{\rho_M \pi a_{ell} b_{ell}^2} \tag{2.3}$$

Here m represents the fragment mass, a_{ell} and b_{ell} are the dimensions of the best fitting ellipsoid of rotation of equal area of projection (Figure 10b) and ρ_M is the material density [Kirchner 2000].

Four stages of the comminution process in the shredder are identified by Kirchner [2000] based on the systematic investigations utilising test bodies of sheet metal. These stages are now described in turn.

2.4.1 Stage I

The first stage of shredding comprises the tearing off a single fragment from the feed material as a result of the combined action of tensile stress, bending and torsion. This occurs in the space close to the feed chute which includes the anvil. The possible comminution process taking place there was examined by means of the modified Izod pendulum. It is clear that breakage can occur only if the specific section modulus $W_{B,bez}$, which can be calculated for the geometry under investigation using

$$W_{B,bez} = \frac{W_B}{w} = \frac{bd^2}{6w} \tag{2.4}$$

exceeds its critical value. W_B is the section modulus of the test body, b and d represent the width and wall thickness of the test body, respectively, and w is the clearance between the impacting tool and the anvil. At values lower than the critical one, the test body is only bent. If the clearances are relatively wide as is the case with industrial shredders, a high section modulus would be necessary in order to initiate breakage during the first stage. From investigations using the small scale horizontal shaft shredder, it can be derived that the first stage of shredding can occur under certain conditions only [Sander 2004]. The feed has to be voluminous and has to contain openings. If it is clamped by the feeding device, the impacting tools can act into the material and tear off fragments.

2.4.2 Stage II

Generally, the second stage of the shredding is characterised by an intense deformation (bending to compaction) of the comparatively large platy fragments, which leads to the formation of flaws. The combined action of the tensile stress, bending and torsion makes the flaws propagate until breakage. This can be verified using the batch test material at varying shredding times and, therefore, at varying specific energy consumptions. In the beginning of the stressing, the fragment size b_{50} (median particle

size, meaning 50% of the particles are greater and 50% of the particles are smaller) decreases whereas the fragment mass m_{50} (median particle mass, meaning 50% particles are heavier and 50% particles are lighter) is hardly changed. At the same time, the degree of bending increases rapidly. This is because of the intense deformation of the material which is not accompanied by comminution at first. As the formation of breakage sets in, the fragment mass starts to drop while the degree of bending remains almost the same. The increase in compaction is not a consequence of the deformation process but is caused by the reduction of the fragment size and fragment mass. The required energy for the deformation and subsequent comminution can only be provided if there is a high relative velocity between the impacting tools and the shredded material. The narrow gap inside the lower part of the housing plays a decisive role. The material is decelerated by the frequent contacts with the wall of the housing. The walls can also act as an abutment for short periods of time. This enables the intense bending to compaction of the fragments and is a precondition for the formation of the effective tensile stress in combination with bending and torsion required for the actual comminution.

The amount of energy required for the deformation preceding the comminution depends on the circumferential velocity v (see Figure 11). The specific energy consumption increases with v (Figure 11a), yielding finer products. But if we regard the median fragment mass m_{50} as a function of the specific energy consumption, it becomes obvious that the comminution at higher circumferential velocity requires less energy. Figure 12 shows the effect of deformation on the process of comminution. In the case of test bodies without preliminary stress, a high amount of energy is required for deformation. Thus, the specific energy consumption per unit increase in surface is very high at the beginning. As the comminution proceeds, it levels off at a constant value of $W_A = 6\mathrm{J/mm}^2$. The comminution of test bodies which

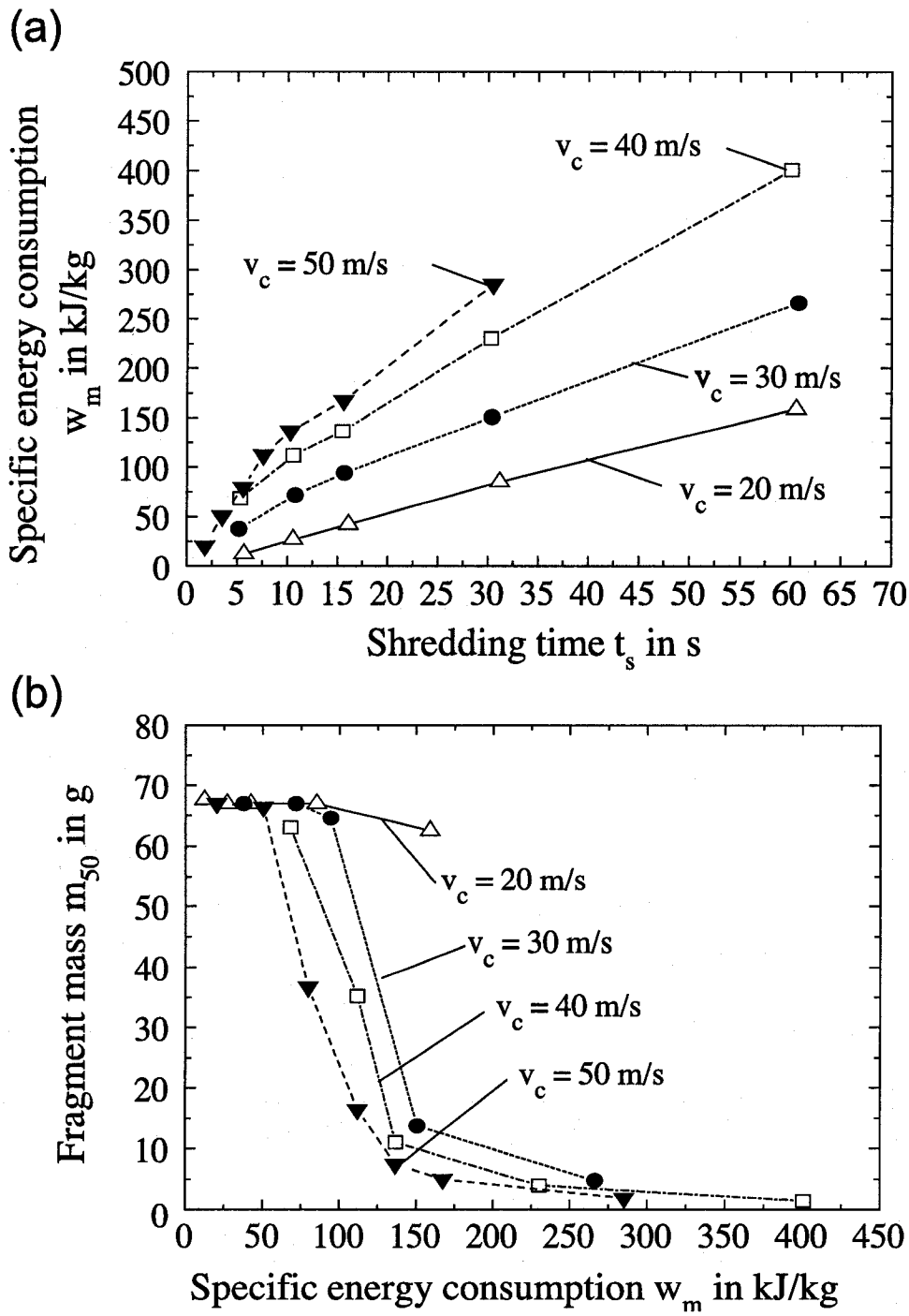

Figure 11: Specific energy consumption vs. shredding time (a) and fragment mass vs. specific energy consumption (b) (Zinc: comminution in small scale horizontal shaft shredder; test body size:$(100 \times 100 \times 100)\mathrm{mm}^3$). [Kirchner 2000]

had been pre-stressed several times prior to feeding consumes less specific energy per unit growth of surface area.

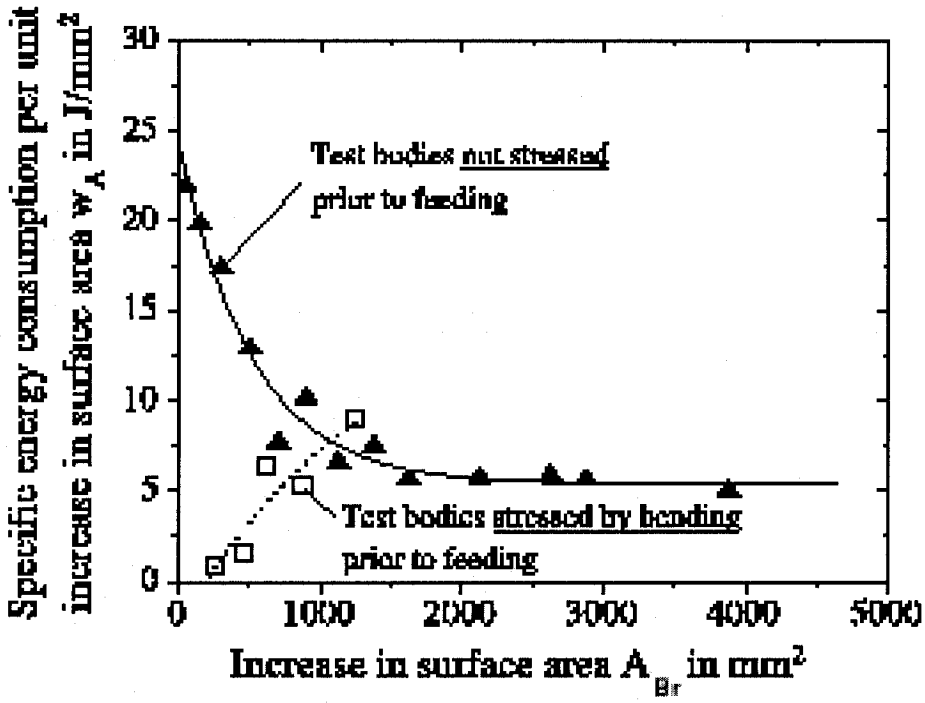

Figure 12: Specific energy consumption per unit increase in surface area vs. growth surface area (Zinc: comminution in small scale horizontal shaft shredder, circumferential velocity: 50 m/s; test body size: $(200 \times 200 \times 1)\text{mm}^3$). [Kirchner 2000]

2.4.3 Stage III

If the fragments are small enough that they can not form abutments inside the lower part of the housing, impacts against the walls of the housing become crucial for further comminution. These impacts cause a proceeding deformation (bending to compaction) of the fragments, which results in the forma-

tion of flaws. Tensile stress is also formed inside the fragments as a consequence of internal deadlock and of locally varying deformations. Gradual cracks extend until breakage takes place. The processes taking place inside the small-scale horizontal shaft shredder can be reproduced by means of the impact apparatus in Figure 9c. Using platy test bodies, Kirchner [2000] determined the specific energy required for breakage as a function of the material properties (Table I).

Material	Number of impacts		Specific energy consumption in kJ/kg	
	Mean value	Standard deviation	Mean value	Standard deviation
Zinc	64	7.8	76	8.7
St14	252	56.2	320	67.1
Aluminum	450	97.8	550	112.3

TABLE I

SPECIFIC ENERGY REQUIRED FOR BREAKAGE AS A FUNCTION OF THE MATERIAL OF THE TEST BODIES (EACH WITH FOUR TEST BODIES; TEST BODY SIZE: $(33\times33\times1)\text{MM}^3$; IMPACT VELOCITY: 50 M/S) [KIRCHNER 2000]

Figure 13 shows the breakage probability distributions of test bodies and fragments selected from products obtained using the small-scale horizontal shaft shredder as a function of the specific energy consumption [Kirchner 2000]. If the test bodies are platy, it can be seen that the value of w_m required in order to obtain an equal breakage probability decreases for heavier test bodies. Although still detectable, this effect is less evident if looking at the fragments, which had been taken from a product of a batch

test. Therefore, it can be assumed that the preliminary stress obtained during the preceding stages of comminution dominates the energy demand of the third stage.

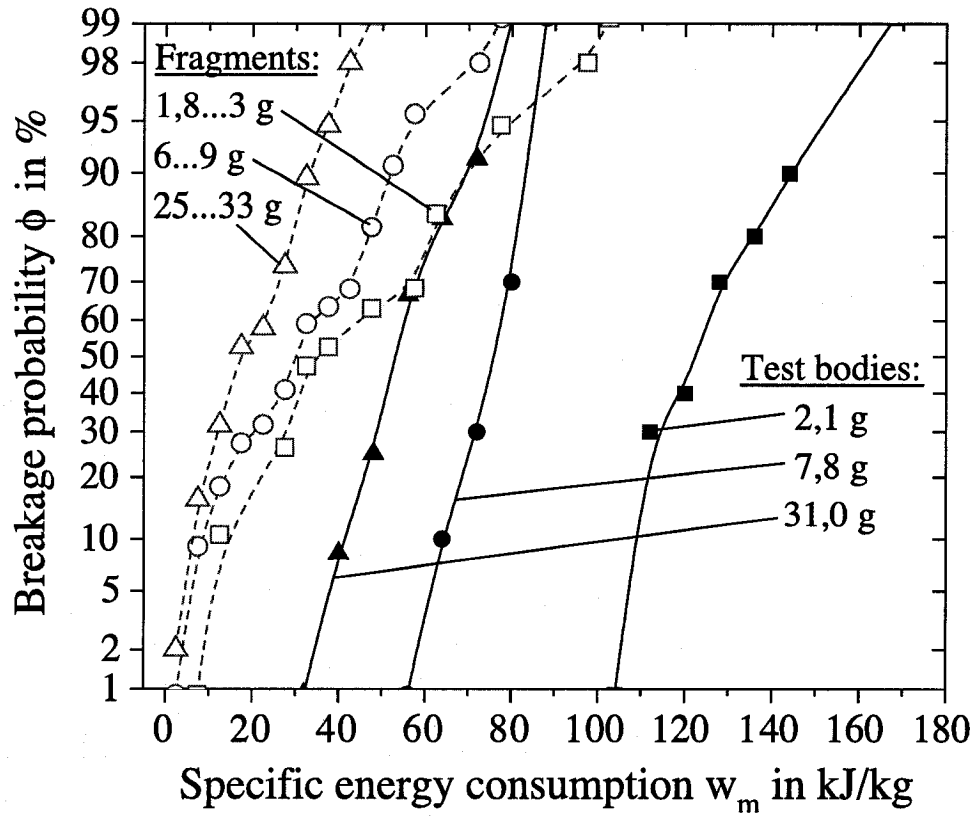

Figure 13: Breakage probability vs.specific energy consumption with mass of the test bodies and fragments's parameter (Zinc; comminution in impact apparatus; impact velocitiy: 50 m/s). [Kirchner 2000]

2.4.4 Stage IV

The 4th stage of comminution is the further intense compaction of fragments until they possess a spherical shape. Simultaneously, the formation of fine particles can be observed. The number of

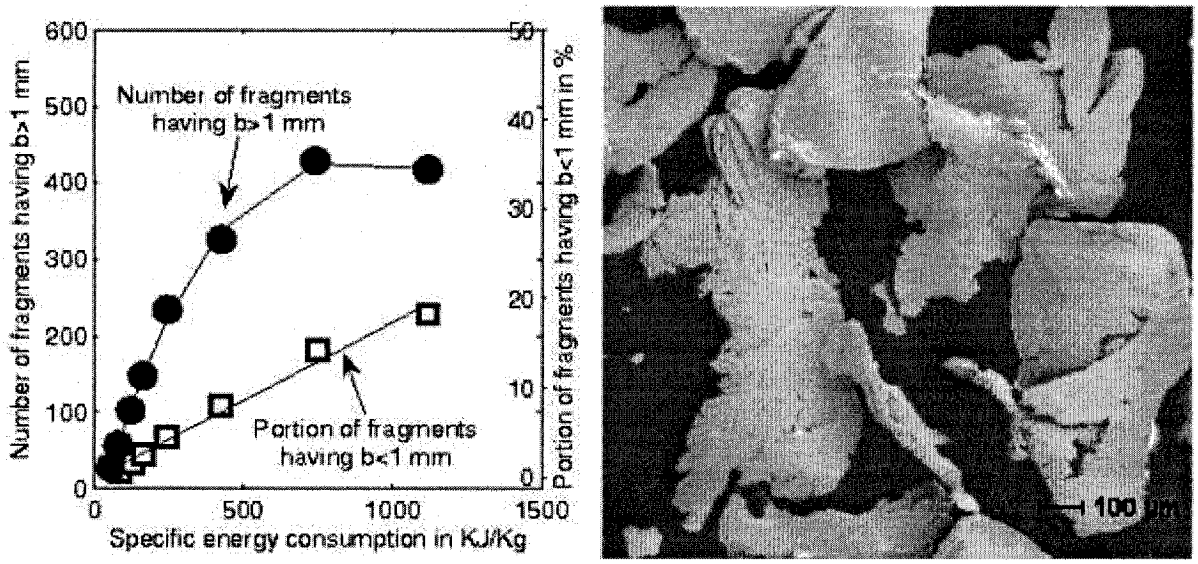

(a) (b)

Figure 14: Number of fragments having $b > 1$ mm and portion of fragments having $b < 1$ mm vs. specific energy consumption (a) and REM (Reflection Electron Microscopy) of fine particles resulting from abrasion (b) (Zinc; comminution in small scale horizontal shaft shredder; circumferential velocity; 50 m/s; test body size: $(200 \times 200 \times 1)\text{mm}^3$. [Kirchner 2000]

fragments with the size b greater than 1 mm levels off for higher shredding times, whereas the portion of fines with size b less than 1 mm increases permanently (Figure 14a). The formation of fine particles is the major shredding mechanism within this stage. This is because of the superficial wear of the stressed material by abrasion. The formed particles are subject to further intense deformation processes (see Figure 14b).

This chapter has provided an overview of the shredder, including its functions and types, and the material shredding process inside a swing-hammer shredder. We will now consider mathematical models of the shredding process.

CHAPTER 3

BASIC CONCEPTS FOR SHREDDER SIMULATION

This chapter covers basic terms, concepts and mathematics relevant to the design and analysis of shredding algorithms. It is intended to be a gentle introduction to the simulation of shredding, the terms introducted here will be used throughout this dissertation, and many of the fundamental ideas used in shredding analysis. Later parts of this dissertation will build upon this base.

3.1 Joints

The term *joints* refers to any material combination (those materials may be same or different) inside the end of life electronic products. They can take any material combinations with different geometries inside the end of life electronic products that will affect the liberation evolution of end of life electronic products in the shredding process. There are a large number of different joint types and geometries present in products. To approach this variability while limiting the complex of the problem, four distinct joint classes are defined here on the basis of the geometry and extent of contact between the two materials in the joint area.

3.1.1 Zero joint class (Z)

The zero joint class is the joint class corresponding to liberated particles. Particles belonging to this class consist of one material only.

3.1.2 P joint class (P)

Point, or P, joints are formed when a mechanical jointing element such as a rivet or bolt is used to connect components at a number of specific points (see Figure 15).

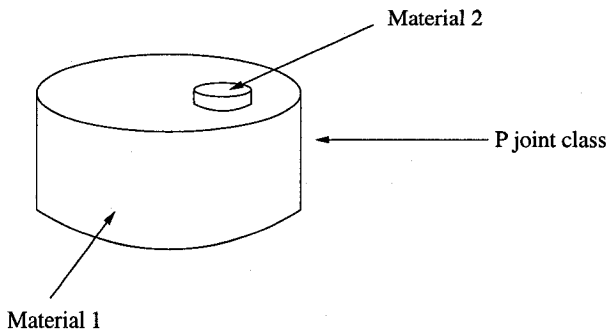

Figure 15: P joint class

3.1.3 L joint class (L)

L joints refer to line joints. In this class of joint, the two materials in the component are jointed along a continuous line (see Figure 16). Common examples are welds and adhesive joints.

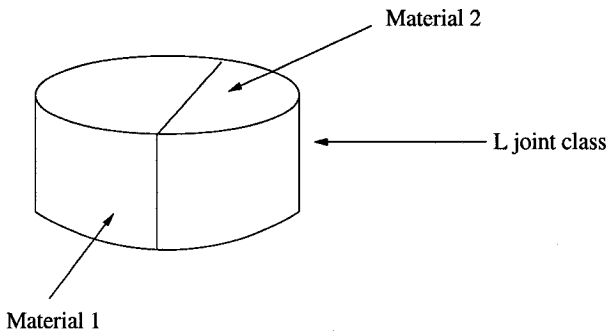

Figure 16: L joint class

3.1.4 S joint class (S)

S joints refer to the surface class. In surface joints, the entire surface of one material is joined to the other material (Figure 17). Examples of such joints are coated materials and laminate composite.

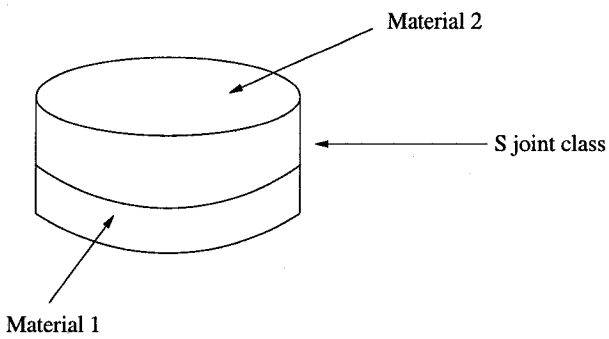

Figure 17: S joint class

3.2 Size transformation matrix

In the shredding process model, a *size transformation matrix* is used to describe the transition of the particle size distribution under shredding. An element of a size transformation matrix is denoted by the symbol Sf_i^{m,p_f,p_y}, in which p_f is the particle size class of the feed f and p_y is the particle size class of the output y. In the size transformation matrix $S = [S_i^{m,p_f,p_y}]$, the element S_i^{m,p_f,p_y} indicates the percentage of source size class p_f which will fall into destination size class p_y of mineral m after shredding. The index m gives the mineral, p_f is the source size class, p_y is the destination size class, and i is the index of the recycling station. The following transformation equation holds in the shredding process:

$$[S_i^{m,p_f,p_y}] \cdot [V_{in}] = [V_{out}] \tag{3.1}$$

where the $[V_{in}]$ is the size class distribution vector of the input to the shredder, and $[V_{out}]$ is the size class distribution vector of the output from the shredder.

Figure 18 illustrates a shredder transformation matrix. Size class 1 is the biggest class and size class N is the smallest class, with particle size decreasing as the index increases from 1 to N.

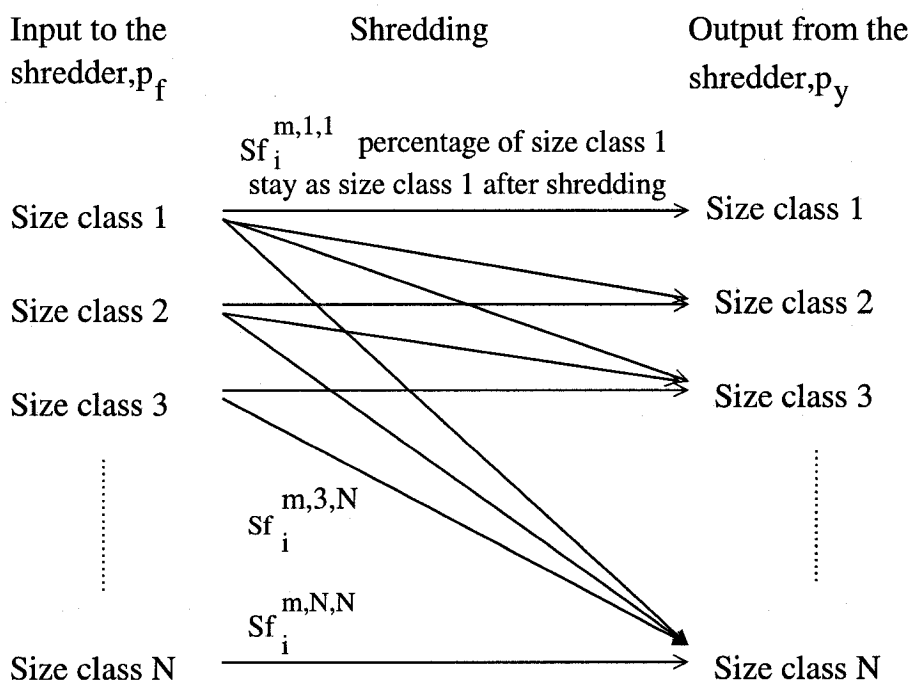

Figure 18: Size transformation matrix, for each input size class j, we assume that the output of that material in size class k will be described by a distribution given by the entries of the matrix S_i^{m,p_f,p_y}.

3.3 Liberation matrix of mineral

Liberation matrix is a matrix used to describe composition distribution of particles within different size classes. The rows of a liberation matrix denote the sizes of particles while its columns denote the

composition grade of particles. Recovery of components of minerals relies on methods that separate particles based on their physical or chemical properties. Individual components can be separated completely only if each particle contains only one component. Two components in the same particle can never be separated using physical separation methods alone. Separating minerals at the particulate level is referred to as liberation since the individual components are liberated from each other in a physical way. The element of liberation matrix can be denoted by the symbol $Lf_i^{m,p,l}$, where Lf indicates it is a liberation matrix entry, i is the processing station index, m signifies the mineral being processed, p is the particle size indicator and l is the liberation class indicator.

Figure 19 is an illustration of a liberation matrix. For mineral m, there are five size classes and five liberation classes (denoted Lc in Figure 19). Each element $Lf_i^{m,p,l}$ means for mineral m in the processing station i, percentage of size class p particles that will fall into liberation class l.

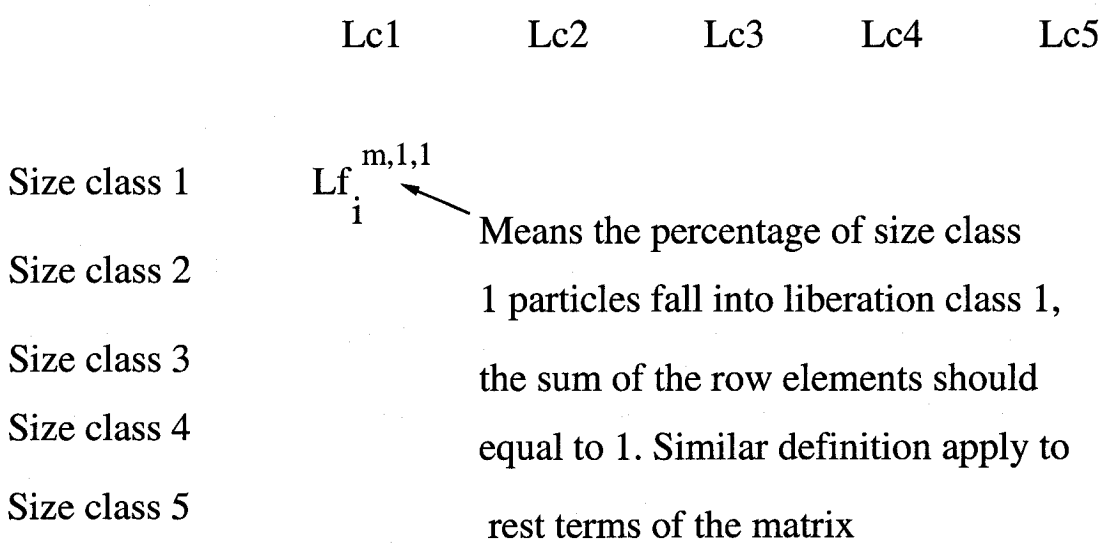

Figure 19: Liberation matrix

Sum of shadow fractions (from a) = This shadow fraction (from b)

(a) (b)

Figure 20: Liberation dispersion

3.4 Liberation dispersion

Liberation dispersion is proposed to take into account the effect on liberation of material dispersion in partcles. This effect is not considered by previous shredder model.

3.4.1 Concept of liberation dispersion

The liberation class tells only how much of a particular mineral is present in a given particle, and does not consider whether that mineral is contiguous. The concept of *liberation dispersion* is introduced here to distinguish how spread out the mineral is throughout a particle. The particles shown in Figure 20(a) and Figure 20(b) have the same shadow fraction ratio. In the shredding simulation model, we use this fraction ration to denote the liberation grade of a particle. The liberation class is the same for

(a) and (b), but the dispersion entropy is not, which will lead to different liberation results in shredding process. This effect is not considered in van Schaik, Reuter & Heiskanen's [2004] model.

3.4.2 Calculation of liberation dispersion

The calculation of liberation dispersion is split into two cases, microscopic and matrix-based.

3.4.3 Liberation dispersion at microscopic level

First of all, let us consider liberation dispersion within a specific particle. To measure the degree of the dispersion of the individual pieces to the local geometric center, the concept of the moment of those shadow pieces relative to the center is adopted to describe the dispersion phenomenon. The moment is calculated according the following formula:

$$I = \sum_{i=1}^{n} s_i \cdot r_i^2 \tag{3.2}$$

where s_i is individual area of each shadow piece and r_i is the distance from the piece to the local geometry center. At the particle level, we use I as measure of liberation dispersion of that particle. The larger I is, the more likely is the formation of a progeny particle with the same liberation grade during shredding process.

3.4.4 Liberation dispersion at matrix level

To incorporate the concept of liberation dispersion into the shredder model we must consider the liberation dispersion at the matrix level. Based on the individual particles' liberation dispersion data, we can fit those data into a matrix entry K_{ij}, where i is the size class of particles and j is the liberation class of particles. that $K_{ij} = f(i, j)$ is expected to fulfill the shredder model. Because of the lack of experiment data and it is enough for the purpose of illustrating simulation algorithm, the values

of elements of dispersion matrix $Dis_{i,j}$ are assumed where i and j are row index and column index respectively.

3.5 Composition matrix

The liberation matrix describes for each particle size class p in a specific mineral flow m a discrete distribution $Lf_i^{m,p}$ of material over the liberation class (i is the recycling station index). The *composition matrix* $C^{m,l,k}$ defines for each mineral m the fraction of chemical elements k of material present in liberation class l for different particle size classes p. Figure 21 gives an example of a composition matrix.

Mineral A	Al wrought	Al cast	Fe	Cu	Rest
Lib class 1	0.5	0.2	0.2	0.05	0.05
Lib class 2	0.65	0.15	0.15	0.03	0.02
Lib class 3	0.75	0.1	0.1	0.03	0.02
Lib class 4	0.87	0.05	0.05	0.02	0.01
Lib class 5	1	0	0	0	0

Figure 21: An example of a composition matrix

3.6 Survival matrix

The survival of joints, understood as the probability that a determined joint will survive at a determined comminution degree, is described using *survival matrices*. Each element of the survival matrix is a statistical distribution describing the probability of survival of a joint-containing particle in the

progeny size class. So far there is no experimental data regarding the survival of joints after shredding, but the survival of the joints after shredding should have a probability distribution of some kind, related to the parent particles size and mechanical properties of the materials and joints used.

3.7 Tensors

An nth-rank tensor in m-dimensional space is a mathematical object that has n indices and m^n components and obeys certain transformation rules. Each index of a tensor ranges over the number of dimensions of space. However, the dimension of the space is largely irrelevant in most tensor equations (with the notable exception of the contracted Kronecker delta). Tensors are generalisations of scalars (that have no indices), vectors (that have exactly one index), and matrices (that have exactly two indices) to an arbitrary number of indices. Tensors provide a natural and concise mathematical framework for formulating and solving problems in areas of physics such as elasticity, fluid mechanics, and general relativity. The notation for a tensor is similar to that of a matrix $(i.e., A = (a_{ij}))$, except that a tensor $a_{ijk...}$, $a^{ijk...}$, $a_i{}^{jk}$..., etc., may have an arbitrary number of indices. In addition, a tensor with rank $r + s$ may be of mixed type (r, s) , consisting of r so-called "contravariant" (upper) indices and s "covariant" (lower) indices [Web 2006*c*]. Note that the positions of the slots in which contravariant and covariant indices are placed are significant so, for example, $\alpha_{\mu\gamma}{}^{\lambda}$ is distinct from $\alpha_{\mu}{}^{\gamma\lambda}$. While the distinction between covariant and contravariant indices must be made for general tensors, the two are equivalent for tensors in three-dimensional Euclidean space, and such tensors are known as *Cartesian* tensors.

Objects that transform like zeroth-rank tensors are called scalars, those that transform like first-rank tensors are called vectors, and those that transform like second-rank tensors are called matrices. In tensor notation, a vector **v** would be written v_i, where $i = 1, ..., m$, and a matrix is a tensor of type $(1, 1)$, which would be written in $a_i{}^j$ tensor notation.

Tensors may be operated on by other tensors (such as metric tensors, the permutation tensor, or the Kronecker delta) or by tensor operators (such as the covariant or semicolon derivatives). The manipulation of tensor indices to produce identities or to simplify expressions is known as index gymnastics, which includes index lowering and index raising as special cases. These can be achieved through multiplication by a so-called metric tensor [Weisstein 2006] g_{ij}, g^{ij}, $g_i{}^j$, etc. [Arfken 1985].

$$g^{ij}A_j = A^i \tag{3.3}$$

$$g_{ij}A^j = A_i \tag{3.4}$$

Tensor notation can provide a concise way of writing vectors and more general identities. For example, in tensor notation, the dot product is simply written

$$\mathbf{u} \cdot \mathbf{v} = u_i v^i \tag{3.5}$$

where repeated indices are summed over, known as Einstein summation.

Similarly, the cross product can be concisely written as

$$(\mathbf{u} \times \mathbf{v})_i = \epsilon_{ijk}\mu^j v^k, \tag{3.6}$$

where $\epsilon_{ijk}\mu^j v^k$ is the permutation tensor. Contravariant second-rank tensors are objects which transform as

$$A'^{ij} = \frac{\partial x_i'}{\partial x_k}\frac{\partial x_j'}{\partial x_l}A^{kl} \tag{3.7}$$

Covariant second-rank tensors are objects which transform as

$$C'_{ij} = \frac{\partial x_k}{\partial x'_i}\frac{\partial x_l}{\partial x'_j}C_{kl} \tag{3.8}$$

Mixed second-rank tensors are objects which transform as

$$B'^{\,i}_{\ j} = \frac{\partial x'_i}{\partial x_k}\frac{\partial x_l}{\partial x'_j}B^k{}_l \tag{3.9}$$

If two tensors A and B have the same rank and the same covariant and contravariant indices, then they can be added in the obvious way:

$$A^{ij} + B^{ij} = C^{ij} \tag{3.10}$$

$$A_{ij} + B_{ij} = C_{ij} \tag{3.11}$$

$$A^i{}_j + B^i{}_j = C^i{}_j \tag{3.12}$$

The generalisation of the dot product applied to tensors is called tensor contraction, and consists of setting two unlike indices equal to each other and then summing using the Einstein summation convention. Various types of derivatives can be taken of tensors, the most common being the comma derivative and covariant derivative.

If the components of any tensor of any tensor rank vanish in one particular coordinate system, they vanish in all coordinate systems. A transformation of the variables of a tensor changes the tensor into another whose components are linear homogeneous functions of the components of the original tensor.

A tensor space of type (r, s) can be described as a vector space tensor product between r copies of vector fields and s copies of the dual vector fields, i.e., one-forms. For example,

$$T^{(3,1)} = TM \otimes TM \otimes TM \otimes T^*M \tag{3.13}$$

is the vector bundle of $(3, 1)$-tensors on a manifold M , where TM is the tangent bundle of M and T^*M is its dual. Tensors of type (r, s) form a vector space. This description generalised to any tensor type, and an invertible linear map $J : V \to W$ induces a map $\tilde{J} : V \otimes V^* \to W \otimes W^*$, where $V^*$is the dual vector space and J the Jacobian, defined by

$$\tilde{J}(v_1 \otimes v_2^*) = (Jv_1 \otimes (J^T)^{-1} v_2^*) \tag{3.14}$$

Here J^T is the pullback map of a form defined using the transpose of the Jacobian. This definition can be extended similarly to other tensor products of V and V^*. When there is a change of coordinates, then tensors transform similarly, with J the Jacobian of the linear transformation.

CHAPTER 4

EXISTING SHREDDER MODELS

This chapter presents an overview of the recycling system,and then delves further into two existing shredder models proposed by van Schaik and Castro. These two models are useful in describing shredding process and will be combined and modified in the subsequent chapter to develop a new computer model for shredding. Their advantages and limitations are also briefly discussed.

4.1 Overview of the recycling system of EOL products

The objective of research on recycling systems is to evaluate optimal solutions taking into consideration conventional economic activities as well as environmental preservation such as waste management and environment investment (i.e., investment allocated to environmental infrastructure to protect and enhance the natural environment) [Masui, Morita & Kyogoku 2000].

Figure 22 shows a simplified AT&T telephone. It consists of three major parts: a cord, a handset, and a telephone base. The handset consists of four parts: parts A and B made from thermoset plastic, part C made from steel, and part D, a printed circuit board [Zussman, Zhou & Caudill 1998].

A typical recycling system consists of successive processes of shredding, mechanical recycling, and metallurgical operations within the interconnected resource cycle system [Verhoef, Reuter & Dijkema 2004]. The recycling system described here is adapted from one for the recycling system for end of life vehicles. Figure 23 contains a flowsheet that shows the basic configuration of the recycling system. It includes a network of unit operations required for recycling the materials, ranging from dismantling, shredding, and mechanical separation to metal producing processes and therefore gives the material flows and structure of the recycling system for end of life products.

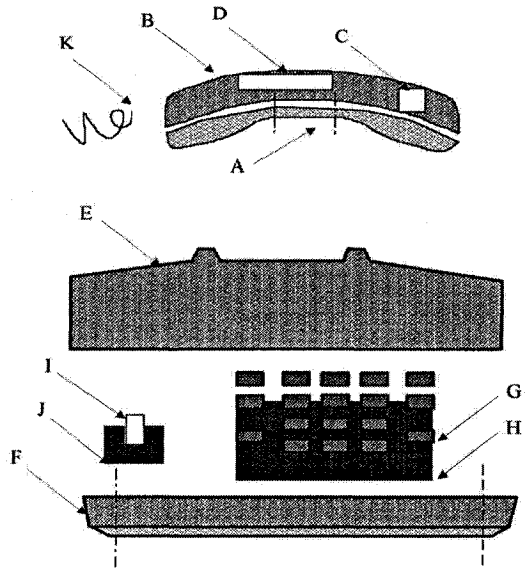

Figure 22: A telephone and its handset [Zussman, Zhou & Caudill 1998].

Figure 23 shows that the first step of shredding is manual dismantling. Materials go into three different streams after dismantling: one stream of dismantled materials is to be processed elsewhere, one goes to spare parts which can be reused and the other stream goes as input to a shredder. Carefully dismantling can get some "functional" parts back at the very early stage of recycling and assure better material stream purity after shredding at the expense of higher labor costs. After shredding, the shredded material stream goes to an air suction station where the dust and fine particles are removed. Materials then go to a magnetic separation station, after which a ferrous stream will go directly to a steel plant, waste will go to trash bins, and a non-ferrous stream will go to eddy current separation. After this eddy current stage, the material experiences several process steps until it is disposed as waste or ends up as alloy after a metallurgical process.

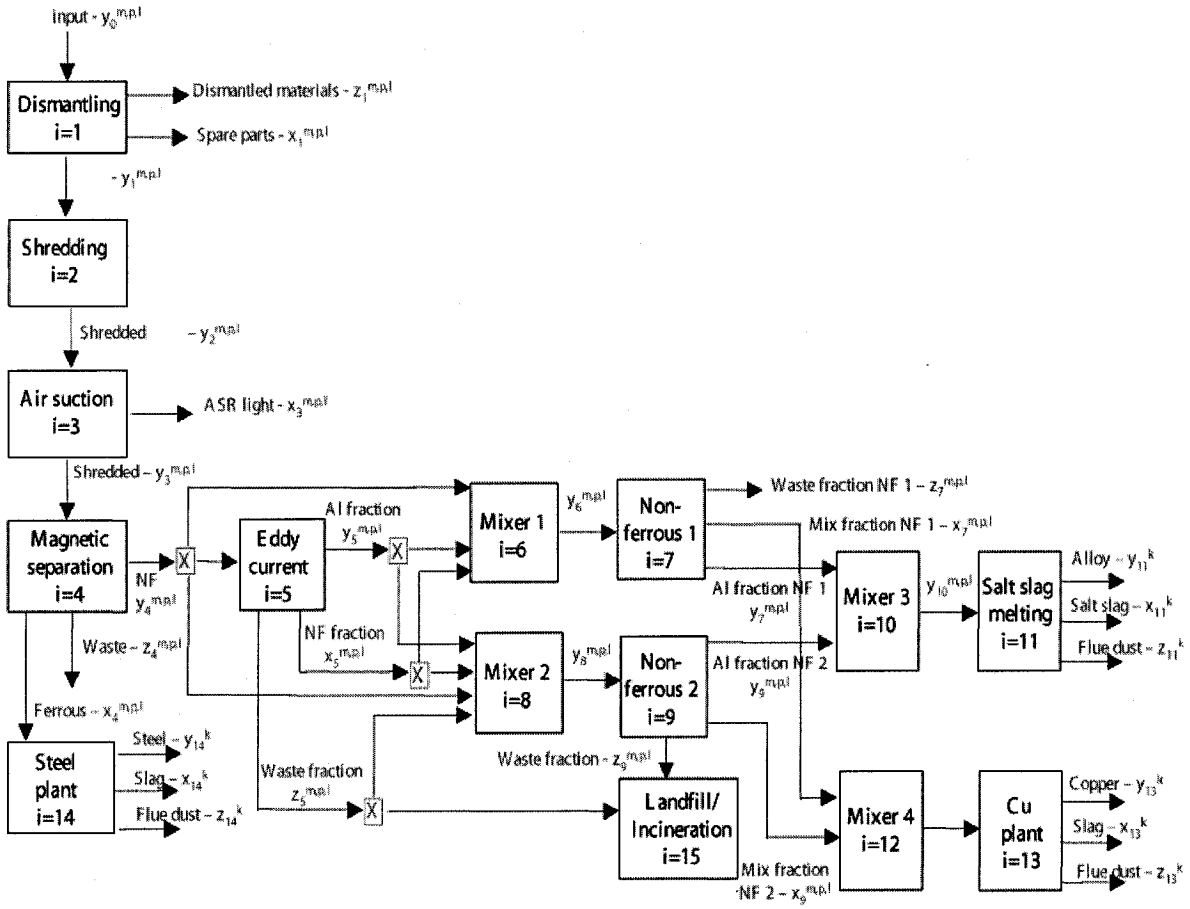

Figure 23: Flow chart of recycling system of end of life products, with m = A - Al wrought based mineral, B - Al cast based mineral, C - remainder based mineral, D - steel based mineral, E - copper based mineral, k = elements Al wrought, Al cast, rest steel, Cu; particle size class p = 1 - 5; liberation class l = 1 - 5; i = plants, unit operations, transport, etc. with i = 1 to n; and α, β, and γ structural parameters. [Reuter & van Schaik 2004]

4.2 Van Schaik's model

Particle size reduction and liberation of materials during the shredding of modern end of life products play an important role in the composition and quality of the intermediate recycling streams and the ultimate material recovery and therefore recycling rate [van Schaik, Reuter & Heiskanen 2004]. Van Schaik's model for shredding presented here is partially based on the modelling techniques applied in traditional minerals processing, demonstrating how classical theory can be applied to solve modern problems. The model describes the influence of breakage on mechanical separation efficiency and material recovery in metallurgical processing for the various materials present in a vehicle. The model has been developed in order to optimise material recovery and to minimise waste generation in recycling of end of life products. The modelling of the breakage behaviour for modern consumer products differs fundamentally from traditional minerals processing.

The design of modern products combines and connects various materials in many complex different ways, making up a complex "mineralogy" (composition, tissue and structure) of the products. This mineralogy changes rapidly and continuously over time. On the other hand, the mineralogy of traditional primary ores and minerals originating from mines, from which the composition is well known, does not change drastically from a particular mine site or even between mine sites. The simulation of classical minerals processing is often not easy due to incomplete descriptions of mineral properties, making the calibration of fundamental models difficult.

Modern end of life products are so complex, diverse and rapidly changing in design that it is difficult to create a fundamental description of them. The closure of the material cycle of modern consumer products requires optimisation of the mutual compatibility of the successive processes of shredding, mechanical recycling and metallurgical operations within the interconnected resource cycle system.

This is only possible if recycling systems are defined more fundamentally than is the case at present [van Schaik, Reuter & Heiskanen 2004].

It is known from traditional minerals processing technology that the behaviour of ore dressing equipment depends on the nature of the individual particles processed [Heiskanen 1993, King 2001]. Both authors propose that the two most important fundamental properties are the size of the particle and its mineralogical composition, which are both determined by the comminution process.

Mineral liberation is the natural link between comminution and mineral recovery operations. Modelling of mineral separation therefore requires the modelling of liberation phenomena. It can be concluded that the same principle applies for the separation of artificial ores, such as modern consumer products, of which the mineralogy is determined by design. King [2001] discusses the quantitative modelling of the unit operations of minerals processing, for which the modelling of particle size and liberation are essential. The modelling of both particle size and liberation is based on combined distributions as well as population balance methodology. Population balance is a well-established method for computing the size distribution of disperse phase, accounting for the break-up and coalescence effects; the philosophy and mathematical details are summarised very well by Randolph & Larson [1971].

The modelling is based on the definition of the distribution of particles in a size-composition space, and can be expressed as a matrix. Liberation is modelled only to the extent that is necessary to provide the link between comminution and mineral recovery. In spite of differences in comminution behaviour of mineral ores compared to man-made products, the same principle for the definition of the relation between particle size and liberation (expressed as grade in minerals processing) can be applied to describe particle sizes related to liberation.

4.2.1 Optimisation model for linking design to recycling of end of life products

Simplified models for the simulation and optimisation of the recycling of end of life products have been developed on the basis of separating particle size and liberation classes. The first optimisation model developed by van Schaik, Reuter, Boin & Dalmijin [2002] defines the separation of the material streams based on particle size classes p and elements $k \in \{\text{Al wrought, Al cast, Rest, Steel, Cu}\}$, whereas the second model describes the material streams in terms of m minerals A to E (representing respectively Al-wrought, Al-cast, Rest, Steel and Cu based metals/minerals) and l liberation classes. The degree of liberation of a product is described by defining, for each of the minerals A to E, the fraction of the various elements k present in the particles of the material flows within the different liberation classes l. In the first model the separation efficiency of the various physical separation steps is defined in terms of grade/recovery curves, whereas the second model describes the separation in terms of recovery only. The grade (based on metals/minerals m) and the exact composition of the streams (based on the elements k) can be calculated from the model.

4.2.1.1 Modelling particle size reduction and liberation in recycling end of life products in relation to modelling minerals processing systems

The particle size reduction and the liberation of materials during shredding, which is determined by product design among other things, will both affect the recycling of end of life products [van Schaik, Reuter, Boin & Dalmijin 2002, van Schaik & Reuter 2004, van Schaik, Castro & Remmerswaal 2003]. This fact is well known from minerals processing technology [King 2001]. In order to define the effect of both particle size and liberation on the separation efficiency, the composition of the intermediate recycling streams and the final metal/material recovery, it is essential to combine these two parameters (particle size reduction and liberation) into one model. Therefore, the models of van Schaik, Reuter,

Boin & Dalmijin [2002], van Schaik & Reuter [2004], and van Schaik, Castro & Remmerswaal [2003] are combined into one final model [van Schaik, Reuter & Heiskanen 2004], which includes the particle size reduction as well as the liberation of the materials to describe the influence of product design (mineralogy), particle size of the product and material flows, and liberation (product/particle composition) on the recycling of end of life modern products and its optimisation. This model is developed using the knowledge available from the modelling and simulation of minerals processing systems [King 2001] and integrating this into simulation models as defined by Reuter & van Deventer [1990].

King [2001] states that during comminution of mineral ores there is a natural tendency towards liberation and particles that are smaller than the mineral grains that occur in the ore can appear as a single mineral. This happens when the particle is formed entirely within a mineral grain, but is impossible when the particle is substantially larger than the mineral grains in the ore. However, King [2001] also states that the distributions of particles with respect to the composition do show some regular features particularly with respect to the variation of the distribution with particle size. This is however not necessarily the case for the comminution of modern consumer products for which the design and the related particle size reduction and liberation behaviour is much more complex than those of mineral ores. This is often the case due to the metals/minerals not being finely divided in the consumer products as is the case for geological ores. Due to the design and construction of the product it is difficult to define a grain size of the minerals/elements in the product. The grain size of any metal/mineral in a modern consumer product is not defined by natural mineralogy, but by continuously changing design, composition, size and connection of the various man-made elements, and can differ from product to product as well as over time. This implies that what is true for classical grinding, i.e., the finer the grind the more liberated particles become, is not necessarily true for shredding of end of life consumer products. The models

for liberation as described by King [2001] are specific to mineralogical textures that consist of only two minerals: a valuable species and all the other minerals that are present and which are classified as gangue minerals. Although the techniques that are used can be applied to multi-component ores, King [2001] discusses that the details of a suitable analysis are not yet worked out and are therefore not discussed. The modelling of the comminution of consumer products can however not be performed on a two component system, but requires the description of all major elements present in the product. Many elements building up the product have to be considered as economically valuable and/or environmentally relevant species. The contamination of one element flow, even with a low quantity of other elements, due to incomplete liberation, could have direct implications for the final recovery rate to be achieved (e.g., the maximum concentration of Cu allowed in steel is 0.25%). As indicated by King [2001], the simulation of multicomponent mineral liberation is difficult.

4.2.1.2 Flowsheet of the model for recycling end of life products

The flowsheet in Figure 23 is derived from a detailed recycling flowsheet for ELV's by van Schaik, Dalmjin & Reuter [2001], and forms the basis for the particle size and liberation based optimisation model discussed here. The flowsheet includes a network of unit operations required for recycling the materials and energy from the product, ranging from dismantling, shredding, and mechanical separation processes to metal producing processes and therefore gives the material flows and structure of the recycling system.

4.2.1.3 Mineral classes m and Particle classes p

The mass (kg) of the material flows $y_i^{m,p}$ in the recycling flowsheet in Figure 23 is described in the model based on the minerals A to E, distributed over the defined particle size classes p (see Table II, Panel A).

Particle size class	Mineral					
	A	B	C	D	E	
Panel A						
Class 1	15	30	250	700	25	
Class 2	0	0	0	0	0	
Class 3	0	0	0	0	0	
Class 4	0	0	0	0	0	
Class 5	0	0	0	0	0	
		Lib. class 1	Lib. class 2	Lib. class 3	Lib. class 4	Lib. class 5
Panel B						
A in ELV	Particle size class 1	0.200	0.200	0.200	0.200	0.200
A in ELV	Particle size class 2	0.000	0.250	0.250	0.250	0.250
A in ELV	Particle size class 3	0.000	0.000	0.333	0.333	0.333
A in ELV	Particle size class 4	0.000	0.000	0.000	0.500	0.500
A in ELV	Particle size class 5	0.000	0.000	0.000	0.000	1.000
Panel C						
Definition of liberation classes						
Mineral A	Al wrought	Al cast	Fe	Cu	Rest	
Lib. class 1	0.5	0.2	0.2	0.05	0.05	
Lib. class 2	0.65	0.15	0.15	0.03	0.02	
Lib. class 3	0.75	0.1	0.1	0.03	0.02	
Lib. class 4	0.87	0.05	0.05	0.02	0.01	
Lib. class 5	1	0	0	0	0	
Mineral B	Al wrought	Al cast	Fe	Cu	Rest	
Lib. class 1	0.2	0.5	0.2	0.05	0.05	
Lib. class 2	0.15	0.65	0.15	0.03	0.02	
Lib. class 3	0.1	0.75	0.1	0.03	0.02	
Lib. class 4	0.05	0.87	0.05	0.02	0.01	
Lib. class 5	0 1	0	0	0		
Mineral C	Al wrought	Al cast	Fe	Cu	Rest	
Lib. class 1	0.04	0.04	0.06	0.06	0.8	
Lib. class 2	0.03	0.03	0.04	0.05	0.85	
Lib. class 3	0.02	0.02	0.03	0.03	0.9	
Lib. class 4	0.015	0.015	0.01	0.01	0.95	
Lib. class 5	0	0	0	0	1	
Mineral D	Al wrought	Al cast	Fe	Cu	Rest	
Lib. class 1	0.01	0.01	0.8	0.08	0.1	
Lib. class 2	0.01	0.01	0.85	0.06	0.07	
Lib. class 3	0.01	0.01	0.9	0.05	0.03	
Lib. class 4	0.005	0.005	0.95	0.02	0.02	
Lib. class 5	0	0	1	0	0	
Mineral E	Al wrought	Al cast	Fe	Cu	Rest	
Lib. class 1	0.01	0.01	0.03	0.8	0.15	
Lib. class 2	0.005	0.005	0.02	0.85	0.12	
Lib. class 3	0.005	0.005	0.01	0.9	0.08	
Lib. class 4	0	0	0.01	0.95	0.04	
Lib. class 5	0	0	0	1	0	

Panel A: mass based particle size distribution of the input $y_i^{m,p}$; Panel B: liberation/particle size matrix $Ly_i^{m,p,l}$; Panel C: composition matrix of liberation classes $C^{m,l,k}$ for mineral A; and also B-E

TABLE II

TYPICAL EXAMPLES OF THE PHASE MODEL AS USED FOR THE SIMULATIONS FOR MINERAL A

4.2.1.3.1 Element classes k and Liberation classes l

For each of the particle size classes in a specific material flow $y_i^{m,p}$, a discrete distribution of material over the liberation classes $l = 1, \ldots, 5$ is defined in the liberation/particle size matrix $Ly_i^{m,p,l}$ (see Table II, Panel B), which is in principle similar in definition to the particle distribution in the size-composition space discussed by King [2001]. The matrix $Ly_i^{m,p,l}$ defines for each mineral m the fraction of material present in liberation classes 1 to 5 for the different particle size classes p for the material stream y_i after each unit operation i. This matrix is also defined for the model input (being the shredded product), describing in this way the particle size classes and liberation classes determined by the design of the product. The composition matrix $C^{m,l,k}$ defines for each mineral m the composition of the different liberation classes l for the elements k (see Table II, Panel C) as discussed by van Schaik, Dalmjin & Reuter [2001]. Panel C of Table II summarises an example for the definition of the composition of the liberation classes in the model for a mineral A (in this case a mineral with Al-wrought being the major component). Similarly there are minerals B (Al-cast rich), C (Plastic rich/rest), D (Steel-rich) and E (Cu-rich). Since data on the composition of the various liberation classes is lacking, estimations on these had to be made as can be seen from Table II. The reason for this lack of data is that recycling systems have not been analysed as systematically as classical minerals processing [King 2001]. This matrix is defined based on a possible description of a multicomponent mineral ore, however it differs fundamentally from the modelling of the two-component minerals system (valuable and gangue) as discussed by King [2001].

4.2.1.3.2 Alloy types

The output of the metallurgical processes has to comply with constraints on the alloy composition. Since each element is described separately in the composition matrices $C^{m,l,k}$ composing the various

minerals, the output of the metallurgical operation can be calculated by adding all elements present in the various material flows, being the input for metallurgical processing (Figure 23). This implies that elements must be added from the different size classes p, of which the composition is defined by combining the liberation/particle size matrix $Ly_i^{m,p,l}$ and the composition matrix $C^{m,l,k}$. The grade of mechanical separation can also be calculated from the model. Aluminium is described in the model as wrought or cast, each with its own specific (average) composition. To be able to calculate the produced alloy type, the composition of the wrought and cast aluminium is described in a separate alloy matrix in the model. Together with the contaminants and alloying elements ending up in the alloy, the exact alloy composition can be calculated from the model based on the degree of liberation and can be controlled by defining boundary conditions on the output ,i.e., the metal quality. Primary materials (aluminium and alloying elements) often have to be added to produce a required alloy composition due to losses in the system. These primary materials are defined as one of the input streams of the model. The addition of primary materials must be kept to a minimum, for economic and environmental reasons. This can be realised by including cost penalties to the primary materials in the objective function of the optimisation model.

4.2.1.4 Separation models

Since the performance of an unit operation is related to the particle size and degree of liberation of the feed of the processes, the separation can be defined for different ranges of size classes p and liberation classes l. The transformation matrices $Ty_i^{m,p,l}$, $Tx_i^{m,p,l}$ and $Tz_i^{m,p,l}$ (see the example in Table III) define the recovery values for each mineral m for each particle size class p and liberation class l for mechanical separation processes i for, respectively, streams y_i, x_i and z_i. The difference in separation efficiency (recovery) is determined by the size class as well as the degree of liberation. However, the

Example of a transformation matrix $Ty_i^{m,p,l}$ with the recovery values for each individual particle size class p and liberation class l defined for m=mineral A for separation process i=5 (eddy current separation) flowing to the product stream y_i

Mineral A	$Ty_i^{m,p,l}$	Lib. class 1	Lib. class 2	Lib. class 3	Lib. class 4	Lib. class 5
i=5 Eddy current	Particle size class 1	0.8000	0.8400	0.8800	0.9200	0.9600
	Particle size class 2	0.8000	0.8400	0.8800	0.9200	0.9600
	Particle size class 3	0.8000	0.8400	0.8800	0.9200	0.9600
	Particle size class 4	0.8000	0.8400	0.8800	0.9200	0.9600
	Particle size class 5	0.2000	0.2000	0.2000	0.2000	0.3000

TABLE III

TRANSFORMATION MATRIX

influence of each individual material present in a non-liberated particle cannot be expressed in the recovery rate for mechanical separation (e.g., the presence of 10% Fe in Al will have another effect on the recovery rate for eddy current separation than the presence of 10% organic materials). An additional distinction should be made for the different material combinations possible in a certain liberation class to be able to model this in future work.

4.2.1.5 Formulation of the optimisation model

From the recycling flowsheet in Figure 23 four different types of processes can be defined: shredding, mechanical separation, mixing and metallurgical processing. Since these operations are fundamentally different, the model describes the flow of materials in the recycling system for these operations in a different way. The description of these unit operations in the optimisation model is discussed below in four separate sections. As discussed by van Schaik, Reuter, Bion & Dalmijin [2002], two types of equations can in principle describe the flow of materials in the system of processes and the structure of the network for each individual mineral/element present in the end-of-life product.

1. mass balance equations, including structural parameters for each mineral m, element k, particle class p, and liberation class l, and
2. separation efficiency models for each of the unit operations for each mineral m, element k, particle class p, and liberation class l.

which are both based on:

1. liberation distributions of liberation classes l for each mineral m and particle size class p, and
2. the composition of each liberation class l based on elements k for each mineral m.

Various parameters playing a role in the efficiency of the material cycle, such as the economy, legislation, etc., can be translated into constraints imposed onto the model, the equations mentioned and an objective function for optimisation [van Schaik, Reuter & Heiskanen 2004]. These theoretical equations comprise the basis of the model, giving the constraints imposed on the system. The material flows for the minerals m (defined based on elements k) in different size classes p and liberation classes l between the unit operations and interconnections between these processes as depicted in the recycling flow sheet of Figure 23 can be simplified and generalised as shown.

4.2.1.6 Formulation of model for shredding

The transition of the particle size as well as of the liberation class distribution within the particle size classes due to the shredding operation can be defined in the model based on shredding transformation matrices. This is similar to the approach taken by Reuter & van Deventer [1990] for milling and flotation plants. However, the transitions of particle size and liberation class are defined in separate transformation matrices.

It is possible to define a transformation matrix for the transition of the particle size distributions over shredding Sf_i^{m,p_f,p_y}, in which p_f is the particle size class of the feed f, whereas p_y is defined

for the output y. The assumption has been made that all materials defined as Al (cast and wrought), Fe, Cu and "Rest" (the rest of the minerals), i.e., minerals A to E, all break according to the same shredding transformation matrix. This is obviously a simplification, since the various materials will break differently due to their specific mechanical properties, joining method, design, and complexity and therefore require different transformation matrices.

Since no data are available on the transition of liberation class distributions during shredding, no reliable definition for the shredding matrix for the liberation class transition could be presented here. Moreover, the definition of a liberation class transition matrix would require detailed insight into the relation between the particle size and liberation class transition, which is unknown for complex products. However, the transition of the liberation class distribution can be described sufficiently based on a mass balance over the shredding operation for the elements k building up the liberation classes l as defined in the composition matrix $C^{m,l,k}$ for liberation. The shredding matrix for particle size class transition changes the distribution of the mass flow of the minerals m over the different particle size classes p after shredding. Therefore, the shredding matrix for the liberation class transition would change the definition of the matrix $Lf_i^{m,p,l}$ to $Ly_i^{m,p,l}$ due to the shredding operation. It changes the distribution of liberation classes in the different particle size classes p for each mineral m.

A mass balance can be set up over the shredding operation, which describes the transition of the mass flow over the particle size classes p for each mineral m (4.1). Since no separation takes place (the input and output of the shredder are both defined as one stream distributed over the particle size classes) no separation efficiency equation for the shredding operation is defined.

$$\left(\sum_{p_f=1}^{p_f=5} Sf_i^{m,p_f,p_y} \cdot f_i^{m,p_f}\right) - y_i^{m,p_y} = 0 \tag{4.1}$$

with

$$\sum_{p_y=1}^{p_y=5} Sf_i^{m,p_f,p_y} = 1 \tag{4.2}$$

4.2.1.7 Liberation during shredding

The shredding operation will change the configuration of the liberation of the various minerals in the different particle size classes p as given in the particle size/liberation matrix $Lf_i^{m,p,l}$. The relation between the liberation class distribution of the input and output of the shredder can be described by the following equation:

$$\sum_{p=1}^{p=5}\left(\sum_{l=1}^{l=5}\left(Lf_i^{m,p,l} \cdot C^{m,l,k}\right)\right) \cdot f_i^{m,p} - \sum_{p=1}^{p=5}\left(\sum_{l=1}^{l=5}\left(Ly_i^{m,p,l} \cdot C^{m,l,k}\right)\right) \cdot y_i^{m,p} = 0 \tag{4.3}$$

with

$$\sum_{l=1}^{l=5} Ly_i^{m,p,l} = 1 \tag{4.4}$$

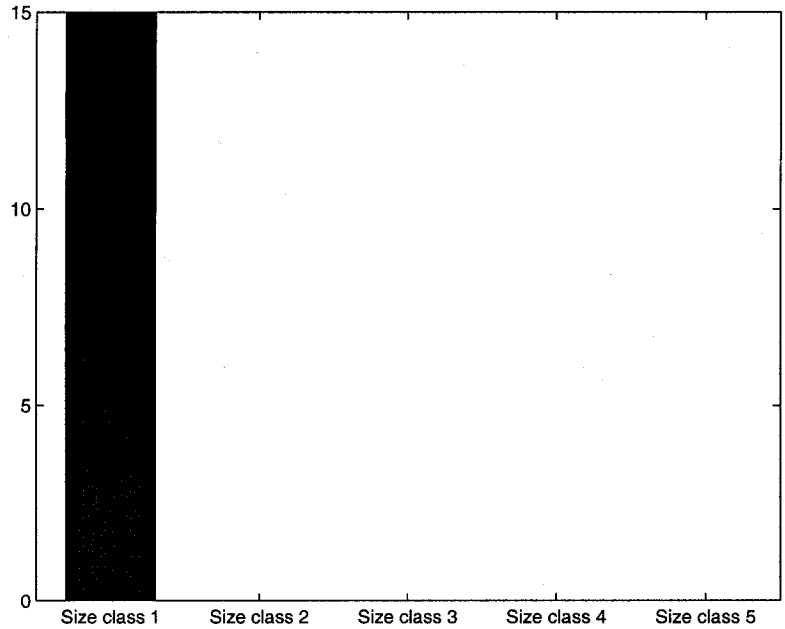

Figure 24: Size distribution before shredding

4.2.2 Simulation with van Schaik's model

Assume mineral A in an ELV has size class distribution of $\begin{bmatrix} 15 \\ 0 \\ 0 \\ 0 \\ 0 \end{bmatrix}$ before shredding (Figure 24), and that the size distribution after shredding is $\begin{bmatrix} 3 \\ 4.5 \\ 4.5 \\ 1.5 \\ 1.5 \end{bmatrix}$ (Figure 25). For scenario 1, the liberation

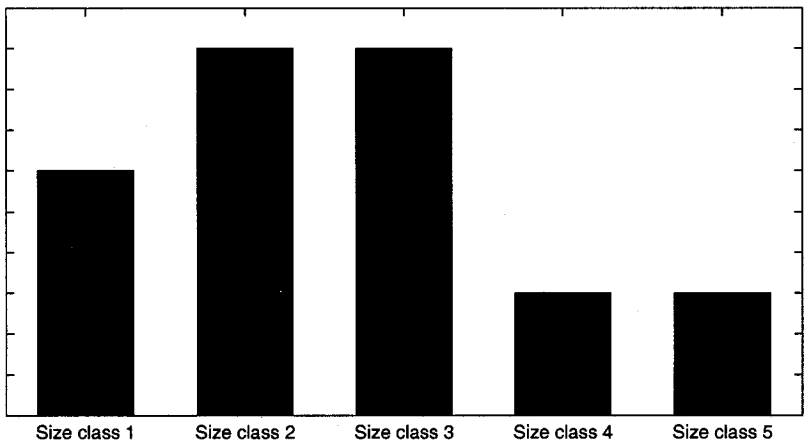

Figure 25: Size distribution after shredding

matrix before shredding is

$$Lf = \begin{bmatrix} 0.1580 & 0.4420 & 0.0000 & 0.3810 & 0.0200 \\ 0.0000 & 1.0000 & 0.0000 & 0.0000 & 0.0000 \\ 0.0000 & 0.0000 & 0.0000 & 0.0000 & 0.0000 \\ 0.0000 & 0.0000 & 0.0000 & 0.0000 & 0.0000 \\ 0.0000 & 0.0000 & 0.0000 & 0.0000 & 0.0000 \end{bmatrix} \tag{4.5}$$

which can be plotted on a bar graph as shown in Figure 26. The liberation matrix after shredding is

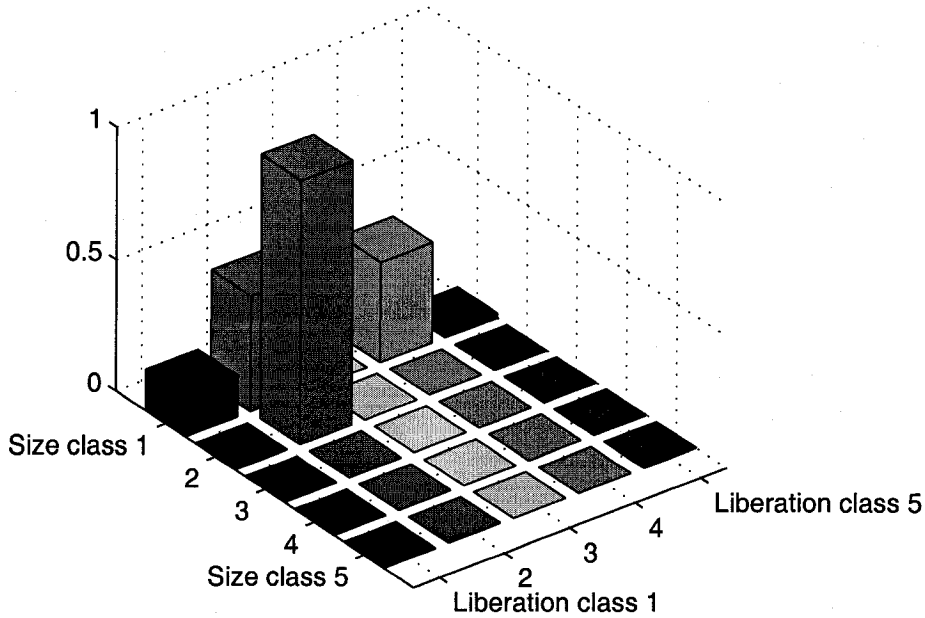

Figure 26: Liberation distribution before shredding

given by

$$Ly = \begin{bmatrix} 0.6320 & 0.3670 & 0.0000 & 0.0000 & 0.0000 \\ 0.0000 & 0.9990 & 0.0000 & 0.0000 & 0.0000 \\ 0.0000 & 0.0000 & 1.0010 & 0.0000 & 0.0000 \\ 0.0000 & 0.0000 & 0.0000 & 0.9990 & 0.0000 \\ 0.0000 & 0.0000 & 0.0000 & 0.0000 & 0.9990 \end{bmatrix} \tag{4.6}$$

with a bar graph as shown in Figure 27. For scenario 2, the liberation matrix before shredding is

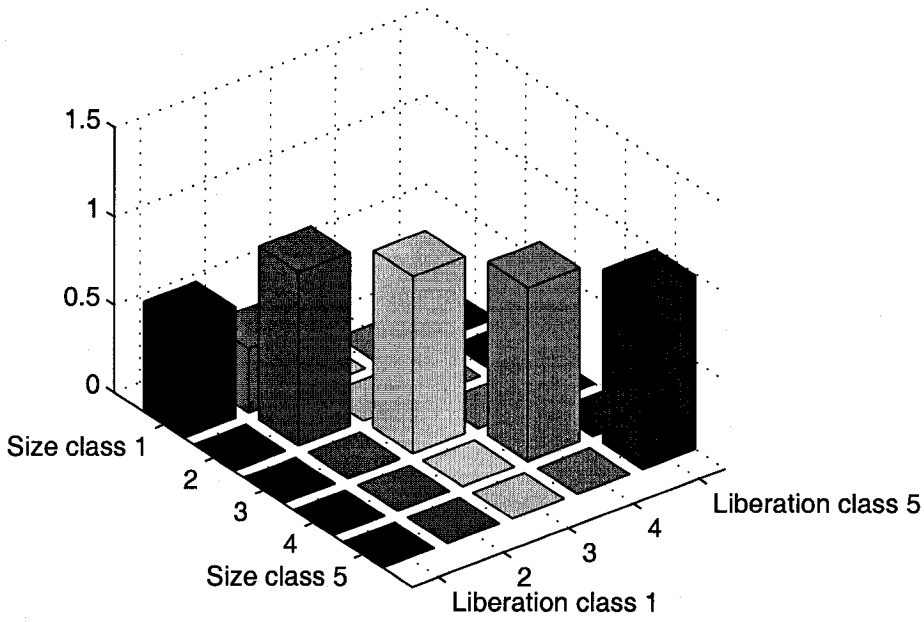

Figure 27: Liberation distribution after shredding

$$Lf1 = \begin{bmatrix} 0.0640 & 0.0580 & 0.0000 & 0.8130 & 0.0660 \\ 0.0000 & 0.9990 & 0.0000 & 0.0000 & 0.0000 \\ 0.0000 & 0.0000 & 1.0010 & 0.0000 & 0.0000 \\ 0.0000 & 0.0000 & 0.0000 & 0.9990 & 0.0000 \\ 0.0000 & 0.0000 & 0.0000 & 0.0000 & 0.9990 \end{bmatrix} \tag{4.7}$$

with a bar graph as shown in Figure 28, while the liberation matrix after shredding is given by

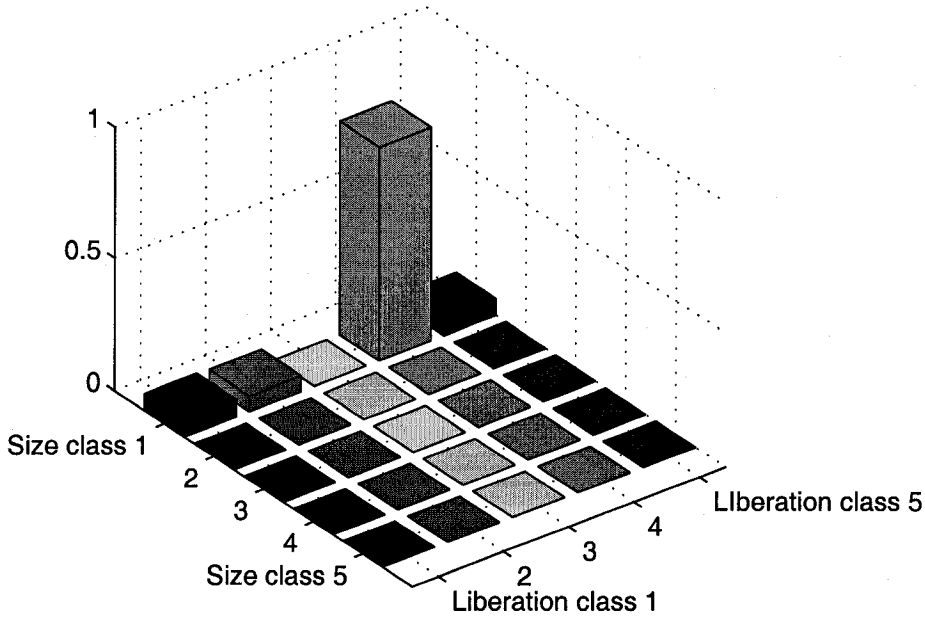

Figure 28: Liberation distribution before shredding

$$Lf1 = \begin{bmatrix} 0.2550 & 0.1290 & 0.2400 & 0.1840 & 0.1900 \\ 0.0000 & 0.1650 & 0.3130 & 0.2860 & 0.2360 \\ 0.0000 & 0.0000 & 0.4610 & 0.2860 & 0.2520 \\ 0.0000 & 0.0000 & 0.0000 & 0.5600 & 0.4410 \\ 0.0000 & 0.0000 & 0.0000 & 0.0000 & 0.9990 \end{bmatrix} \tag{4.8}$$

with a bar graph as shown in Figure 29. Using van Schaik's model, we find that the size transformation

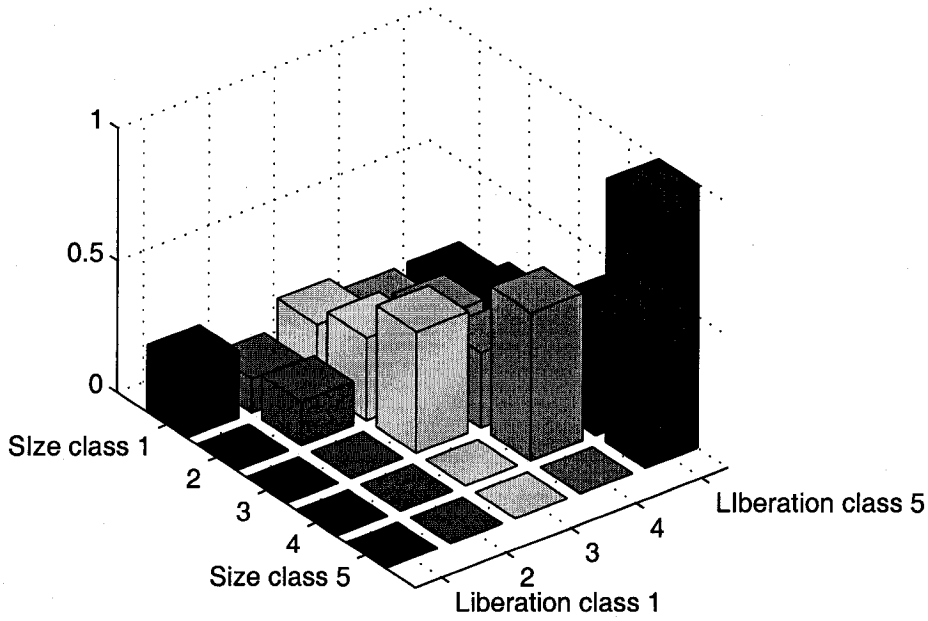

Figure 29: Liberation distribution after shredding

matrix is

$$Lf1 = \begin{bmatrix} 0.2000 & 0.0000 & 0.0000 & 0.0000 & 0.0000 \\ 0.3000 & 0.5000 & 0.0000 & 0.0000 & 0.0000 \\ 0.3000 & 0.1000 & 0.7000 & 0.0000 & 0.0000 \\ 0.1000 & 0.3000 & 0.1000 & 0.5000 & 0.0000 \\ 0.1000 & 0.1000 & 0.2000 & 0.5000 & 1.0000 \end{bmatrix} \tag{4.9}$$

The element composition matrix is found using MATLAB to be:

$$C^{m,l,k} = \begin{bmatrix} 0.6890 \\ 0.5502 \\ 0.4058 \\ 0.2344 \\ 0.0547 \end{bmatrix} \tag{4.10}$$

4.3 Castro's model

While there is extensive research on liberation modelling for mineral processing system, much of which is mentioned by King [2001], literature on comminution and liberation modelling of recycling streams is very recent and scarce. One of the difficulties in developing models is that the shredding processes can not be observed directly, the phenomena occurring in the comminution chamber must be deduced from the results [Kirchner 2000]. Furthermore, recycling streams have specific properties distinct from natural minerals: large particle size, high ductility, large variations in size, shape and mineralogy.

The model proposed by Castro, Remmerswaal, Brezet, van Schaik & Reuter [2005] is another simulation computer model for comminution and liberation process of shredders.

It models the comminution and liberation of five interconnected minerals. All of the minerals simulated in Castro's model are binary minerals, meaning that they are composed of only two different materials. The plastic deformation of materials is responsible for the largest amount of breakage enegy absorbed in ductile materials. Because of intensive plastic deformation and the three dimensionality of the breakage phenomena, fracture mechanics can only handle breakage in plastic materials with numerical methods [Anderson 1995]. These numerical methods require exact knowledge of the applied force. However, the particles to comminute have complex geometries and unknown varying coordinates during shredding. Therefore, a statistical approach is necessary for modelling the breakage and liberation in the shredder model, using distribution functions.

In Castro's model, products are modelled as a set of materials and a set of joints. The amount of materials ("minerals") is limited to five: Aluminium cast (Al_c), Aluminium wrought (Al_w), Copper (Cu), Ferrous (Fe) and Rest (Rest). The choice of five materials was also made in order to make this model compatible with the physical and metallurgic recycling optimisation model developed by van Schaik, Reuter & Heiskanen [2004].

All joints are modelled as binary combinations. Joints between the same or similar materials (e.g., two steel alloys) are not considered as joints because they do not influence the liberation for recycling purposes. Because comminution and liberation occur simultaneously and are coupled during the shredding process, they are modelled as coupled phenomena.

4.3.1 Particle size classes and liberation classes

Five particle size classes (SC) were defined to classify particles according to size: SC5 $\leq$ 10mm; 10 $<$ SC4 $\leq$ 20mm; 20 $<$ SC3 $\leq$ 35mm; 35 $<$ SC2 $\leq$ 50mm; SC1 $>$ 50mm. The reason for this number of size classes is that it is approximately the same as used in the industrial screening of recycling streams.

Liberation classes (LC) were defined to describe the liberation of the EOL product before shredding and of the particles originating from shredding. To describe all possible non-liberated binary material combinations, ten liberation classes were defined ($Al_c - Al_w$, $Al_c - Cu$, $Al_c - Fe$, $Al_c - Rest$, $Al_w - Cu$, $Al_w - Fe$, $Al_w - Rest$, $Cu - Fe$, $Cu - Rest$, $Fe - Rest$). The ten binary materials are named according as shown in Table IV. To describe the composition of the particles in each liberation class, each combination is further divided into ten composition ratio subclasses, as shown in 4.11.

Liberation materials	Name	A	B	C	D	E
	Mineral	Al_c	Al_w	Cu	Fe	Rest
Non-liberated material combinations	Name	F	G	H	I	J
	Mineral	$Al_c - Al_w$	$Al_c - Cu$	$Al_c - Fe$	$Al_c - Rest$	$Al_w - Cu$
	Name	K	L	M	N	O
	Mineral	$Al_w - Fe$	$Al_w - Rest$	Cu-Fe	Cu-Rest	Fe-Rest

TABLE IV

LIST OF NAMES USED FOR THE MINERALS IN CASTRO'S MODEL

Ten ratio composition subclasses were applied to cover these possible liberation classes of shredded particles belonging to five size classes within each composition class. An example of the liberation class

for $Al_c - Al_w(F)$ is shown in 4.11. For calculation purposes, the liberation classes were defined both as mass ratios (LC_m) and as volume ratios (LC_v).

$$LC_{mAl_cAl_w} = \begin{bmatrix} 0.1000 & 0.9000 & 0.0000 & 0.0000 & 0.0000 \\ 0.2000 & 0.8000 & 0.0000 & 0.0000 & 0.0000 \\ 0.3000 & 0.7000 & 0.0000 & 0.0000 & 0.0000 \\ 0.4000 & 0.6000 & 0.0000 & 0.0000 & 0.0000 \\ 0.4900 & 0.5100 & 0.0000 & 0.0000 & 0.0000 \\ 0.5100 & 0.4900 & 0.0000 & 0.0000 & 0.0000 \\ 0.7000 & 0.3000 & 0.0000 & 0.0000 & 0.0000 \\ 0.8000 & 0.2000 & 0.0000 & 0.0000 & 0.0000 \\ 0.9000 & 0.1000 & 0.0000 & 0.0000 & 0.0000 \\ 0.9500 & 0.0500 & 0.0000 & 0.0000 & 0.0000 \end{bmatrix} \quad (4.11)$$

4.3.2 Particle geometry

Geometric variations in particles and shredders are not included in Castro's model. For simplification of modelling, the particle geometry chosen is an average geometry: a circular disk of varying thickness, illustrated by Figure 30. The particle diameter is an estimated diameter of the corresponding size class and its thickness an estimated average thickness for that size class.

4.3.3 Joint geometry and dimension

Joint classes are defined in Castro's model to describe the effect of different types and geometries of joints on liberation phenomena. There are many different joint types and geometries present in most products. To approach this variability while limiting the complexity of the model, four distinct joint

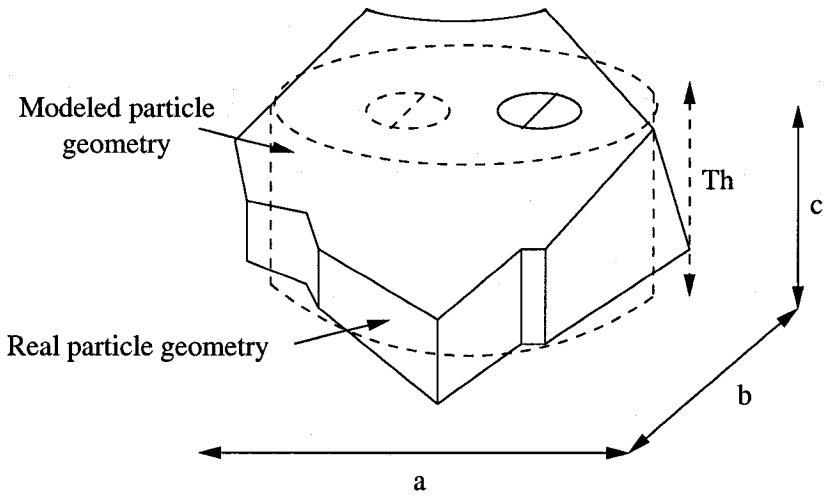

Figure 30: Modelling of the irregular shaped non-liberated particles produced by shredding as circular disks of varying thickness, containing one joint each

classes were defined, according to the geometry and extent of contact surface between the two materials in the joint area (see chapter 3).

4.3.4 Partitioning

The product to shred is a large bulk product, always much larger than the particles produced by shredding. Castro proposed to describe the EOL product as a mineral, after which the liberation is calculated.

The EOL product is a bulk mineral particle belonging to the largest size class (SC1). To calculate the liberation level of the EOL product, it is partitioned in cubes with a side dimension L corresponding to the largest mesh size of the sieve used to process the shredded particles, Φ_1. This is shown schematically in Figure 31. The exact position of the P type joints in the EOL product is unknown, so it is assumed for simplification that the joints are randomly distributed, and that each partition volume contains one joint only. This produces a conservative measure of the liberation of the EOL product.

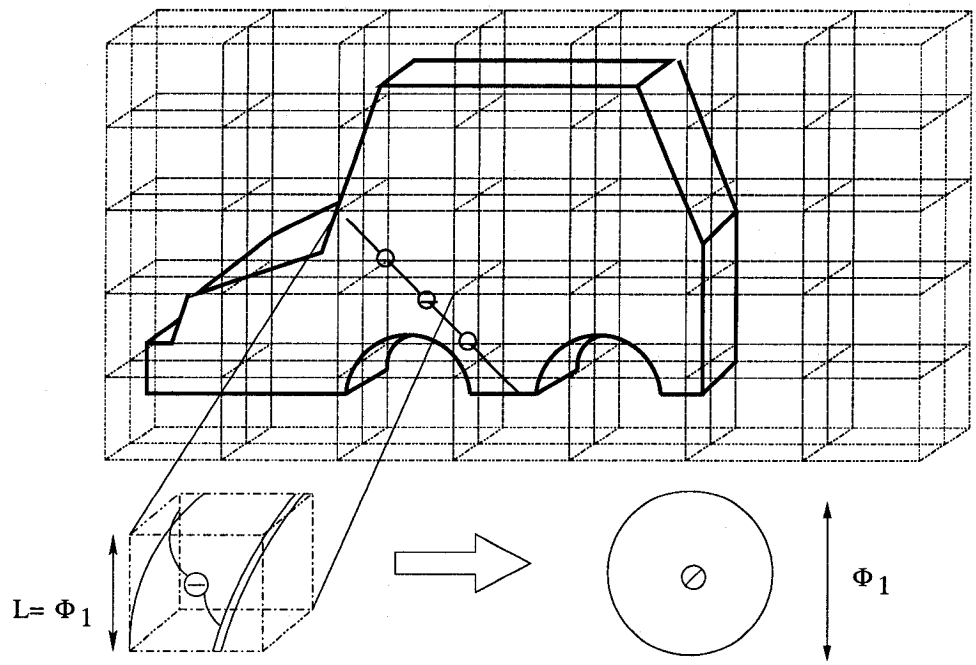

Figure 31: Schematic EOL product partitioning with detail of one partition containing a P joint (bolt)

4.3.5 Transformation matrices

Transformation matrices were defined to relate the design parameters of the product and the liberation level of the product's mineral description. A transformation matrix establishes a relationship between a joint of determined joint class and dimensions and an amount of material. Specific transformation matrices are defined for each each joint class and per mineral. These transformatrices are different from those transformation matrices in van Schaik's model since they are using to transfer product design parameters into initial size class distribution before shredding here, while in van Schaik's model they are describing size class transformation before and after shredding.

4.3.6 Calculation of the liberation level of the EOL product

The amount of non-liberated material n in the mineral description of the EOL product, per mineral and joint class, is calculated by using 4.12, which transforms each joint from each material combination n into a mass of a mineral with a particular liberation ratio:

$$W_{init_n}^{P,L,S} = T_{np\_1}^{P,l,S} \cdot Joint_{p\_1}^{P,L,S} \otimes (LC_{V_n,i} \cdot \rho_i) \otimes Vol_1^{P,L,S} + T_{np\_2}^{P,L,S} \cdot Joint_{p\_2}^{P,L,S} \otimes (LC_{V_n,i} \cdot \rho_i) \otimes Vol_1^{P,L,S} \tag{4.12}$$

where n denotes the mineral (or composition subclass), p is the joint size class and i is the liberated mineral A to E. $Joint_{p_1}^{P,L,S}$ is the joint vector (Figure 32). The subscripts "1" and "2" are used to distinguish the two joint vectors of a determined joint vectors of a determined joint class and mineral XY:

the joint vector where mineral X is the major material and the joint vector where material Y is the main material. The transformation matrices with subscripts "1" and "2" regard the respective vectors with the same underscore.

The liberated materials do not contain a joint is calculated by making

the mass balance of each material from the original mass of that material in the EOL product using:

$$W_{init_n}^{Z} = \sum M_i - \sum (W_{init_n}^{P,L,S} \otimes LC_{v_{n,i}}) \tag{4.13}$$

where n is the minerals A to O describe in Table IV and i the liberated materials A to E. The elements of W_{init}^{Z} are non-zero only for the single minerals A, B, C, D and E.

The final matrix $W_{init}^{P,L,S,Z}$ in 4.14 is formed by adding all the components, per mineral n and joint class, P, L, S, Z:

$$W_{init}^{P,L,S,Z} = \sum_{n}(W_{init_n}^{P,L,S} + W_{init_n}^{Z}) \tag{4.14}$$

where n is the minerals A to O described in Table IV.

4.3.7 Liberation transition during shredding

The modelling of the coupled comminution-liberation phenomena is based on three proposed hypotheses:

Hypothesis 1. The probability of fracture of a joint is lower than that of the rest of the material around it.

Hypothesis 2. Joint destruction is complete only if the particle size formed is smaller than the joint size.

Hypothesis 3. Materials joined by chemical joints can not be liberated by shredding.

Particles containing P joints become partly or completely liberated after shredding. Particles containing L joints become partly liberated. Particles containing S joints do not become further liberated during comminution.

The coupled comminution-liberation phenomena are described in Castro's model by the use of two coupled matrices, a size distribution matrix and a survival matrix. The size distribution matrix describes the comminution process, in terms of the mass fraction of initial material in the EOL products that transits to a determined size class. For simplicity, only one size distribution matrix is used for all liberated minerals and another for the binary minerals in the model.

4.3.8 Particle survival

The survival of joints, understood as the probability of a determined joint to survive a determined comminution degree, is described using survival matrices. Elements of the survival matrix are the statistic distributions describing the probabilities of the survival of joint-containing particles in progeny size class. Because there is no experimental data about the survival of joints after shredding, Castro et al. [2005] believe the survival of joints after shredding has a probability distribution of some kind, related to the parent particle size and mechanical properties of the materials and joints used.

In Castro's model, one survival matrix is used for each joint class, but in reality there should be one matrix per joint dimension and materials combined, to translate the Hypotheses 1 and 2 conveniently. In the absence of experimental results regarding this matrix, Castro et al. [2005] considered a single matrix to be sufficient to illustrate the modelling methodology.

Product components and mass (kg)

Component	Al_c	Al_w	Cu	Fe	Rest
x	30	25	8	600	200
y	50	0.5	1	30	1
z	0	5	5	0	1

Product Joints

M1-M2	Amount	Type	Size
Al_c-Fe	30	P	M15 (Ø15)

TABLE V

PRODUCT DESIGN INFORMATION

$$Joint^{P}_{Al_2Fe_1} = \begin{bmatrix} 0 \\ 0 \\ 0 \\ 0 \\ 0 \\ 30 \end{bmatrix} \quad Joint^{P}_{Al_2Fe_2} = \begin{bmatrix} 0 \\ 0 \\ 0 \\ 0 \\ 0 \\ 0 \end{bmatrix}$$

Figure 32: Vector of joints, according to the information on Table IV

4.3.9 Calculation of the liberation level of the comminuted material

Shredding of an EOL product will produce a set of particles constituted by the defined minerals, distributed over composition subclasses and classed by size. The comminution is calculated using the following equations:

(a) Non-comminuted P, L, S and Z particles and comminuted Z and S particles

$$W^{Z,P,L,S}_{fin_{n,s}} = W^{Z,P,L,S}_{init_n} \cdot (SD^{Z,P,L,S}_{n,s})^T \otimes (SUR^{Z,P,L,S}_{n,s})^T \tag{4.15}$$

where n is the mineral and s the size class. T indicates that the transposed matrix is used.

(b) Liberated material from comminuted P and L particles

$$Lib^{P,L}_{n,s} = W^{Z,P,L,S}_{init_n} \cdot (SD^{P,L}_{n,s})^T \otimes (SUR^{P,L}_{n,s})^T \cdot (1 - \frac{Vol^{P,L}_s}{Vol^{P,L}_1}) \tag{4.16}$$

(c) Comminuted P and L particles

$$W_{fin_{n,s}}^{P,L} = W_{init_n}^{P,L} \cdot (SD_{n,s}^{P,L})^T \otimes (SUR_{n,s}^{P,L})^T - Lib_{n,s}^{P,L} \tag{4.17}$$

(d) Particles that did not survive

$$N_{surv_{n,s}}^{P} = W_{init_n}^{P} \cdot (SD_{n,s}^{P})^T \otimes (NSUR_{n,s}^{P})^T \tag{4.18}$$

(e) The amount of liberated material after shredding is calculated, per material, using the mass balance equation:

$$W_{f_{i,s}}^{Z} = W_{fin_{i,s}}^{Z} + \sum(Lib_{n,s}^{P} \cdot LC_{m_{n,i}}) + \sum(Nsurv_{n,s}^{P} \cdot LC_{m_{n,j}}) + \sum(Lib_{n,7-s}^{L} \cdot LC_{m_{n,i}}) \tag{4.19}$$

where i is the liberated mineral A to E, n is the mineral and s the size class.

In (4.19), the index of the matrices with liberated material is $(n, 7-s)$. This is because only a single breakage event is modelled, in the absence of more specific data. A liberated particle originating from a particle that ends up, e.g., in size class 2, must be a small particle, being assigned size class 5, and a liberated particle originating from a particle that ends up, e.g., in size class 3 is a bit larger, being assigned size class 4, etc. The liberated material is attributed to the Z class as belonging to size class $(7-s, s)$, s being the size class of the correponding non-liberated particle.

CHAPTER 5

COMPUTER MODEL OF SHREDDER

In this chapter, a modified shredder model based on van Schaik's and Castro's models discussed in Chapter 4 is developed. The principal improvement of this shredder model is the complete partition schedule for the inputs to the shredder and the incorporation of the dispersion effect on liberation which was not previously considered. The procedure to simulate the shredding process is detailed as below. Some simulation results of this model are discussed so that the effectiveness of this model can be evaluated.

5.1 Partitioning

Since the EOL products to shred are large bulk productsm, always much larger than the particles produced by shredding, it is necessary to propose a procedure to describe the EOL products in the sense of mineral context before shredding. Here the Castro partitioning procedure is adopted to partition the EOL product wreck (see Figure 31).

(a) The EOL product is partitioned in cubes with a side dimension L corresponding to the largest mesh size of the sieve used to process the shredded particles, $\emptyset_1$.

(b) The exact position of the P type joints in the EOL product is unknown, and it is assumed for simplicity that the joints are randomly distributed, and that each partition volume contains one joint only.

5.2 Transformation of design parameters of EOL product to liberation matrix

Transformation matrices were defined to relate the design parameters of the product to the liberation level of the product's mineral description. A transformation matrix establishes a relationship between a joint of determined joint class and dimensions and an amount of material corresponding to the volume $L^3\ m^3$. Specific transformation matrices are defined for each joint class and mineral. The transformation matrices for all P joints are coincidently the same. For each individual joint of the L and S joint classes, the transformation matrix is defined using an algorithm based on the data on the thickness ratio of the materials.

5.3 Generating the liberation matrix

Since all pseudo-particles of end of life electronic products before shredding belong to the largest size class, the liberation level information obtained in the above step can be used directly to generate the liberation matrix before shredding.

5.4 Calculation of the size transformation in the shredding process

The size class distribution transition before and after shredding is calculated using 4.1 with the constraint condition 4.2.

5.5 Calculation of the liberation transition of the particles in the shredding process

Liberation transformation in the shredding process is considered to be affected by three factors in this model: size, liberation, and dispersion. For the liberation matrix transition, each element in the liberation matrix before shredding will split into fractions that will go to different elements of the liberation matrix after shredding, see Figure 33.

Any specific element Lf_{32} in the liberation matrix before shredding theoretically will go to five different liberation classes after shredding. Lf_{32}^{11} is the fraction of Lf_{32} that makes up part of the

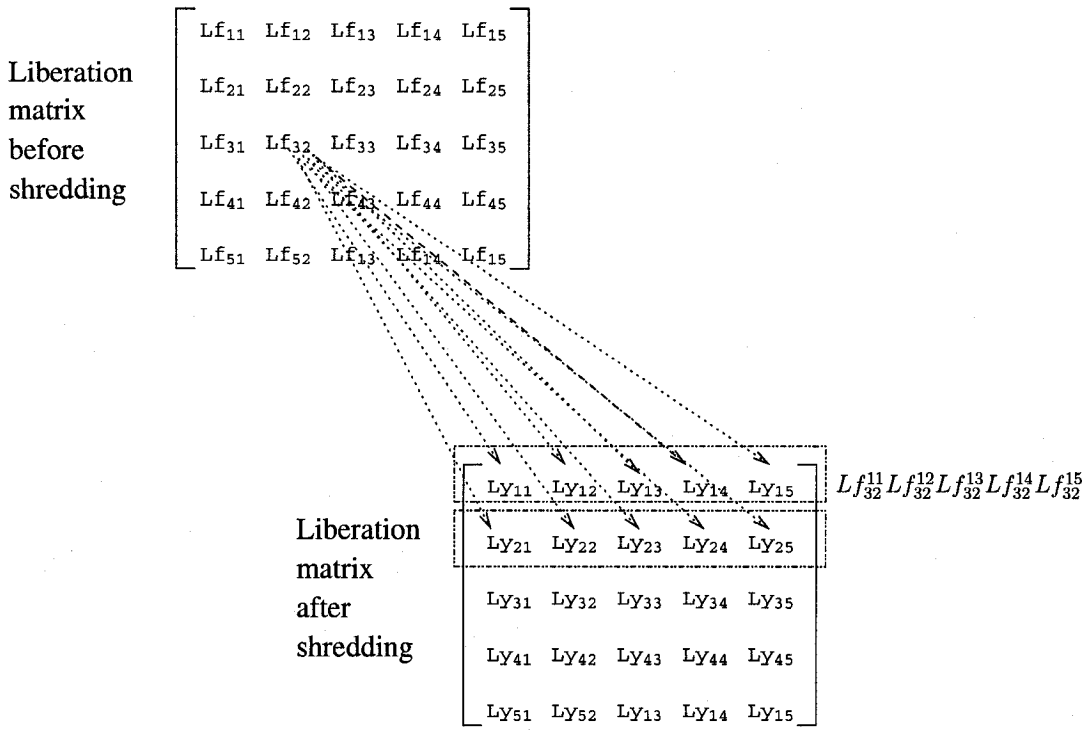

Figure 33: Liberation matrix transition in shredding process

element Ly_{11} of the liberation matrix after shredding, Lf_{32}^{12} is the fraction of Lf_{32} that makes up part of the element Ly_{12} of the liberation matrix after shredding, and so on. Let

$$Ly_{32}^{1} = Ly_{32}^{11} + Ly_{32}^{21} + \quad Ly_{32}^{31} + Ly_{32}^{41} + Ly_{32}^{51} \tag{5.1}$$

$$Ly_{32}^{2} = Ly_{32}^{12} + Ly_{32}^{22} + \quad Ly_{32}^{32} + Ly_{32}^{42} + Ly_{32}^{52} \tag{5.2}$$

$$\cdots$$

$$Ly_{32}^{5} = Ly_{32}^{15} + Ly_{32}^{25} + \quad Ly_{32}^{35} + Ly_{32}^{45} + Ly_{32}^{55} \tag{5.3}$$

The distribution density of Lf_{32}^{l} is assumed to be normal:

$$Lf_{32}^{l} = k \cdot \frac{1}{\sigma\sqrt{2\pi}} exp(-\frac{(x-l)^2}{2\sigma^2}) \tag{5.4}$$

where l is liberation level, and k is the coefficient which for any size class s should conserve

$$\int_0^1 k \cdot Lf_{32}^{l} dl = 1 \tag{5.5}$$

The variance σ^2 corresponds to the reciprocal of the dispersion of particles within a specific size class and liberation class (assumed to be a function of liberation class and size class). Then we have

$$Ly_{32}^{1} = \int_0^{0.05} Lf_{32}^{l} dl \tag{5.6}$$

$$Ly_{32}^{2} = \int_{0.05}^{0.3} Lf_{32}^{l} dl \tag{5.7}$$

$$\cdots$$

$$Ly_{32}^{5} = \int_{0.9}^{1} Lf_{32}^{l} dl \tag{5.8}$$

Applying (5.6)-(5.8) to each of 25 elements in the liberation matrix before shredding and summing those terms with the same liberation index "l", we can get the below equations

$$Ly^{1} = K1 \tag{5.9}$$

$$Ly_{2}^{2} = K2 \tag{5.10}$$

$$\cdots$$

$$Ly_{5} = K5 \tag{5.11}$$

where $K1, K2, \cdots, K5$ are calculation numerical values.

The statistical distribution entropy of the liberation matrix after shredding can be expressed as below

$$\text{Entropy}_{\text{row1}} = -\sum_{i=1}^{5} Ly_{1i} \cdot Log(Ly_{(1i)}) \tag{5.12}$$

$$\text{Entropy}_{\text{row2}} = -\sum_{i=1}^{5} Ly_{2i} \cdot Log(Ly_{(2i)}) \tag{5.13}$$

$$\cdots$$

$$\text{Entropy}_{\text{row5}} = -\sum_{i=1}^{5} Ly_{5i} \cdot Log(Ly_{(5i)}) \tag{5.14}$$

After the shredding process, (5.12)–(5.14) will try to reach their maximum values. Combining equations (4.1)–(4.4) and equations (5.9)–(5.14), a problem to find the minimum of a contrained nonlinear multivariable function can be constructed. The problem is specified by

$$\begin{aligned} &\min_{x} f(x) \quad subject\ to \\ &A \cdot x \leq b \\ &Aeq \cdot x = beq \\ &0 \leq x \leq 1 \end{aligned}$$

where x is the element of the liberation matrix after shredding and function $f(x)$ and matrices A and Aeq and vectors b and beq can be worked out from those equations discussed above. This problem can be solved by the MATLAB toolbox function fmincon. The simulation example is given in the next chapter.

CHAPTER 6

FEM NUMERICAL SHREDDING

In this chapter, an FEM-based numerical "pseudo-shredder" is developed. This is one of the contributions of this thesis since in previous models, how to get the size distribution after shredding is not clear. At the same time, the liberation distribution calculated from FEM simulaton can serve as a kind of experimental data to evaluate the effectiveness of the shredder model in Chapter 5. This numerical pseudo-shredder is built on a solid mechanics model which is different from the computer models discussed in previous chapters. The "shredding force" for this shredder is generated randomly both in magnitude and orientation, and a finite element method is used to calculate the stresses.

The end of life electronic product which will be shredded is assumed to be a cell phone. Some assumptions and simplications about this cell phone are made before this "numerical shredding". The assumed geometry and materials of different part of this cell phone are detailed in the following paragraphs. Based on this information, we can generate the size distribution matrix and liberation distribution matrix before shredding. After that an FEM model based on fundamental solid mechanics is built. Using this FEM model, we can calculate the size distribution matrix and liberation distribution matrix after shredding. The calculation results of are treated as experimental data to evalute the shredder simulation model of Chapter 5. The FEM model is coded in MATLAB and a Java script is written to generate the grid for the FEM algorithm.

6.1 Simplifications and assumptions

The following simplifications and assumptions are made for the simplified cell phone (Figure 34) in building the simulation model:

1. The simulation is assumed to be a two-dimensional problem.
2. The cell phone is assumed to be a rectangle with two rectangles with different material properties attached on it.
3. The interaction between the cell phone and shredder can be modelled as random forces (some statistical rules may apply) applied on the cell phone.
4. The forces transferred from the shredder knife to the cell phone can be substitued by the equivalent node forces of random magnitude acting at a random orientation (denoted by a random angle θ).
5. The fracture mechanism for all materials assumes that cracks will be initiated along the direction perpendicular to the principal stress acting line (when this exceeds the maximum strength) and will propagate until they hit the boundary of the cell phone or another crack which propagates to the intersection first.
6. The shredding process is treated as a plane stress problem.

6.2 Procedure

The following are the steps required to build the FEM model. After the model is constructed the shredding results of the numerical experiment can be obtained.

6.2.1 Geometrical description of the theoretical shredded cell phone

1. The EOL cell phone to be shredded is assumed to be a rectangle of material A with coordinates: lower left (0,0), size (10,4). This simplicity makes the simulation simple without losing the generality of the simulation method.
2. One part of the cell phone is assumed to be a small rectangle of material B attached to the cell phone with coordinates: lower left (4,0.8), size (1.3333,1.6).

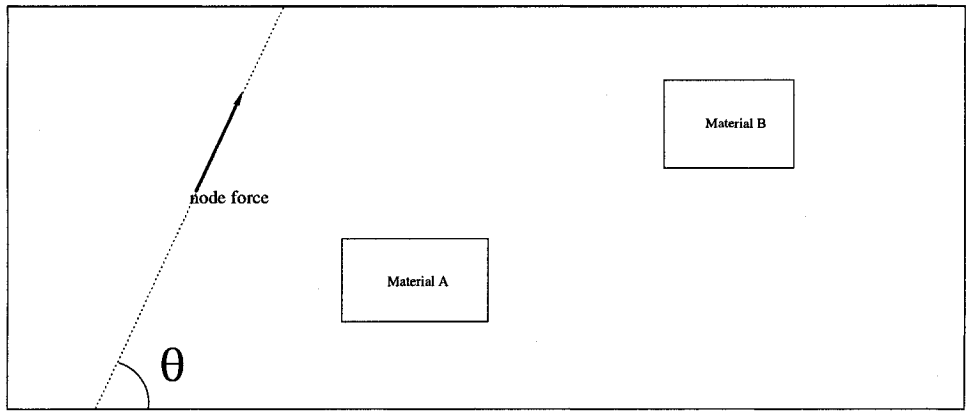

Figure 34: Theoretical shredded cell phone

3. Another part of the cell phone is assumed to be a small rectangle of material C attached to the cell phone with coordinates: lower left (6.6667, 2.4), size (1.3333,1.6).

4. For simplification, the three-part simplified cell phone suffices to illustrate the simulation method.

6.2.2 Material description of the theoretical shredded cell phone

Three different materials are involved in this "pseudo-shredding": matrix material high-impact polystyrene, component material copper and component material aluminum. The following lists their material property parameters that will be used in the FEM model.

6.2.2.1 Material A: PS-HI (Polystyrene, High Impact)

The source of data for material A is Web [2006*d*].

Property	Approximate Value	
	PS	PS-HI (High Impact)
Tensile Strength	55-80 MN/m^2	30-55 MN/m^2
Tensile Modulus	3-4 GN/m^2	2-3 GN/m^2
Elongation at Break	$<$10%	10-50%
Flexural Strength	50-100 MN/m^2	50-100%
Notched Impact Strength	$<$3KJ/m^2	3-15KJ/m^2
Specific Heat	1.25-1.70 KJ/kg/°C	1.25-1.70KJ/kg/°C
Glass Transition Temperature	100°C	100°C
Heat Deflection Temperature	$<$100°C	$<$100°C
Coefficient of Thermal Expansion	5-10$\times 10^{-5}$/°C	5-15$\times 10^{-5}$/°C
Long Term Service Temperature	70-85°	60-80°
Specific Gravity	1.0-1.2	1.0-1.2
Mould Shrinkage	0.001-0.005m/m	0.001-0.01m/m
Water Absorption	0.1-0.5%(50%rh)	0.1-0.5%(50%rh)
Transparency	Transparent	Opaque

Its chemical makeup is shown in Figure 35.

6.2.2.2 Material B: Copper

Web [2006*b*] is the source of data for material B.

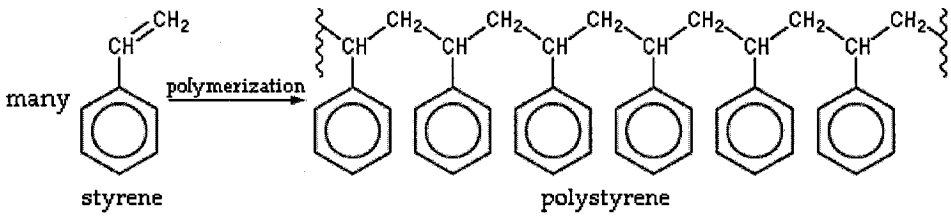

Figure 35: Chemical makeup of polystyrene

Density:	8800-8940kg/m^3
Melting Point:	1082°C
Elastic Modulus:	117GPa
Poisson's Ration:	0.34
Tensile Strength:	170-220MPa
Yield Strength:	62-69MPa
Percent Elongation:	40-50%
Hardness:	40-45(HB)

6.2.2.3 Material C: Aluminum

Data for material C comes from Web [2006*a*].

Material	Elastic Modulus (GPa)	Shear Modulus (GPa)	Poisson's Ratio	Yield Stress (MPa)	Ultimate Stress (MPa)	Elongation (%)
Aluminum [Al]	70	26	0.33	20	70	60

6.2.3 Calculation of the stress distribution using FEM

The procedures to calculate the stress distribution are discussed below. This is the FEM calculation based on solid mechanics, after which information can be collected to construct the particles after shredding.

1. Grid the cell phone. Choose a suitable coordinate system and number. Triangular elements are used in the FEM procedure (Figure 36) . For more details about FEM modelling, please refer to Rockey & Evans [1983].

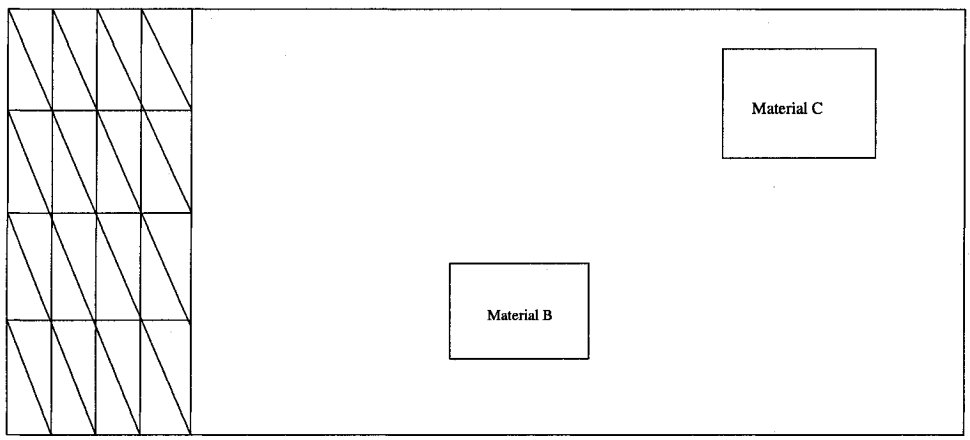

Figure 36: Gridding plan for the shredded cell phone

The Cartesian coordinate system used is shown in Figure 37, with three nodes numbered 1, 2, and 3 using an anti-clockwise convention. The positions of these nodes in terms of the Cartesian coordinates are (x_1, y_1), (x_2, y_2), and (x_3, y_3).

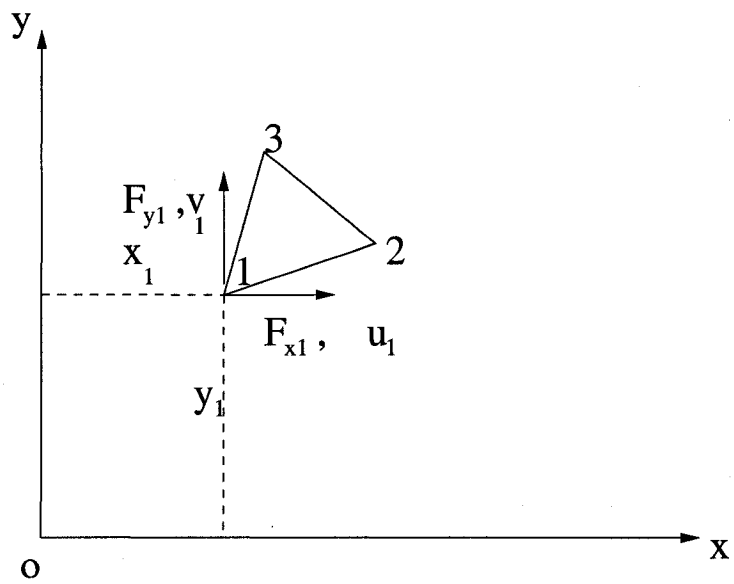

Figure 37: Coordinate system

2. Choose a displacement function $[f(x, y)]$ that defines the displacement $\delta(x, y)$ at any point in an element.

3. Express the displacement $\delta(x, y)$ within the element in terms of nodal displacements δ^e.

4. Relate strains $\varepsilon(x, y)$ at any point in the element to displacements $\delta(x, y)$ and hence to nodal displacements δ^e.

5. Relate internal stresses $\sigma(x, y)$ to strains $\varepsilon(x, y)$ and to nodal displacements δ^e.

6. Replace internal stresses $\sigma(x, y)$ with statically equivalent nodal forces F^e. Relate nodal forces to nodal displacements δ^e and hence obtain element stiffness matrix $[K^e]$.

7. Establish the stress-displacement matrix $[H]$.

8. Calculate the stress distribution of the shredded cell phone.

9. Calculate the principal stress of the shredded cell phone.

10. Pick up those points whose pricipal stresses exceed the strength of the material and record those points with their stress information.

11. Construct the physical particle based on stress information. The initial particle boundary before shredding and final particle "cut line" after shredding are combined to construct the particles after shredding.

6.3 Simulation example

Figure 38 presents the configuration of the FEM progam. Other parameters and calculation results of a simulation example are discussed in the following.

6.3.1 Gridding plan

Figure 39 shows the gridding plan generated by Java based on the information discussed above.

6.3.2 Applied load

The shredder load applied to the cell phone is assumed to be a random force vector because we do not have enough information about the interaction between shredder blade and shredded materials inside shredder. The force vector is constructed to pair x and y components of node force for each node from node 1 to node 96:(Figure 40)

6.3.3 Shredding result

Figure 41 presents the shredding result of the "numerical shredder". This is the calculation result by FEM method based on assumptions and parameters assumed earlier in this chapter. The blue lines in Figure 41 are the "cut lines" of the shredded cell phone, that means material will separate along those lines after shredding.

Combining this information with the initial particle boundaries, particles after shredding can be constructed.

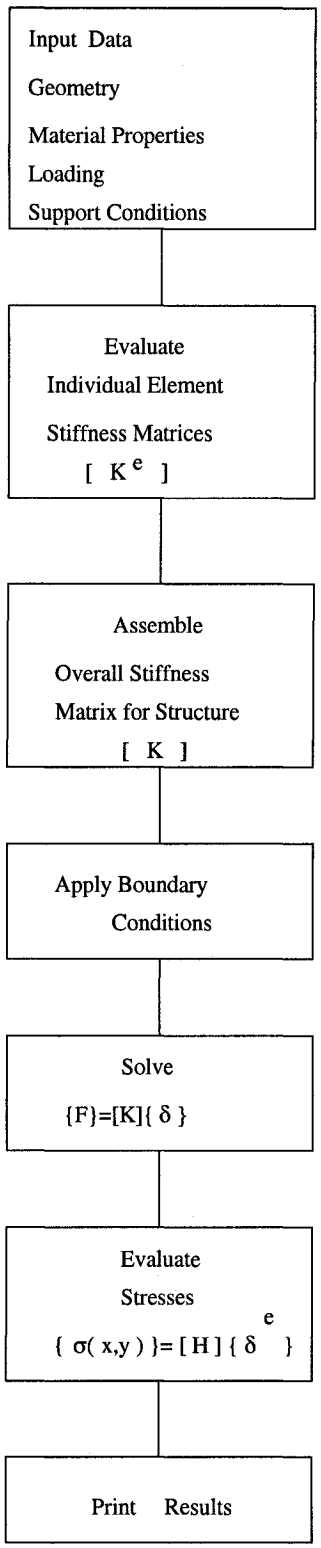

Figure 38: Flow chart of the computer program for the solution of the finite element method

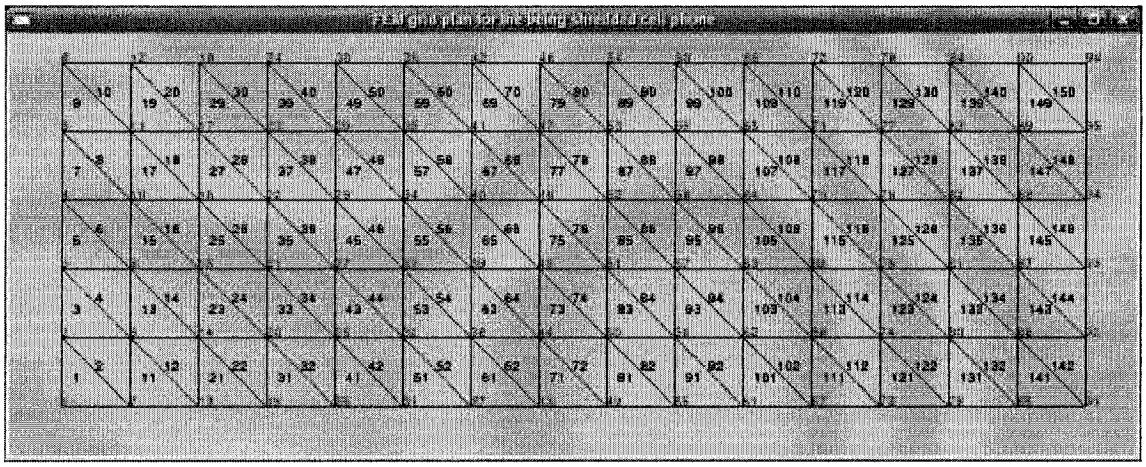

Figure 39: Element and node number system for FEM of the shredded phone

F = [-0.3138 -0.2711 0.4205 -0.4280 -1.4832 0.0742 0.6438 -0.4523 2.0592 -0.0573 -0.2383 0.2671
-0.1763 -1.1569 -1.2037 -0.1404 0.8339 0.1079 0.2768 -0.1536 1.9851 0.6458 -0.4631 0.8419 0.1506
0.0413 -0.3795 0.0543 0.0868 -1.1182 1.0756 -1.9010 -1.4493 -0.8723 0.8092 -0.6161 0.7637 -0.3663
-0.3253 -0.3645 -1.2243 -1.3630 -1.2222 -0.3390 0.6735 -1.2530 -1.1344 0.7602 -1.6144 0.0387
-2.3541 -1.3719 -0.7570 -1.2380 1.9273 0.0733 0.4805 0.9248 -0.5644 -0.4675 1.5315 1.1259 0.8663
0.6447 0.5315 -1.0223 -0.0364 -0.5450 -0.0915 1.2929 -0.3044 0.2936 -0.7568 -1.0763 -1.4717 1.6672
0.4392 1.1296 0.8349 0.8164 -0.7689 1.2655 -1.4576 0.1141 2.3012 -0.9264 0.7399 -1.2026 1.2001
0.3796 -0.2564 0.8979 0.0913 -0.1863 0.3483 0.6505 1.3026 -0.5538 0.2646 -1.2080 -0.6241 0.0569
1.3614 1.6597 2.2170 -0.5030 0.6141 0.7943 -0.8401 -1.7130 -0.2200 -0.0469 -1.4466 1.5455 1.1429
-1.6563 0.0820 0.7817 -0.2441 -0.9951 0.3931 -2.0684 -0.6561 -0.7869 0.0868 -1.5503 -0.4552 2.1685
-2.4084 -0.5863 0.3634 0.3385 1.7983 1.3369 0.3598 0.7758 1.6272 -0.9807 -0.9230 0.2325 -0.6368
1.3296 0.2455 -1.7169 0.5202 -0.4369 -1.0749 0.1516 0.3663 -0.5803 -0.5214 0.8384 -1.2093 -1.6731
1.2364 -1.2359 -0.4669 -1.0723 0.4633 -0.2652 -1.1811 -2.1277 2.4852 1.3532 1.2796 -0.7893 -0.9955
1.0413 -1.7720 0.0561 -0.2933 -0.7310 -0.1309 -0.8991 -0.5078 -0.5691 -0.3940 0.3585 1.5426
0.3861 -0.1829 0.0831 0.7680 -0.6294 -1.1220 0.8691 0.1201 0.9099 1.5699 -0.5329 0.0936 -0.2528]

Figure 40: Applied load

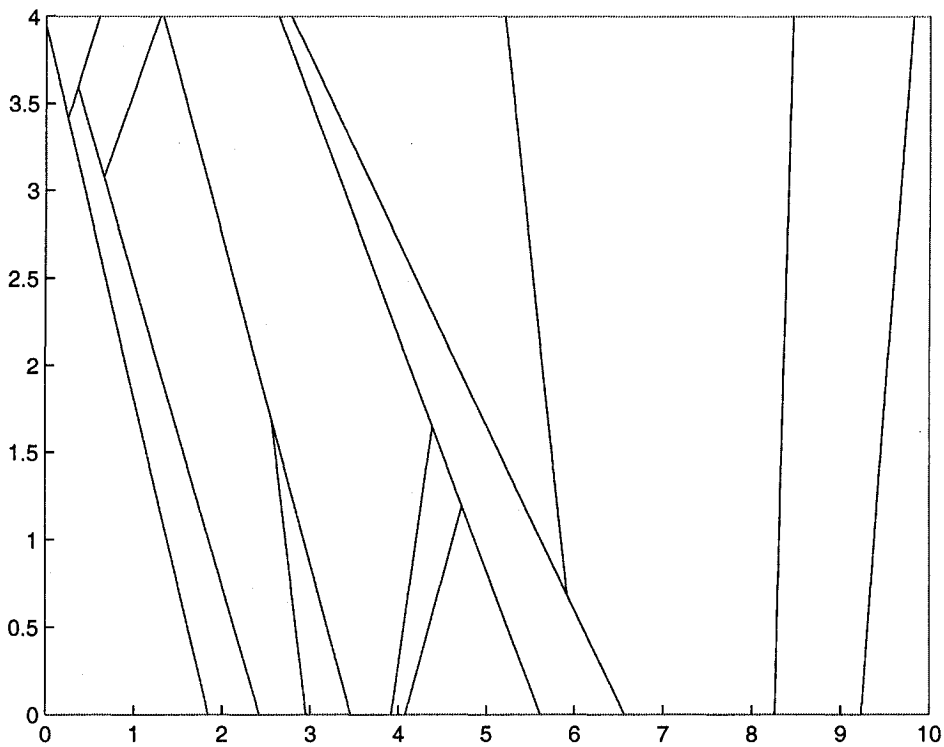

Figure 41: Shredding result of the FEM simulation

CHAPTER 7

SIMULATION WITH THE SHREDDER MODEL

In this chapter, an abstracted model of a cell phone is proposed to simulate the shredding process using the proposed shredder model. The simulation results will be compared with the results of a numerical experiment.

7.1 Description of the cell phone to be shredded

The following is the basic information about the cell phone in the simulation of the shredder model.

1. Materials: The abstracted cell phone is composed of three materials. Material A is high impact polystyrene, material B is copper and material C is aluminum.
2. Sizes and positions of materials: Material A is the matrix material. It is a rectangle ten units in length and four in height with lower left corner coordinates (0,0). Material B is a rectangle of size 1.3333 in length and 1.6 in height with the lower left corner at the point (4, 0.8). Material C is a rectangle of size 1.3333 in length and 1.6 in height with lower left corner at the point (6.6667, 2.4).
3. Mesh size: The following mesh size series are used for size (based on length) classification. Size class 1 contains particles of size greater than 2 units. Size class 2 contains particles between 2 and 1.414 units. Size class 3 contains particles between 1.414 and 1. Size class 4 contains particles between 1 and 0.707, and size class 5 contains all sizes less than 1.

7.2 Data preparation for the shredder model

The geometry layout for the cell phone outlined in Figure 42 prepares the input data for the shredder simulation model. According to this partitioning scheme, sieve series with size (1.4142, 1.1892,

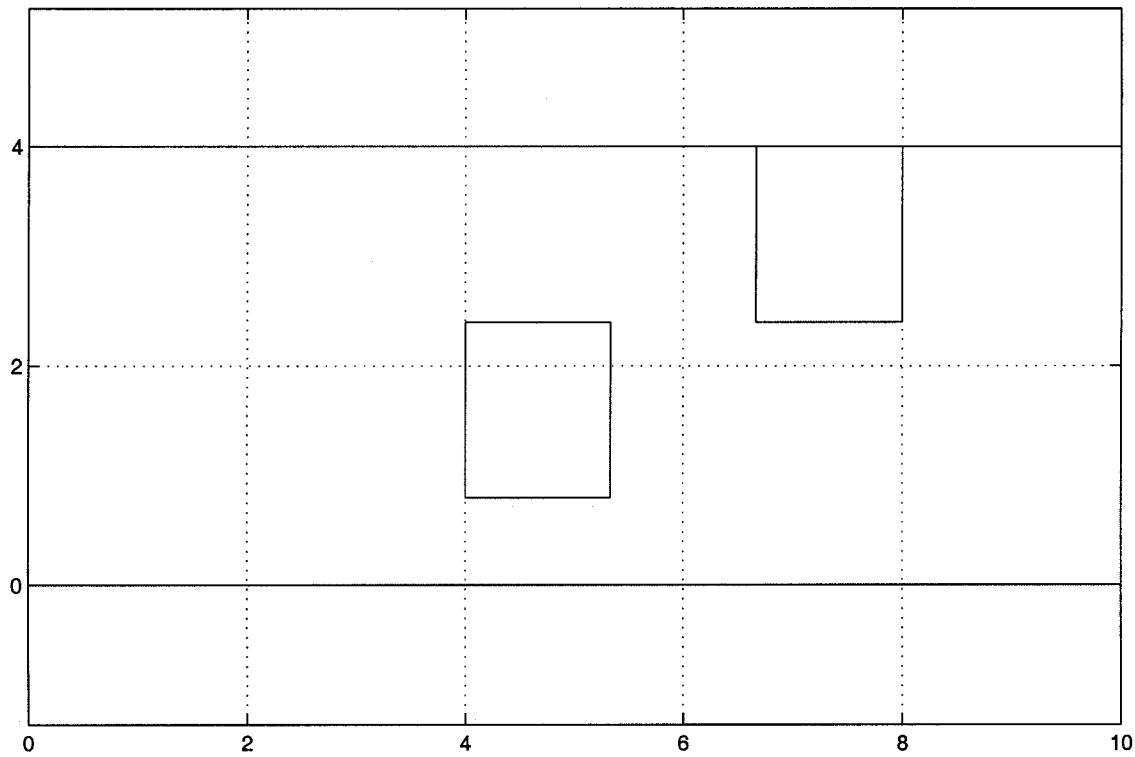

Figure 42: Partitioning scheme for the cell phone.

1.0905, 1.0443, 1.0219) are taken, the liberation class series is defined (liberation class 1, 0–5% secondary material, liberation class 2, 5–30% secondary material, liberation class 3, 30–60% secondary material, liberation class 4, 60–90% secondary material, liberation class 5, 90–100% secondary material), and the input data to the shredder are as follows:

1. Properties of material A, B and C. Please refer to chapter 6 for the physical properties for these materials. The density for material A is taken as 1100 kg/m^3, density for material B is taken as 8900 kg/m^3 and density of material C is taken as 2700 kg/m^3.

2. The size class distribution for minerals consisting of materials A and B is:

$$\text{Size}_{AB}^{\text{input}} = \begin{bmatrix} 36 \\ 0 \\ 0 \\ 0 \\ 0 \end{bmatrix} \tag{7.1}$$

The size class distribution for minerals consisting of materials A and C is:

$$\text{Size}_{AC}^{\text{input}} = \begin{bmatrix} 32 \\ 0 \\ 0 \\ 0 \\ 0 \end{bmatrix} \tag{7.2}$$

3. The liberation distribution for minerals consisting of materials A and B is:

$$\text{Liberation}_{AB}^{\text{input}} = \begin{bmatrix} 0.7778 & 0.0000 & 0.1111 & 0.0000 & 0.1111 \\ 0.0000 & 0.000 & 0.0000 & 0.0000 & 0.0000 \\ 0.0000 & 0.0000 & 0.0000 & 0.0000 & 0.0000 \\ 0.0000 & 0.0000 & 0.0000 & 0.0000 & 0.0000 \\ 0.0000 & 0.0000 & 0.0000 & 0.0000 & 0.0000 \end{bmatrix} \tag{7.3}$$

Liberation distribution for minerals consist of material A and material C is:

$$\text{Liberation}_{AC}^{\text{input}} = \begin{bmatrix} 0.8750 & 0.0000 & 0.0000 & 0.1250 & 0.0000 \\ 0.0000 & 0.000 & 0.0000 & 0.0000 & 0.0000 \\ 0.0000 & 0.0000 & 0.0000 & 0.0000 & 0.0000 \\ 0.0000 & 0.0000 & 0.0000 & 0.0000 & 0.0000 \\ 0.0000 & 0.0000 & 0.0000 & 0.0000 & 0.0000 \end{bmatrix} \tag{7.4}$$

7.3 Calculation of the size distribution evolution and liberation distribution evolution

According to (4.1), we can get the size distribution as in Figure 43. Using Scion Imaging® software, the size distribution matrix can be extracted from Figure 43 (a MATLAB script sizedisgem.m is written to calculate the size distribution matrix) as the following:

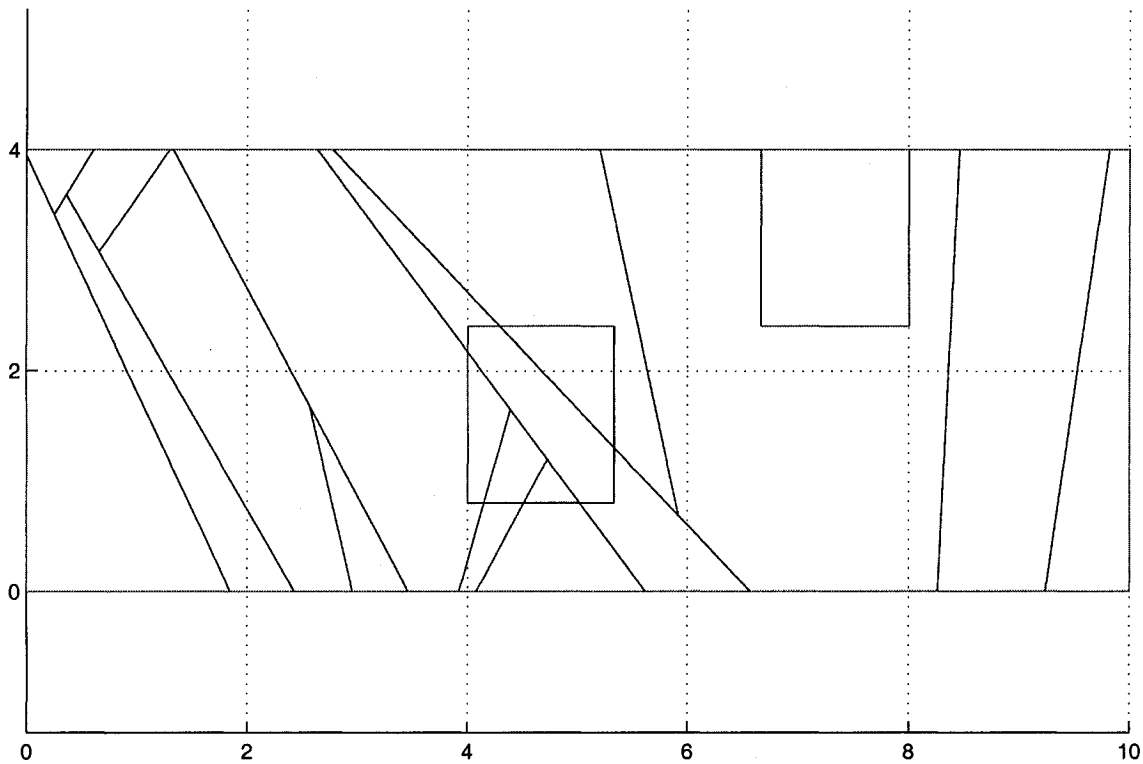

Figure 43: Calculation graph of the simulation result

1. The size class distribution for the mineral consisting of materials A and B is:

$$\text{Size}_{AB}^{\text{output}} = \begin{bmatrix} 18.5063 \\ 1.5949 \\ 3.7975 \\ 1.1646 \\ 10.7276 \end{bmatrix} \tag{7.5}$$

2. The size class distribution for the mineral consisting of materials A and C is:

$$\text{Size}_{AC}^{\text{output}} = \begin{bmatrix} 19.8734 \\ 1.5949 \\ 2.4810 \\ 0 \\ 7.8567 \end{bmatrix} \tag{7.6}$$

The liberation dispersion matrix before shredding for the mineral consisting of materials A and B is assumed to be

$$\text{Dispersion}_{AB} = \begin{bmatrix} 10.501 & 8.6210 & 7.1543 & 5.0571 & 1.5789 \\ 3.3114 & 5.5647 & 8.9194 & 10.355 & 4.5287 \\ 7.0684 & 1.1850 & 10.218 & 10.169 & 9.1317 \\ 5.8598 & 9.2141 & 8.3821 & 5.1027 & 1.0986 \\ 9.9130 & 5.4470 & 2.7627 & 9.9365 & 2.3889 \end{bmatrix} \tag{7.7}$$

The liberation dispersion matrix before shredding for the mineral consisting of materials A and C is assumed to be

$$\text{Dispersion}_{AC} = \begin{bmatrix} 1.4905 & 10.327 & 3.0927 & 4.1930 & 2.9984 \\ 8.5534 & 2.3098 & 5.5509 & 4.7490 & 1.4949 \\ 9.9481 & 10.408 & 1.8107 & 9.6780 & 6.6671 \\ 3.8615 & 8.0185 & 9.5112 & 4.7218 & 2.2192 \\ 3.5120 & 9.4768 & 6.6205 & 1.7369 & 6.2211 \end{bmatrix} \tag{7.8}$$

The composition matrix for element **Cu** of the mineral consisting of material A and material B is assumed to be

$$\text{Composition}_{AB} = \begin{bmatrix} 0 \\ 0.15 \\ 0.45 \\ 0.75 \\ 0.95 \end{bmatrix} \tag{7.9}$$

The compostion matrix for element **Al** of the mineral consist of materials A and C is assumed to be

$$\text{Composition}_{AC} = \begin{bmatrix} 0 \\ 0.15 \\ 0.45 \\ 0.75 \\ 0.95 \end{bmatrix} \tag{7.10}$$

According to 4.3, we have the following equation for the mineral consisting of materials A and B:

$$\begin{aligned} 5.5980 - (&2.78 \times l12 + 8.33 \times l13 + 13.9 \times l14 + 17.6 \times l15 + .239 \times l22 + .718 \times l23 + \\ &1.20 \times l24 + 1.52 \times l25 + .570 \times l32 + 1.71 \times l33 + 2.85 \times l34 + 3.61 \times l35 + \\ &.175 \times l42 + .524 \times l43 + .874 \times l44 + 1.11 \times l45 + 1.61 \times l52 + 4.83 \times l53 + \\ &8.05 \times l54 + 10.2 \times l55) = 0 \end{aligned} \tag{7.11}$$

and the following equation for the mineral consisting of materials A and C:

$$\begin{aligned} 3 - (&2.98 \times lc12 + 8.94 \times lc13 + 14.9 \times lc14 + 18.9 \times lc15 + .239 \times lc22 + .718 \times lc23 + \\ &1.20 \times lc24 + 1.52 \times lc25 + .372 \times lc32 + 1.12 \times lc33 + 1.86 \times lc34 + 2.36 \times lc35 + \\ &1.18 \times lc52 + 3.54 \times lc53 + 5.89 \times lc54 + 7.46 \times lc55) = 0 \end{aligned} \tag{7.12}$$

The dispersion matrix's effect on liberation is given by the following matrix, calculated by the MATLAB program libdism.m:

$$\text{DispLib}_{AB} = \begin{bmatrix}
0.8119 & 0.1881 & 2.887 \times 10^{-15} & 0.0 & 0.0 \\
0.01476 & 0.9846 & 0.0005950 & 4.502 \times 10^{-11} & 0.0 \\
3.657 \times 10^{-13} & 0.003573 & 0.4964 & 0.5000 & 0.00000003725 \\
0.0 & 0.000000005846 & 0.00007157 & 0.5003 & 0.4948 \\
0.0001712 & 0.008410 & 0.03262 & 0.3292 & 0.4940 \\
0.3219 & 0.6654 & 0.01258 & 0.0001876 & 0.0000000004806 \\
0.06450 & 0.9170 & 0.01853 & 0.00001455 & 0.0 \\
0.0 & 0.0003988 & 0.4996 & 0.5000 & 9.915 \times 10^{-12} \\
0.0 & 0.0 & 3.442 \times 10^{-15} & 0.5000 & 0.5000 \\
0.0 & 1.118 \times 10^{-13} & 0.000000009652 & 0.01622 & 0.6832 \\
0.6243 & 0.3757 & 0.0000001064 & 1.554 \times 10^{-15} & 0.0 \\
0.08294 & 0.4335 & 0.2124 & 0.2238 & 0.04294 \\
0.0 & 0.00006103 & 0.4999 & 0.5000 & 7.716 \times 10^{-15} \\
0.0 & 0.0 & 1.033 \times 10^{-14} & 0.5000 & 0.5000 \\
0.0 & 0.0 & 0.0 & 0.000002687 & 0.5722 \\
0.5373 & 0.4627 & 0.00001050 & 3.849 \times 10^{-11} & 0.0 \\
0.01019 & 0.9895 & 0.0002657 & 2.122 \times 10^{-12} & 0.0 \\
0.0 & 0.0008119 & 0.4992 & 0.5000 & 0.0000000001458 \\
0.0 & 0.000000004316 & 0.00006227 & 0.5003 & 0.4951 \\
0.003909 & 0.05475 & 0.08639 & 0.3755 & 0.3800 \\
0.7859 & 0.2141 & 9.026 \times 10^{-14} & 0.0 & 0.0 \\
0.06715 & 0.9122 & 0.02068 & 0.00002144 & 1.110 \times 10^{-16} \\
0.001889 & 0.1468 & 0.3509 & 0.4816 & 0.01863 \\
0.0 & 0.0 & 3.941 \times 10^{-14} & 0.5000 & 0.5000 \\
0.00000004690 & 0.00008033 & 0.002148 & 0.1848 & 0.6224
\end{bmatrix} \quad (7.13)$$

$$\text{DispLib}_{AC} = \begin{bmatrix}
0.1482 & 0.5896 & 0.1697 & 0.08766 & 0.004693 \\
0.004766 & 0.9952 & 0.00005158 & 4.108 \times 10^{-15} & 0.0 \\
0.0007220 & 0.1215 & 0.3776 & 0.4901 & 0.009967 \\
9.270 \times 10^{-14} & 0.000001130 & 0.0008102 & 0.5013 & 0.4843 \\
9.643 \times 10^{-12} & 0.0000007988 & 0.0001317 & 0.1026 & 0.6707 \\
0.7163 & 0.2837 & 0.0000000001259 & 0.0 & 0.0 \\
0.1099 & 0.6516 & 0.1875 & 0.05070 & 0.0003154 \\
0.00000001287 & 0.01844 & 0.4816 & 0.5000 & 0.00001495 \\
0.0 & 0.00000004242 & 0.0001779 & 0.5006 & 0.4921 \\
0.0003256 & 0.01230 & 0.04017 & 0.3419 & 0.4759 \\
0.7875 & 0.2125 & 7.383 \times 10^{-14} & 0.0 & 0.0 \\
0.004496 & 0.9955 & 0.00004550 & 2.554 \times 10^{-15} & 0.0 \\
0.01456 & 0.2191 & 0.2590 & 0.4247 & 0.07710 \\
0.0 & 0.0 & 1.698 \times 10^{-13} & 0.5000 & 0.5000 \\
0.0 & 0.0 & 0.0 & 0.0005202 & 0.6258 \\
0.3716 & 0.6247 & 0.003673 & 0.00001326 & 3.886 \times 10^{-13} \\
0.02096 & 0.9778 & 0.001287 & 0.0000000008216 & 0.0 \\
0.0 & 0.0001743 & 0.4998 & 0.5000 & 4.265 \times 10^{-13} \\
1.110 \times 10^{-16} & 0.00000005026 & 0.0001923 & 0.5006 & 0.4918 \\
0.0000003513 & 0.0002451 & 0.004194 & 0.2137 & 0.6022 \\
0.3402 & 0.6516 & 0.008192 & 0.00007449 & 4.044 \times 10^{-11} \\
0.008582 & 0.9912 & 0.0001832 & 5.151 \times 10^{-13} & 0.0 \\
1.585 \times 10^{-11} & 0.006400 & 0.4936 & 0.5000 & 0.0000003203 \\
0.0007043 & 0.02774 & 0.08210 & 0.4694 & 0.3577 \\
0.0 & 0.0 & 3.997 \times 10^{-15} & 0.001161 & 0.6380
\end{bmatrix} \tag{7.14}$$

The statistical entropy of the liberation distribution after shredding can be used as the objective function. Using MATLAB's fmincon function, the liberation matrices 7.15 and 7.16 after shredding can be calculated. The liberation matrices before shredding can be used as the starting point for fmincon.

The liberation matrix for the mineral consisting of materials A and B is:

$$Liberation_{AB} = \begin{bmatrix} 0.6221 & 0.3031 & 0.07242 & 0.001000 & 0.001362 \\ 0.2391 & 0.2284 & 0.1971 & 0.1754 & 0.1599 \\ 0.2981 & 0.2545 & 0.1900 & 0.1417 & 0.1157 \\ 0.2277 & 0.2162 & 0.2001 & 0.1834 & 0.1726 \\ 0.4821 & 0.3181 & 0.1381 & 0.06076 & 0.001000 \end{bmatrix} \tag{7.15}$$

The liberation matrix for the mineral consisting of materials A and C is given by:

$$Liberation_{AC} = \begin{bmatrix} 0.8074 & 0.1809 & 0.009722 & 0.001000 & 0.001000 \\ 0.2743 & 0.2458 & 0.1935 & 0.1526 & 0.1338 \\ 0.3181 & 0.2680 & 0.1811 & 0.1306 & 0.1022 \\ 0.0000 & 0.0000 & 0.0000 & 0.0000 & 0.0000 \\ 0.5590 & 0.3042 & 0.09219 & 0.03064 & 0.01390 \end{bmatrix} \tag{7.16}$$

CHAPTER 8

EXPERIMENTAL PROCEDURE TO VERIFY THE SHREDDER MODEL

In this chapter, an experimental procedure which can be used to collect and analyze the shredding data and validate the effectiveness of the shredder model is proposed. In the shredding process, the end of life electronic products are comminuted, their sizes are reduced and "mineral ingredients" are liberated. The most important characteristics in shredding evolution are size distribution transition and composition liberation distribution transition. Thus those data which are to be collected are size distribution and liberation distribution of end of life electronic products before and after shredding. Because of the characteristics of shredded particles, image analysis is proposed here as an appropriate measure to analyze shredding data and evaluate the shredder model. The fundamental knowledge of image analysis and basic calculation formulas are introduced here and the transformation of the 2D image data to real world 3D data is proposed.

8.1 Mineral liberation during the shredding process

Recovery of materials from end of life electronic products is based on methods that separate particles on the basis of their physical or chemical properties. Individual materials can be separated completely only if each particle contains only one mineral. Two materials in the same particle can never be separated using physical separation alone. Separating materials at the particulate level is referred to as liberation since the individual material flows are liberated from each other in a physical way.

In practice, however, the comminution processes that are used to reduce mineralogical raw materials to the particulate state are, for the most part, unselective and, apart from a few unusual cases, the particles that are formed consist of mixtures of the mineral components that are present in original ore. During

comminution there is, however, a natural tendency towards liberation and particles that are smaller than the mineral grains that occur in the ore can appear as a single mineral. This happens when the particle is formed entirely within a mineral grain [Web 2006*g*]. Obviously this will occur more frequently the smaller the particle size and it is impossible when the particle is substantially larger than the mineral grains in the ore. Mineralogical textures have indeterminate geometries which are to a greater or lesser extent random in size, shape, orientation, and position. The mineralogical scale of a mineralogical texture is difficult to specify and often the different mineral components are present in the texture at vastly different size scales. In spite of this it is useful to regard each mineral as having a characteristic size that is commensurate with the size of individual grains in the texture. It is not possible to assign a definite value to this size because every mineral grain will be different in size and shape. Except in the most regular crystalline structures, it is not possible to assign a unique size to a grain of irregular shape. In spite of this, the concept of grain size is useful in that it provides some idea of the size to which the material must be reduced by comminution in order to achieve liberation of the phase. The concept of some characteristic grain sizes has been used in a semi-quantitative sense for many years in mineral processing and this concept is developed here by using a hypothetical liberation size as the main parameter in the development of a quantitative model for mineral liberation during comminution.

8.2 Characterisation of chemical composition by image analysis

Because the texture of the shredded end of life electronic product particles are so irregular in their geometrical construction, it is possible to characterise the texture only in terms of its statistical properties. This requires that many individual observations must be made and the relevant statistical properties of the texture must be estimated from these observations. Figure 44, Figure 45 and Figure 46 contain images of some mineral textures.

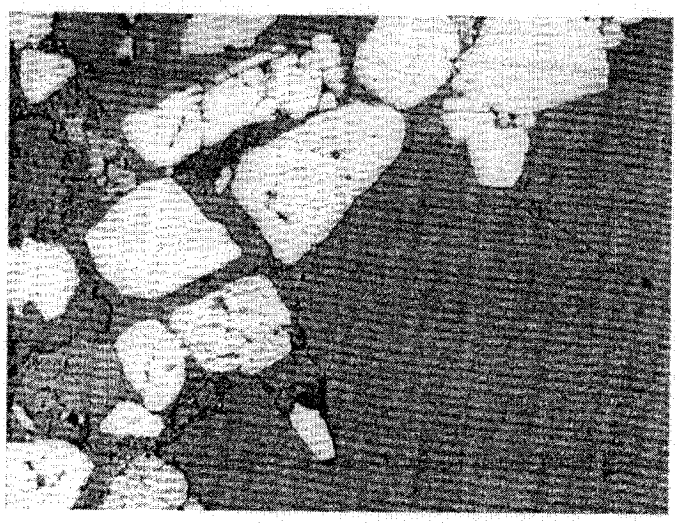

Figure 44: Typical image of a section through mineral-bearing ore. Bright phase is pyrite, gray phase are silicates.

Figure 45: Texture of coal. Bright phase is pyrite, gray phase is ash-forming mineral matter and dark phase is the desired carbonaceous material.

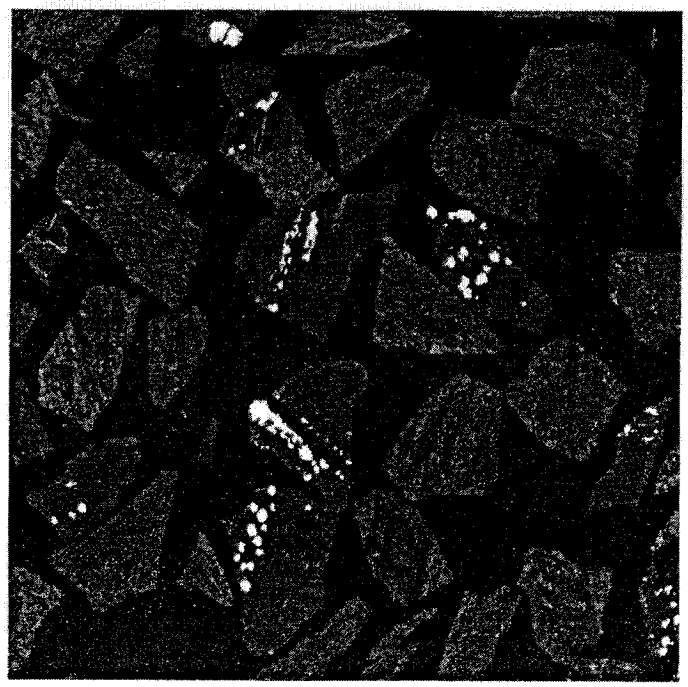

Figure 46: Coal particles that were formed by comminution of the texture shown in Figure 45

The most useful properties to measure are those that will give some measure of the nature of the particles that are formed during shredding. Unfortunately it is not possible to know in advance how any particular piece of ore will fragment during the comminution operations. The sizes and shapes of these particles are characterised by the distribution of linear intercepts which is determined by measuring the length of very many intercept lengths across the particles. This linear intercept pattern characterises the particle population and the linear intercept distribution can be used to generate the particle size distribution by solving the integral equation for the mesh size distribution density $p(D)$ [King 2001]:

$$P(l) = \bar{l} \int_0^\infty P(l|D) \frac{p(D)}{\bar{l}_D} dD \tag{8.1}$$

where $\bar{l}$ is the average intercept over the whole population and $\bar{l_D}$ is the conditional average intercept length for particles that have mesh size D. The kernel function $P(l|D)$ can be measured experimentally but usually only for a sample of particles in a mesh size interval such as $\sqrt{2}$ series. A function that has been found to be representative of particles that are typically found in the products of comminution operation is:

$$P(l|\Delta D_R) = 1 - \{1 - \frac{l}{1.2D_{i-1}}\} \exp\{-\frac{R^2 l}{1.2D_{i-1}}\} \quad \text{for } l \leq 1.2D_{i-1} \quad (8.2)$$

$$= 1.0 \quad \text{for } l > 1.2D_{i-1} \quad (8.3)$$

The conditional variable ΔD_R indicates that this distribution applies to a sample of particles in a mesh size interval rather than at a single size D.

The image of the unbroken assembly is sampled by superimposing linear samples drawn from the population defined by (8.1). Each linear sample will cover one or more of the phases and consequently can be characterised by its fraction of its length that covers the mineral phase.

The sample lengths can be sorted into sizes and the distribution of linear grades can be easily estimated for each different linear sample length which generates the conditional linear grade distribution for the shredded electronic product. This provides the necessary characterisation of the shredded electronic product texture from which its liberation characteristics can be calculated. The images that are used must be larger than the largest dimension of any texture characteristic of the shredded particles. This can be difficult to achieve if the size scales of the different materials in the shredded end of life products are greatly different. The image must be collected at sufficiently high resolution to capture all of the essential features of the texture of the finest material grains and at the same time they must reveal the full texture of the largest material grains. Generally this is not possible in a single image since the

field of view of any microscope is limited. This problem can usually be overcome by collecting images that are contiguous and then stitching these together to form a single long image from the sequence of smaller images. The linear sample lines can be sufficiently long to cover the largest feature in the texture while the full resolution of original image is maintained. The liberation distribution that can be expected when this end of life electronic product is comminuted can be calculated using the following two-step procedure.

In the first step the measured distribution of linear grades from the linear samples are combined with the linear intercept distribution density $p(l|D)$ of the particles that are expected to be formed during the shredding process. This produces the distribution of linear grades in particles of size D from the following equation [King 2001]:

$$P(g_L|D) = \int_0^\infty P(g_L|l)p(l|D)\,dl \tag{8.4}$$

This equation represents exactly the measurement of the linear grade distribution by sampling particle sections from size D.

8.3 Algorithm to transform the linear grades to 3-D grades

This section presents the algorithm to transform the distribution of linear grades that was calculated using 8.4 stereologically generating the distribution of grades in the real three-dimensional particles. The stereological transformation is a typical inverse problem and requires the solution of the integral equation

$$P(g_L|d_p) = \int_0^1 P(g_L|g, d_p)p(g|d_p)dg \tag{8.5}$$

The above equation can not be solved in a straightforward manner because the required solution is the function $P(g|D)$ that appears under the integral in the right hand side. However, appropriate solution methods are available and the solution can be generated easily using a number of computer software packages [King 2001].

The measured apparent grade distributions must be stereologically transformed to convert them to the desired grade distribution. The stereological transformation is typically an inverse problem and requires the solution of the integral (8.5), where g_L represents the measured apparent grade, either linear or areal, and g represents the true grade of a particle. $P(g_L|d_p)$ is the cumulative distribution of apparent grades that is measured in the image. The above equation provides the basis of calculating the distribution of volumetric grades $p_v(g_v|D)$ in a population of particles when the distribution of linear grades $P_l(g_L|D)$ has been measured or calculated from a theoretical model. It is convenient to use a matrix notation so that the above equation becomes

$$P_l = K p_v \tag{8.6}$$

where K is the 12×12 transformation kernel, P_l is the vector of 12 measured cumulative linear grades and p_v is the desired vector of fractional volumetric grades. The inherently ill-posed nature of the stereological correction problem is reflected in the very high condition number of the transformation matrix K so that the apparently straightforward solution by direct inversion

$$p_v = K^{-1} P_l \tag{8.7}$$

is useless because even very small errors in the measured distribution, which must always be present, are magnified by the inversion and swamp the true solution p_v. In spite of these difficulties, useful and reliable numerical solutions can be generated by imposing the following constraints on the solution given by

$$\sum_{i=1}^{12} p_v^i = 1.0 \tag{8.8}$$

and

$$p_v^i \geq 0 \text{ for } i = 1, 2...12 \tag{8.9}$$

with p_v^i representing the ith element of the vector p_v. The solution is obtained by imposing additional regularization conditions which reflect the relative smoothness that would be expected for the distribution function $p_v(g|D)$ in any real sample, and the transformed distribution is obtained as the solution to the constrained minimisation problem

$$\text{Minimise } ||100(Kp_v - P_l)|| + \lambda \sum_{i=1}^{12} p_v^i ln\, p_v^i \tag{8.10}$$

subject to the equality constraint 8.8 and inequalities 8.9. The term

$$-\sum_{i=1}^{12} p_v^i ln\, p_v^i$$

measures the entropy of the distribution and increases as the distribution becomes smoother. The regularization parameter λ is arbitrary and controls the weight given to maximisation of the entropy of the distribution relative to minimisation of the residual norm. Large λ favors larger entropy and therefore

$P_l(g_l|g_v) =$

1.0000	0.8190	0.5508	0.3758	0.2633	0.1905	0.1411	0.1041	0.0727	0.0433	0.0144	0.0000
1.0000	0.9028	0.6960	0.5101	0.3640	0.2571	0.1809	0.1254	0.0826	0.0470	0.0151	0.0000
1.0000	0.9288	0.7645	0.5987	0.4521	0.3318	0.2367	0.1621	0.1033	0.0561	0.0171	0.0000
1.0000	0.9460	0.8149	0.6716	0.5329	0.40825	0.3002	0.2087	0.1324	0.0701	0.0205	0.0000
1.0000	0.9584	0.8543	0.7334	0.6073	0.4843	0.3688	0.2632	0.1693	0.0894	0.0255	0.0000
1.0000	0.9677	0.8857	0.7861	0.6753	0.5590	0.4410	0.3247	0.2139	0.1143	0.0323	0.0000
1.0000	0.9745	0.9106	0.8307	0.7368	0.6312	0.5157	0.3927	0.2666	0.1457	0.0416	0.0000
1.0000	0.9795	0.9299	0.8676	0.7913	0.6998	0.5918	0.4671	0.3284	0.1851	0.0540	0.0000
1.0000	0.9829	0.9439	0.8967	0.8379	0.7633	0.6682	0.5479	0.4013	0.2355	0.0712	0.0000
1.0000	0.9849	0.9530	0.9174	0.8746	0.8191	0.7429	0.6360	0.4899	0.3040	0.0972	0.0000
1.0000	0.9856	0.9567	0.9273	0.8959	0.8589	0.8095	0.7367	0.6242	0.4492	0.1810	0.0000
1.0000	1.0000	1.0000	1.0000	1.0000	1.0000	1.0000	1.0000	1.0000	1.0000	1.0000	1.0000

Figure 47: A useful kernel

smoother solutions at the cost of larger residual norms. In practice a value of $\lambda = 1.0$ has been found to be a satisfactory choice in most cases [King 2001].

In general the kernel matrix should be determined separately for every sample that is analyzed but obviously this is a time-consuming and tedious task. A useful kernel that will produce good results for many natural minerals is given in Figure 8.3.

If the kernel $P_l(g_l|g_v)$ (which is the matrix used to generate linear distribution if the voluminal distribution is known) is known, solution to (8.10) with the constraint (8.8) and (8.9) will give the 3D data p_v (voluminal distribution) based on the 2D data. After this transformation operation, the data p_v can be used as experimental data to verify simulation model.

CHAPTER 9

CONCLUSIONS

Successful environmental protection and the economic advantages to be gained from the reuse of materials depend on an optimised recycling system in which the shredding process plays a very important role. The research presented in this thesis explores a simulation method for shredding which incorporates the complexity of end of life electronic products and the feasiblity of quantitative simulation. The long run objective for shredding simulation is to optimise the overall recycling system and yield design advice in view of recycling purpose to electronic product designers.

9.1 Shredding equipment

The shredding equipment is a shredder, a size reduction machine that tears objects into small pieces. Different types of shredders are is use in industry today. The swing-hammer shredder is one typical type.

9.2 Shredding process

The main shredding process is the interaction between the shredder blade and shredded materials. Four stages can be distinguished based on the kinetics of the interaction.

1. Stage I: The combined action of tensile stress, bending and torsion cause the tearing of single fragments from the feed material.
2. Stage II: Intense deformation leads to the formation of flaws on the comparatively large platy fragments.
3. Stage III: Impacts cause a proceeding deformation which results in the formation of further flaws.

4. Stage IV: Fragments are intensely compacted until they possess a spherical shape and fine particles are formed.

9.3 Mathematics and physics elements in shredding simulation model

The data of interest both before and after shredding are sizes and compositions of end of life electronic products. Because of the characteristics of those data, matrix and related mathematics manipulation are suit tools to build shredding model.

9.4 Shredder simulation algorithm

There are two main steps in the simulation of shredding. The first step to map the end of life electronic product design parameters to size and liberation distribution (which are matrices) before shredding. The second step is simulating the size and liberation evolution in the shredding process. The core ideas for this process are mass balance and liberation dispersion constrains.

9.5 MATLAB and FEM

MATLAB and FEM have been shown to be powerful tools in the simulation model. Their flexibility and power can be further explored in future work.

9.6 Image analysis

One of the proposed verification procedure is to collect the image data of those particle after shredding. After the 2D to 3D transformation, those image data can be built up as experimental data to validate the simulation model. This image analysis procedure does not involve complex chemical operations and is simple to implement.

9.7 Contributions of this thesis

The following are direct contributions of this thesis to the field:

1. Combine Castro partition scheme and Van Schaik liberation concept to generate the matrix description of end of life electronic products before shredding.
2. Develop an FEM based shredding simulation which will generate the size distribution after shredding and also supply the liberation distribution results after shredding for comparison with the modified shredder model.
3. Propose the liberation dispersion concept and build it into shredder model.
4. Propose an image analysis based experiment procedure and data processing method for verification of the shredder model of end of life electronic product.

9.8 Future work

In this research, for the purpose of simplicity and illustrating the simulation method, most of those material/geometry specific matrices are assumed to be "generic". This is obviously not the case in reality. To develop a more accurate simulation model, each matrix should be built in its own properties.

Neural networks provide an effective approach for a broad spectrum of applications. Neural networks excel at problems involving pattern mapping, pattern completion and pattern classification. Neural networks utilise a parallel processing structure that has large numbers of processors and many interactions between them. These processors are much simpler than typical central processing units, or CPU's. In a neural network each processor is linked to many of its neighbors (typically hundreds or thousands) so that there are more interconnectionss than processors. The power of neural networks lies in their tremendous number of interconnections. A lot of neural network variants are adopted to optimise the disassembly procedure [Zussman & Zhou 1999]. In the future, a neural network algorithm could be incorporated into the computer simulation model for shredding end of life electronic products.

CITED LITERATURE

Anderson, T.L. 1995. *Fracture Mechanics.* USA: CRC Press.

Arfken, G. 1985. *Mathematical Methods for Physicists.* Orlando, FL: Academic Press.

Castro, M.B., J.A.M. Remmerswaal, J.C. Brezet, A. van Schaik & M.A. Reuter. 2005. "A simulation model of the comminution-liberation of recycling streams relationships between product design and the liberation of materials during recycling." *International Journal of Mineral Processing* 75:255–281.

Consumer Electronics Association. 2005. CEA Market Research Report *Comsumer Electronics Reuse and Recycling*. October 2005.

Gay, S.L. 2004. "A liberation model for comminution based on probability theory." *Minerals Engineering* 17:525–534.

Heiskanen, K. 1993. *Particle Classification.* London,Great Britain: Chapman & Hall.

King, B.P. 2001. *Modeling and Simulation of Mineral Processing Systems.* United States: Butterworth Heinemann.

Kirchner, J. 2000. Mikroprozesse und Einflußgrössen bei der Zerkleinerung der Schrotte und Metalle in Shreddern mit horizontal angeordnetem Rotor PhD thesis TU Bergakademie Freiberg.

Kotera, Yoshikazu & Shin'ya Sato. 1997. An Integrated Recycling Process for Electric Home Appliance. R&d progress report Mitsubishi Electric.

Lastra, R. 2002. "A Comparision of Liberation Determinations by Particle Area Percentage and Exposed Particle Perimeter Percentage in a Flotation Concentrator." *Journal of Minerals & Materials Characterization & Engineering* 1(1):31–37.

Masui, T., T. Morita & J. Kyogoku. 2000. "Analysis of recycling activities using multi-sectoral economic model with material flow." *European Journal of Operational Research* 122:405–415.

Randolph, A.D. & M.A. Larson. 1971. *Theory of particulate processes.* London: Academic Press.

Reuter, M.A. & A. van Schaik. 2004. The Effect of Design on Recycling Rates for Cars. In *REWAS'04 - Global Symposium on Recycling, Waste Treatment and Clean Technology*. REWAS pp. 35–58.

Reuter, M.A. & J.S.J. van Deventer. 1990. "The use of linear programming in the optimal design of flotation circuits incorporating regrind mills." *International Journal of Mineral Processing* 28:15–43.

Rockey, K. C. & H. R. Evans. 1983. *The Finite Element Method.* New York: John Wiley & Sons.

Sander, S. 2004. "The fundamentals of the comminution of metals in shredders of the swing-hammer type." *Int. J. Miner. Process* 74:385–393.

Schneider, C.L. 1995. Measurement and calculation of liberation in continuous milling circuits PhD thesis University of Utah.

van Schaik, A. & M.A. Reuter. 2004. "The time-varying factors influencing the recycling rate of products." *Resources, Conservation and Recycling* 40(4):301–328.

van Schaik, A., M.A. Reuter & K. Heiskanen. 2004. "The influence of particle size reduction and liberation on the recycling rate of end-of-life vehicles." *Mineral Engineering* 17:331–347.

van Schaik, A., M.A. Reuter, U Bion & W.L. Dalmijin. 2002. "Dynamics modelling and optimisation of the resource cycle of passenger vehicles." *Minerals Engineering* 15(11) Suppl. 1:1001–1016.

van Schaik, A., M.A. Reuter, U.M.J. Boin & W.L. Dalmijin. 2002. "Dynamic modelling and optimisation of the resource cycle of passenger vehicles." *Minerals Engineering* 15:1001–1016.

van Schaik, A., M.B. Castro & J.A.M Remmerswaal. 2003. The role of product design and liberation in the optimisation of recycling passenger vehicles. In *Proceedings XXII International Mineral Processing Congress.* pp. 1768–1777.

van Schaik, A., W. L. Dalmjin & M.A. Reuter. 2001. Impact of economy on the secondary material cycle. In *Proceedings COM Waste Processing and Recycling in Mineral and Metallurgical Industries IV.* Waste Processing and Recycling in Mineral and Metallurgical Industries. Toronto, Canada,pp. 407-423.

Verhoef, E.V., M.A. Reuter & G.P.J. Dijkema. 2004. "Process knowledge, system dynamics and metal ecology." *Journal of Industrial Ecology, JIE* 8:23–43.

Web, Efunda. 2006*a*. "Mechanical Properties of Aluminum." web reference.
URL: *http://www.efunda.com/materials/common_matl/Common_Matl.cfm ?MatlPhase=Solid&MatlProp=Mechanical#MechanicalStrength*

Web, Efunda. 2006*b*. "Mechanical Properties of Copper." web reference.
URL: *http://www.efunda.com/materials/alloys/copper/properties.cfm*

Web, MATLAB. 2006*c*. "Tensors, Contravariant and Covariant." web reference.
URL: *http://www.mathpages.com/rr/s5-02/5-02.htm*

Web, TangramTechnology. 2006*d*. "TI POLYMER PS." web reference.
URL: *http://www.tangram.co.uk/TI-Polymer-PS.html*

Web, Wikipedia. 2006*e*. "comminution." web reference.
URL: *http://en.wikipedia.org/wiki/Comminution*

Web, Wikipedia. 2006*f*. "compaction." web reference.
URL: *http://en.wikipedia.org/wiki/Compaction*

Web, Wikipedia. 2006*g*. "Crystallite." web reference.
URL: *http://en.wikipedia.org/wiki/Einstein_notation*

Web, Wikipedia. 2006*h*. "Shredder." web reference.
URL: *http://wikipedia.org/wiki/Shredder_(device)*

Wei, X. & S. Gay. 1999. "Liberation Modelling Using a Dispersion Equation." *Minerals Engineering* 12(2):219–227.

Weisstein, Eric W. 2006. "Metric Tensor." web reference.
URL: *http://mathworld.wolfram.com/MetricTensor.html*

Zussman, Eyal & MengChu Zhou. 1999. "A Methodology for Modeling and Adaptive Planning of Disassembly Processes." *IEEE Transactions on Robotics and Automation* 15:190–194.

Zussman, Eyal, MengChu Zhou & Reggie Caudill. 1998. Disassembly Petri Net Approach to Modeling and Planning Disassembly Process of Electronic Products. In *Proc. of 1998 IEEE International Symposium on Electronics and the Environment*. IEEE pp. 331–336.

APPENDIX

SOURCE CODE

A.1 Java source code to generate FEM grid

```
//Java core packages

import java.awt.*; //import class Graphics

import java.awt.event.*;


//Java extension packages

import javax.swing.*;


public class femgrid extends JFrame {


//set window's title bar String and dimensions

public femgrid( )

{

super("FEM grid plan for the being shredded cell phone");

setSize(1000,400);

setVisible ( true );

}
```

APPENDIX (Continued)

```
// display grid on the pop window

public void paint (Graphics g)

{

// call superclass's paint method

super.paint(g);

g.setColor(Color.blue);

g.drawRect(50,50,900,300);

for (int i=1;i<=4 ;i++){ g.drawLine(50,50+i*300/5,950,50+i*300/5);

}

for (int i=1;i<=14;i++){

g.drawLine(50+i*900/15,50,50+i*900/15,350);

} //draw the middle ten oblique lines

for( int i=0;i<=10;i++){ g.drawLine(50+i*900/15,50,50+(i+5)*900/15,350); }

//draw the left four oblique lines

for (int i=1;i<=4;i++){ g.drawLine(50,50+i*300/5,50+5*900/15-i*900/15,350); }

//draw the right four oblique lines

for (int i=1;i<=4;i++){

g.drawLine(950-5*900/15+i*900/15,50,950,350-i*300/5);

} // put node number in the grid system

int counter=1;

g.setColor(Color.red);

for (int i=1;i<=16;i++){
```

APPENDIX (Continued)

```
for(int j=1;j<=6;j++){
g.drawString(String.valueOf(counter),50+(i-1)*900/15,350-(j-1)*300/5);
counter=counter+1;
}}
// put element number in the grid system, odd part
counter=1;
g.setColor(Color.black); for (int i=1;i<=15;i++){
for(int j=1;j<=5;j++){
g.drawString(String.valueOf(counter),50+(i-1)*900/15+10,350-(j-1)*300/5-100/5);

counter=counter+2; }}
// put element number in the grid system, even part
counter=2;
g.setColor(Color.black);
for (int i=1;i<=15;i++){
for(int j=1;j¡=5;j++)
g.drawString(String.valueOf(counter),50+i*900/15-30,350-(j-1)*300/5-30);
counter=counter+2; }}

    }
```

APPENDIX (Continued)

```
//execute application

public static void main (String args[])  femgrid application = new femgrid( );

application.setDefaultCloseOperation(JFrame.EXIT_ON_CLOSE);

//end class femgrid
```

A.2 Matlab FEM code to calculate stress distribution

```
% Assume the length of cell phone is 10 cm and its width is 4 cm

% In the direction of length, we will divide the the length into 15 equal segments, in the direction of

width, we will divide the width into 5 equal segments

% We number the nodes in the sequence from bottom to top, from left to the right

% We also assume the thickness of the discarded cell phone is 1 cm

java;

femgrid;

K=zeros(2*96); % initialize the system stiffness matrix with 96 nodes

deltx=10/15;

delty=4/5;

for i=1:96

x(i)=floor((i-1)/6)*deltx; % abscissa x for all those nodes

y(i)=mod((i-1),6)*delty; % ordinate y for all those nodes

end

% calculate all those element stiffness matrix from node 1 to node 96 for

% material A, ps

for j=1:15
```

APPENDIX (Continued)

```
i1=1+6*(j-1);
for k=i1:i1+4
l1=k;
l2=k+6;
l3=k+1;
eatm=[1 x(l1) y(l1);1 x(l2) y(l2);1 x(l3) y(l3)] % 1/2 of element area of triangle, matrix form
eatd=det(eatm) % 1/2 of element area of triangle, determinant of corresponding matrix
B=(1/(2*eatd))*[y(l2)-y(l3) 0 y(l3)-y(l1) 0 y(l1)-y(l2) 0;0 x(l3)-x(l2) 0 x(l1)-x(l3) 0 x(l2)-x(l1);x(l3)-
x(l2) y(l2)-y(l3) x(l1)-x(l3) y(l3)-y(l1) x(l2)-x(l1) y(l1)-y(l2)] % intermediate matrix needed to calculate
system stiffness matrix
v=0.3;% poisson's ratio of ps
E=3.5;% tensile modulus of ps
DA=[E/(1-v^2) v*E/(1-v^2) 0;v*E/(1-v^2) E/(1-v^2) 0;0 0 E/(2*(1+v))] % intermediate matrix needed
to calculate system stiffness matrix
i2=2*j-1;
% element matrix needed to calculate element stresses
ek(:,:,2*k-i2)=DA*B;
ke(:,:,2*k-i2)=B.'*ek(:,:,2*k-i2) % element stiffness matrix
end
for k=i1:i1+4
l1=k+1;
l2=k+6;
```

APPENDIX (Continued)

```
l3=k+7;
eatm=[1 x(l1) y(l1);1 x(l2) y(l2);1 x(l3) y(l3)] % 1/2 of element area of triangle, matrix form
eatd=det(eatm) % 1/2 of element area of triangle, determinant of corresponding matrix
B=(1/(2*eatd))*[y(l2)-y(l3) 0 y(l3)-y(l1) 0 y(l1)-y(l2) 0;0 x(l3)-x(l2) 0 x(l1)-x(l3) 0 x(l2)-x(l1);x(l3)-
x(l2) y(l2)-y(l3) x(l1)-x(l3) y(l3)-y(l1) x(l2)-x(l1) y(l1)-y(l2)] % intermediate matrix needed to calculate
system stiffness matrix
v=0.3;% poisson's ratio of ps
E=3.5;% tensile modulus of ps
DA=[E/(1-v^2) v*E/(1-v^2) 0;v*E/(1-v^2) E/(1-v^2) 0;0 0 E/(2*(1+v))] % intermediate matrix needed
to calculate system stiffness matrix
i2=2*j-1;
% element matrix needed to calculate element stresses
ek(:,:,2*k-(i2-1))=DA*B;
ke(:,:,2*k-(i2-1))=B.'* ek(:,:,2*k-(i2-1))% element stiffness matrix
end
end


% calculate all those element stiffness matrix from node 1 to node 96 to
% incorporate material B,copper
for j=1:3
i1=38+6*(j-1);
for k=i1:i1+1
```

APPENDIX (Continued)

```
l1=k;
l2=k+6;
l3=k+1;
eatm=[1 x(l1) y(l1);1 x(l2) y(l2);1 x(l3) y(l3)] % 1/2 of element area of triangle, matrix form
eatd=det(eatm) % 1/2 of element area of triangle, determinant of corresponding matrix
B=(1/(2*eatd))*[y(l2)-y(l3) 0 y(l3)-y(l1) 0 y(l1)-y(l2) 0;0 x(l3)-x(l2) 0 x(l1)-x(l3) 0 x(l2)-x(l1);x(l3)-
x(l2) y(l2)-y(l3) x(l1)-x(l3) y(l3)-y(l1) x(l2)-x(l1) y(l1)-y(l2)] % intermediate matrix needed to calculate
system stiffness matrix
v=0.34;% poisson's ratio of copper
E=117;% tensile modulus of copper
DA=[E/(1-v^2) v*E/(1-v^2) 0;v*E/(1-v^2) E/(1-v^2) 0;0 0 E/(2*(1+v))] % intermediate matrix needed
to calculate system stiffness matrix
i2=13+2*(j-1);
% element matrix needed to calculate element stresses
ek(:,:,2*k-i2)=DA*B;
ke(:,:,2*k-i2)=B.'*ek(:,:,2*k-i2) % element stiffness matrix
end


for k=i1:i1+1
l1=k+1;
l2=k+6;
l3=k+7;
```

APPENDIX (Continued)

```
eatm=[1 x(l1) y(l1);1 x(l2) y(l2);1 x(l3) y(l3)] % 1/2 of element area of triangle, matrix form
eatd=det(eatm) % 1/2 of element area of triangle, determinant of corresponding matrix
B=(1/(2*eatd))*[y(l2)-y(l3) 0 y(l3)-y(l1) 0 y(l1)-y(l2) 0;0 x(l3)-x(l2) 0 x(l1)-x(l3) 0 x(l2)-x(l1);x(l3)-
x(l2) y(l2)-y(l3) x(l1)-x(l3) y(l3)-y(l1) x(l2)-x(l1) y(l1)-y(l2)] % intermediate matrix needed to calculate
system stiffness matrix
v=0.34;% poisson's ratio of ps
E=117;% tensile modulus of ps
DA=[E/(1-v^2) v*E/(1-v^2) 0;v*E/(1-v^2) E/(1-v^2) 0;0 0 E/(2*(1+v))] % intermediate matrix needed
to calculate system stiffness matrix
i2=13+2*(j-1);
% element matrix needed to calculate element stresses
ek(:,:,2*k-(i2-1))=DA*B;
ke(:,:,2*k-(i2-1))=B.'*ek(:,:,2*k-(i2-1)) % element stiffness matrix
end
end

% calculate all those element stiffness matrix from node 1 to node 96 to
% incorporate material c,aluminum
for j=1:3
i1=64+6*(j-1);
for k=i1:i1+1
l1=k;
```

APPENDIX (Continued)

```
l2=k+6;

l3=k+1;

eatm=[1 x(l1) y(l1);1 x(l2) y(l2);1 x(l3) y(l3)] % 1/2 of element area of triangle, matrix form

eatd=det(eatm) % 1/2 of element area of triangle, determinant of corresponding matrix

B=(1/(2*eatd))*[y(l2)-y(l3) 0 y(l3)-y(l1) 0 y(l1)-y(l2) 0;0 x(l3)-x(l2) 0 x(l1)-x(l3) 0 x(l2)-x(l1);x(l3)-
x(l2) y(l2)-y(l3) x(l1)-x(l3) y(l3)-y(l1) x(l2)-x(l1) y(l1)-y(l2)] % intermediate matrix needed to calculate
system stiffness matrix

v=0.33;% poisson's ratio of copper

E=70;% tensile modulus of copper

DA=[E/(1-v^2) v*E/(1-v^2) 0;v*E/(1-v^2) E/(1-v^2) 0;0 0 E/(2*(1+v))] % intermediate matrix needed
to calculate system stiffness matrix

i2=21+2*(j-1);

% element matrix needed to calculate the stresses of the element

ek(:,:,2*k-i2)=DA*B;

ke(:,:,2*k-i2)=B.'*ek(:,:,2*k-i2) % element stiffness matrix

end


for k=i1:i1+1

l1=k+1;

l2=k+6;

l3=k+7;

eatm=[1 x(l1) y(l1);1 x(l2) y(l2);1 x(l3) y(l3)] % 1/2 of element area of triangle, matrix form
```

APPENDIX (Continued)

```
eatd=det(eatm) % 1/2 of element area of triangle, determinant of corresponding matrix
B=(1/(2*eatd))*[y(l2)-y(l3) 0 y(l3)-y(l1) 0 y(l1)-y(l2) 0;0 x(l3)-x(l2) 0 x(l1)-x(l3) 0 x(l2)-x(l1);x(l3)-
x(l2) y(l2)-y(l3) x(l1)-x(l3) y(l3)-y(l1) x(l2)-x(l1) y(l1)-y(l2)] % intermediate matrix needed to calculate
system stiffness matrix
v=0.33;% poisson's ratio of ps
E=70;% tensile modulus of ps
DA=[E/(1-v^2) v*E/(1-v^2) 0;v*E/(1-v^2) E/(1-v^2) 0;0 0 E/(2*(1+v))] % intermediate matrix needed
to calculate system stiffness matrix
i2=21+2*(j-1);
% element matrix needed to calculate the stresses of the element ek(:,:,2*k-(i2-1))=DA*B;
ke(:,:,2*k-(i2-1))=B.'*ek(:,:,2*k-(i2-1)) % element stiffness matrix
end
end

% assembly the system stiffness matrix
counter=1;
for jj=1:6:85

for j1=jj:jj+4
g=ke(:,:,2*j1-counter);
% procedure to replace the 36 matrix elements of each element stiffness
% into the big system stiffness matrix
```

APPENDIX (Continued)

```
j=2*(j1-1)+1;

% operation of row 1 of element stiffness matrix

K(j,j)=K(j,j)+g(1,1);

K(j,j+1)=K(j,j+1)+g(1,2);

K(j,j+12)=K(j,j+12)+g(1,3);

K(j,j+13)=K(j,j+13)+g(1,4);

K(j,j+2)=K(j,j+2)+g(1,5);

K(j,j+3)=K(j,j+3)+g(1,6);


% operation of row 2 of element stiffness matrix

K(j+1,j)=K(j+1,j)+g(2,1);

K(j+1,j+1)=K(j+1,j+1)+g(2,2);

K(j+1,j+12)=K(j+1,j+12)+g(2,3);

K(j+1,j+13)=K(j+1,j+13)+g(2,4);

K(j+1,j+2)=K(j+1,j+2)+g(2,5);

K(j+1,j+3)=K(j+1,j+3)+g(2,6);


% operation of row 3 of element stiffness matrix

K(j+12,j)=K(j+12,j)+g(3,1);

K(j+12,j+1)=K(j+12,j+1)+g(3,2);

K(j+12,j+12)=K(j+12,j+12)+g(3,3);

K(j+12,j+13)=K(j+12,j+13)+g(3,4);
```

APPENDIX (Continued)

```
K(j+12,j+2)=K(j+12,j+2)+g(3,5);

K(j+12,j+3)=K(j+12,j+3)+g(3,6);


% operation of row 4 of element stiffness matrix

K(j+13,j)=K(j+13,j)+g(4,1);

K(j+13,j+1)=K(j+13,j+1)+g(4,2);

K(j+13,j+12)=K(j+13,j+12)+g(4,3);

K(j+13,j+13)=K(j+13,j+13)+g(4,4);

K(j+13,j+2)=K(j+13,j+2)+g(4,5);

K(j+13,j+3)=K(j+13,j+3)+g(4,6);


% operation of row 5 of element stiffness matrix

K(j+2,j)=K(j+2,j)+g(5,1);

K(j+2,j+1)=K(j+2,j+1)+g(5,2);

K(j+2,j+12)=K(j+2,j+12)+g(5,3);

K(j+2,j+13)=K(j+2,j+13)+g(5,4);

K(j+2,j+2)=K(j+2,j+2)+g(5,5);

K(j+2,j+3)=K(j+2,j+3)+g(5,6);


% operation of row 6 of element stiffness matrix

K(j+3,j)=K(j+3,j)+g(6,1);

K(j+3,j+1)=K(j+3,j+1)+g(6,2);
```

APPENDIX (Continued)

```
K(j+3,j+12)=K(j+3,j+12)+g(6,3);

K(j+3,j+13)=K(j+3,j+13)+g(6,4);

K(j+3,j+2)=K(j+3,j+2)+g(6,5);

K(j+3,j+3)=K(j+3,j+3)+g(6,6);

end


% assemble the system matrix, even number part

for j1=jj:jj+4

g=ke(:,:,2*j1-(counter-1));

% procedure to replace the 36 matrix elements of each element stiffness

% into the big system stiffness matrix

j=2*j1-1;

% operation of row 1 of element stiffness matrix

K(j+2,j+2)=K(j+2,j+2)+g(1,1);

K(j+2,j+3)=K(j+2,j+3)+g(1,2);

K(j+2,j+12)=K(j+2,j+12)+g(1,3);

K(j+2,j+13)=K(j+2,j+13)+g(1,4);

K(j+2,j+14)=K(j+2,j+14)+g(1,5);

K(j+2,j+15)=K(j+2,j+15)+g(1,6);


% operation of row 2 of element stiffness matrix

K(j+3,j+2)=K(j+3,j+2)+g(2,1);
```

APPENDIX (Continued)

```
K(j+3,j+3)=K(j+3,j+3)+g(2,2);

K(j+3,j+12)=K(j+3,j+12)+g(2,3);

K(j+3,j+13)=K(j+3,j+13)+g(2,4);

K(j+3,j+14)=K(j+3,j+14)+g(2,5);

K(j+3,j+15)=K(j+3,j+15)+g(2,6);


% operation of row 3 of element stiffness matrix

K(j+12,j+2)=K(j+12,j+2)+g(3,1);

K(j+12,j+3)=K(j+12,j+3)+g(3,2);

K(j+12,j+12)=K(j+12,j+12)+g(3,3);

K(j+12,j+13)=K(j+12,j+13)+g(3,4);

K(j+12,j+14)=K(j+12,j+14)+g(3,5);

K(j+12,j+15)=K(j+12,j+15)+g(3,6);


% operation of row 4 of element stiffness matrix

K(j+13,j+2)=K(j+13,j+2)+g(4,1);

K(j+13,j+3)=K(j+13,j+3)+g(4,2);

K(j+13,j+12)=K(j+13,j+12)+g(4,3);

K(j+13,j+13)=K(j+13,j+13)+g(4,4);

K(j+13,j+14)=K(j+13,j+14)+g(4,5);

K(j+13,j+15)=K(j+13,j+15)+g(4,6);
```

APPENDIX (Continued)

```
% operation of row 5 of element stiffness matrix

K(j+14,j+2)=K(j+14,j+2)+g(5,1);

K(j+14,j+3)=K(j+14,j+3)+g(5,2);

K(j+14,j+12)=K(j+14,j+12)+g(5,3);

K(j+14,j+13)=K(j+14,j+13)+g(5,4);

K(j+14,j+14)=K(j+14,j+14)+g(5,5);

K(j+14,j+15)=K(j+14,j+15)+g(5,6);


% operation of row 6 of element stiffness matrix

K(j+15,j+2)=K(j+15,j+2)+g(6,1);

K(j+15,j+3)=K(j+15,j+3)+g(6,2);

K(j+15,j+12)=K(j+15,j+12)+g(6,3);

K(j+15,j+13)=K(j+15,j+13)+g(6,4);

K(j+15,j+14)=K(j+15,j+14)+g(6,5);

K(j+15,j+15)=K(j+15,j+15)+g(6,6);


end

counter=counter+2;

end


% We assume the following boundary condition for this shredding cell phone

% This being shredded cell phone is fixed at its four nodes, node 1, node
```

APPENDIX (Continued)

```
% 6,node 91 and node 96


% The following operation is to insert the boundary condition into the
% system stiffness matrix
K(1,1)=K(1,1)*10^10;
K(2,2)=K(2,2)*10^10;
K(11,11)=K(11,11)*10^10;
K(12,12)=K(12,12)*10^10;
K(181,181)=K(181,181)*10^10;
K(182,182)=K(182,182)*10^10;
K(191,191)=K(191,191)*10^10;
K(192,192)=K(192,192)*10^10;


% Assume the random forces on each node from the shredder
% Assume the mean for those forces is 0 and standard deviation is 1
% Initialize rand to a different state each time
randn('state',sum(100*clock));
F=randn(192,1);
% calculate the displacement for each node
dis=inv(K)*F
```

APPENDIX (Continued)

```
% calculate stresses for each individual element

% initialize those element matrices to 0

dise=zeros(6,150)

% connectivity matrix

cot=[

1 7 2; 2 7 8; 2 8 3; 3 8 9; 3 9 4; 4 9 10; 4 10 5; 5 10 11; 5 11 6; 6 11 12; 7 13 8; 8 13 14; 8 14 9; 9 14 15;

9 15 10; 10 15 16; 10 16 11; 16 11 17; 11 17 12; 12 17 18; 13 19 14; 14 19 20; 14 20 15; 15 20 21;

15 21 16; 16 21 22; 16 22 17; 17 22 23; 17 23 18; 18 23 24; 19 25 20; 20 25 26; 20 26 21; 21 26 27;

21 27 22; 22 27 28; 22 28 23; 23 28 29; 23 29 24; 24 29 30; 25 31 26; 26 31 32; 26 32 27; 27 32 33;

27 33 28; 28 33 34; 28 34 29; 29 34 35; 29 35 30; 30 35 36; 31 37 32; 32 37 38; 32 38 33; 33 38 39;

33 39 34; 34 39 40; 34 40 35; 35 40 41; 35 41 36; 36 41 42; 37 43 38; 38 43 44; 38 44 39; 39 44 45;

40 45 46; 40 45 46; 40 46 41; 41 46 47; 41 47 42; 42 47 48; 43 49 44; 44 49 50; 44 50 45; 45 50 51;

45 51 46; 46 51 52; 46 52 47; 47 52 53; 47 53 48; 48 53 54; 49 55 50; 50 55 56; 51 50 56; 51 56 57;

51 57 52; 52 57 58; 52 58 53; 53 58 59; 53 59 54; 54 59 60; 55 61 56; 56 61 62; 56 62 57; 57 62 63;

57 63 58; 58 63 64; 58 64 59; 59 64 55; 59 65 60; 60 65 66; 61 67 62; 62 67 68; 62 68 63; 63 68 69;

63 69 64; 64 69 70; 64 70 65; 65 70 71; 65 71 66; 66 71 72; 67 73 68; 68 73 74; 68 74 69; 69 74 75;

69 75 70; 70 75 76; 70 76 71; 71 76 77; 71 77 72; 72 77 78; 73 79 74; 74 79 80; 74 80 75; 75 80 81;

75 81 76; 76 81 82; 76 82 77; 77 82 83; 77 83 78; 78 83 74; 79 85 80; 80 85 86; 80 86 81; 81 86 87;

81 87 82; 82 87 88; 82 88 83; 83 88 89; 83 89 84; 84 89 90; 85 91 86; 86 91 92; 86 92 87; 87 92 93;

87 93 88; 88 93 94; 88 94 89; 89 94 95; 89 95 90; 90 95 96]
```

APPENDIX (Continued)

```
for i=1:150
dise(1,i)=dis(2*cot(i,1)-1,1);
dise(2,i)=dis(2*cot(i,1),1);
dise(3,i)=dis(2*cot(i,2)-1,1);
dise(4,i)=dis(2*cot(i,2),1);
dise(5,i)=dis(2*cot(i,3)-1,1);
dise(6,i)=dis(2*cot(i,3),1);
end

% calculate the stresses for each element
% we use fe to denotate the element stress
for i=1:150
fe(:,i)=ek(:,:,i)*dise(:,i);
end

% calculate the maxium principal stress for each element and its
% corresponding orientation
% initialize this matrix
psor=zeros(2,150);
for i=1:150
psor(1,i)=(fe(1,i)+fe(2,i))/2+sqrt(((fe(1,i)-fe(2,i))/2)^2+fe(3,i)^2);
psor(2,i)=1/2*atan(2*fe(3,i)/(fe(1,i)-fe(2,i)));
```

APPENDIX (Continued)

```
end

% calculate the centroid of each individual triangle elements use the
% formula xc=1/3*(x1+x2+x3), yc=1/3*(x1+x2+x3)

intx=(0+0+deltx)/3;
inty=(0+0+delty)/3;
% initialize counter and k and cc

counter=1;

for i=1:15
cc=0;
for j=1:10
if (mod(j,2) =0) && j =1
cc=cc+1;
end
xc(counter)=intx+(1-mod(j,2))*intx+(i-1)*deltx;
yc(counter)=inty+(1-mod(j,2))*inty+cc*delty;
counter=counter+1;
end
```

APPENDIX (Continued)

```
end

% generate the quiver vector from psor
for i=1:150
u(i)=psor(1,i)*cos(psor(2,i));
v(i)=psor(1,i)*sin(psor(2,i));
end
quiver(xc,yc,u,v,1.6);
```

A.3 Maltab source code for the post process treatment of FEM calculation

```
% This function is used to generate particles of shredded cell phone after
% fem simulation

% function y = fempp(px,py, psor)
% FEM post process for FEM simulation of shredded cell phone
% This function take input from the previous FEM simulation

[m,n]=size(xc); % get the size of matrix px
ms=mean(abs(psor(1,:))); % get the average stress of the stress vector

ct=1;% tracker
iteration_times=0;
```

APPENDIX (Continued)

```
for i=1:n

if (abs(psor(1,i))) >= (1.6*ms) % we assume the material will fail only when the stress is 8 times the

mean stress, this parameter can be adjusted

npsm(ct)=psor(1,i);

npsd(ct)=pi/2+psor(2,i);

npx(ct)=xc(i);

npy(ct)=yc(i);

ct=ct+1;

end

end

% y=0;


% solve for those intersection points of all those cracks


[i,tcp]=size(npx);

for i=1:tcp

% elements of matrix xin and yin on diagonal line

xin(i,i)=npx(i);

yin(i,i)=npy(i);


for j=i+1:tcp

if (npsd(i)==npsd(j) ) || abs(npsd(i)-npsd(j))==pi
```

APPENDIX (Continued)

```
xin(i,j)=10^5;

yin(i,j)=10^5;% since line i and line j is almost parrellel, so assume their intersection is very big numbers

else %% Sunday October 01 revise xc and yc to npx and npy

xin(i,j)=((npy(j)-tan(npsd(j))*npx(j)) - ( npy(i) - tan(npsd(i))*npx(i)))/( tan(npsd(i))-tan(npsd(j))); % x

abscissa of the intersection

yin(i,j)=polyval([tan(npsd(i)) (npy(i) - tan(npsd(i))*npx(i))],xin(i,j));

end

xin(j,i)=xin(i,j);

yin(j,i)=yin(i,j); % make use of the symmetry of the matrix to generate the complete matrix


end

end


% initialize the initial node crack pass flag to 0

for i=1:tcp

for j=1:tcp

ncpf(i,j)=0;

end

end


% get the sorted version of matrices xin and yin
```

APPENDIX (Continued)

```
for i=1:tcp
% shift the rows of matrices xin and yin first
xin1=circshift(xin,1-i);
yin1=circshift(yin,1-i);

amcd=[xin1(:,i) yin1(:,i)]; % auxiliary matrix to calculate distance
opdt=pdist(amcd); % get the distance vector for each pair between point i and the rest tcp-1 points
fdt=opdt(1:tcp-1); % we take only the firt tcp-1 elements of vector opdt
[sfdt,ix]=sort(fdt,2,'ascend');

six(i,1:tcp-1)=ix; % assemble system index matrix
end

% let us get the calibrated version of system index matrix
for i=1:tcp
for j=1:tcp-1
if six(i,j)+i >= tcp
sixc(i,j)=six(i,j)+i-tcp;
else
sixc(i,j)=six(i,j)+i;
end
end
```

APPENDIX (Continued)

```
end

% draw those cracks on the shredded cell phone

ctr=1;
for i=1:tcp
ctr1(i)=1;
ctr2(i)=1;
end
delt=0.00067;% time step size

hold on; % keep all those plots on the same figure

% initialize those dynamic points to npx and npy
for i=1:tcp
k1(i)=npx(i);
k2(i)=npy(i);
k3(i)=npx(i);
k4(i)=npy(i);
end
```

APPENDIX (Continued)

```
while ctr>0


for i=1:tcp

k10(i)=k1(i);

k20(i)=k2(i);

k30(i)=k3(i);

k40(i)=k4(i);

k1(i)=k1(i)+ctr1(i)*delt*abs(npsm(i))*cos(npsd(i));

k2(i)=k2(i)+ctr1(i)*delt*abs(npsm(i))*sin(npsd(i));

k3(i)=k3(i)-ctr2(i)*delt*abs(npsm(i))*cos(npsd(i));

k4(i)=k4(i)-ctr2(i)*delt*abs(npsm(i))*sin(npsd(i));

% deal with the situation when a crack hits one intersection

for j=1:tcp

while (i~=j)


if (xin(i,j)-k1(i))*(xin(i,j)-k10(i))<=0

if ncpf(i,j)==1

ctr1(i)=0;

k1(i)=xin(i,j);

k2(i)=yin(i,j);

else

ncpf(i,j)=1;
```

APPENDIX (Continued)

```
ncpf(j,i)=1;
end
end

if (xin(i,j)-k3(i))*(xin(i,j)-k30(i))<=0
if ncpf(i,j)==1
ctr2(i)=0;
k3(i)=xin(i,j);
k4(i)=yin(i,j);
else
ncpf(i,j)=1;
ncpf(j,i)=1;
end
end
break;
end
end

% deal with the conditions when cracks hit boundary of the shredded cell % phone
% left boundary condition
if (0-k1(i))*(0-k10(i))<=0
k1(i)=0;
```

APPENDIX (Continued)

```
k2(i)=npy(i)+tan(npsd(i))*(k1(i)-npx(i));

ctr1(i)=0;

end

if (0-k3(i))*(0-k30(i))<=0

k3(i)=0;

k4(i)=npy(i)+tan(npsd(i))*(k3(i)-npx(i));

ctr2(i)=0;

end


% right boundary condition

if (10-k1(i))*(10-k10(i))<=0

k1(i)=10;

k2(i)=npy(i)+tan(npsd(i))*(k1(i)-npx(i));

ctr1(i)=0;

end

if (10-k3(i))*(10-k30(i))<=0

k3(i)=10;

k4(i)=npy(i)+tan(npsd(i))*(k3(i)-npx(i));

ctr2(i)=0;

end
```

APPENDIX (Continued)

```
% upper boundary condition
if (4-k2(i))*(4-k20(i))<=0
k2(i)=4;
k1(i)=(k2(i)-npy(i))/tan(npsd(i))+npx(i);
ctr1(i)=0;
end
if (4-k4(i))*(4-k40(i))<=0
k4(i)=4;
k3(i)=(k4(i)-npy(i))/tan(npsd(i))+npx(i);
ctr2(i)=0;
end
% lower boudary condition

if (0-k2(i))*(0-k20(i))<=0
k2(i)=0;
k1(i)=(k2(i)-npy(i))/tan(npsd(i))+npx(i);
ctr1(i)=0;
end
if (0-k4(i))*(0-k40(i))<=0
k4(i)=0;
k3(i)=(k4(i)-npy(i))/tan(npsd(i))+npx(i);
ctr2(i)=0;
```

APPENDIX (Continued)

```
end

end


ctr=sum(ctr1)+sum(ctr2);


iteration_times=iteration_times+1

end


for i=1:tcp

line([k1(i);k3(i)],[k2(i);k4(i)]);

end

plot([0 0 10 10 0],[0 4 4 0 0],'r'); % draw the boundary lines of the shredded cell phone

hold off;
```